UNESCO-IHE
INSTITUTE FOR WATER EDUCATION

Modelling of Cohesive Sediment Transportation, Deposition and Resuspension in the Haringvliet Mouth

Ye,Qinghua

MSc Thesis (WSE-HI.06-15)
April 2006

UNESCO-IHE
Institute for Water Education

UNESCO-IHE
Institute for Water Education

Modelling of Cohesive Sediment Transportation, Deposition and Resuspension in the Haringvliet Mouth

Master of Science Thesis
by
Ye, Qinghua

Supervisors
Prof. Dr. J.A. Roelvink (UNESCO-IHE / WL | Delft Hydraulics)
Dr. D.P.Solomatine (UNESCO-IHE)
Dr. B. Bhattacharya (UNESCO-IHE)

Examination committee
Prof. Dr. R.K. Price (UNESCO-IHE), Chairman
Prof. Dr. J.A. Roelvink (UNESCO-IHE / WL | Delft Hydraulics)
Dr. Ir. T. van Kessel (WL | Delft Hydraulics)
Dr. B. Bhattacharya (UNESCO-IHE)

This research is done for the partial fulfilment of requirements for the Master of Science degree at the UNESCO-IHE Institute for Water Education, Delft, the Netherlands

Delft
April, 2006

The findings, interpretations and conclusions expressed in this study do neither necessarily reflect the views of the UNESCO-IHE Institute for Water Education, nor of the individual members of the MSc committee, nor of their respective employers.

To my mother...

Abstract

In the Dutch coastal zone, where the marine environment is characterized by shallow depths and highly energetic hydrodynamic conditions, the cohesive sediments, or mud, play an important role in the local morphology. For instance, mud deposits and high concentrations of suspended particulate matter (SPM) occur frequently, especially during extreme wave conditions, which lead to a great concern to transportation authorities and coastal managers. Several researchers contributed to the understanding of the cohesive sediment dynamics in the Dutch coastal zone. Nevertheless, the mechanism of cohesive sediment transportation, deposition and resuspension, especially due to wave effects, needs further studies and careful formulation.

The main objective of this study is to increase the understanding of the complex patterns of cohesive sediments transportation, deposition and resuspension due to wave effects with tide, wind, density-driven flow in the Dutch coastal area. The study focuses on the areas adjacent to the approach channel of the port of Rotterdam and Haringvliet Mouth, which are characterized by complex interactions between hydrodynamics and sedimentation.

Based on the scale linkage theory of de Vriend and rules of Roelvink to keep models simple, the study is carried out with three models at different spatial and temporal scale. Firstly, the study starts with the extension of the existing ZUNO model of the North Sea in a macro spatial scale using Delft3D FLOW and WAVE modules. The sediment movements under wave dynamics are verified as well. Secondly, the domain decomposition technology to generate locally refined grid to cover the studied area. Simulations are carried out with flow, wave, sediments, and morphology modules of Delft3D.

Thirdly, the simulated results with the ZUNO coarse grid model is utilised as the boundary condition of another fine grid model of the Haringvliet Mouth. This model is set up to study the influence of waves upon the cohesive sediments in the Haringvliet Mouth in a meso-temporal and spatial scale.

The specific boundary conditions of the model are introduced intentionally with harmonic tidal forcing and real time discharge from the Haringvliet Sluice. After the calibration of the wave model and cohesive sediment transportation model, the coupled models show the correct pattern of the cohesive sediment distribution in the area. It reproduces successfully the cohesive sediment transportation, deposition and resuspension pattern mainly due to wave effects in the areas adjacent to the approach channel of the port of Rotterdam and Haringvliet Mouth, which has been verified by measured sediments data. The model results show that the wave dynamics is one of the most significant processes behind the sediment movements in the Haringvliet Mouth.

A distributed simulation solution software is developed to utilize the distributed computation abilities in the local area network based on the named pipe technology. And it has been proved to be efficient during the models simulations.

Keywords: wave, cohesive sediments, transportation, deposition, resuspension, Haringvliet Mouth, Delft 3D

Acknowledgements

Writing this page, I am at the end of the period of the six month study, during then, I am greatly enjoyed.

The study presented here was a MSC study for UNESCO-IHE Institute for Water Education. The study is financially supported by World Bank JJ/WBGSP scholarship. I am quite grateful for this support, with which I can choose the interesting topic inspired by Prof. J.A. Roelvink and Dr. D.P. Solomatine.

I want to thank my supervisors, Prof. J.A. Roelvink and Dr. D.P.Solomatine for providing such a nice interdisciplinary surrounding among different departments and institutes. During the meetings with different people and personal direction in the office, so many interesting topics and amazing ideas were sparkling, some of which had been included in this study, while a lot of still need further study.

I want to thank Dr. Biswanath Bhattacharya for his daily advices, and pleasant ways of constructive criticism.

I want to thank the colleagues from WL | Delft Hydraulics, Dr. Thijs Van Kessel, Theo van der Kaaij, Dr. Johan Winterwerp, for prototype of the model I used in the study and beneficial helps during the models setup, especially for local refined model with domain decomposition.

Many thanks to Prof. Roland Price and Prof. Arthur Mynett, thank you for all kind of directions and advice given by you during the last 20 months.

Many thanks to Prof. M.B. Abbott, your interesting lectures, open minds, fascinating topics will be with me in the rest of life.

Many thanks to Dr. Z. Vojinovic, Dr. A.H. Lobbrecht, Dr. A. Jonoski and Dr. I. Popescu for your support and accompany in the best parts of the last years.

Many thanks to PhD researchers, Mr. Durga Lal Shrestha, Mr. Gerald Corzo Perez, Mrs. Li, Hong, Mr. Wilmer Barreto, Mr. S. J. van Andel for your valuable contributions and discussions during the study.

Many thanks to Mick van Der Wegen, and colleagues from ICT group for the help on the model software and computer facilities.

Many thanks to Dr. Z.B. Wang, Prof. M. Stive, Prof H. de Vriend, Prof. G.S. Stelling, Dr. Reniers, A.J.H.M for interesting discussions.

Many thanks to the PhD researcher of the Civil Engineering department, Mr. Li, Yu, Mr. Wang, Wen, Mr. Zhu, Yonghui for advice and kind criticisms.

Many thanks to Mr. J. Luijendijk, Jeltsje Kemerink, Edwin Hes, Klaas Schwartz and all members of the gorgeous IHE running team, with your accompaniment, I survived in the cold winter of Holland.

Many thanks to the colleagues of 2004-2006 Hydroinformatics group. We shared the

fun and pain all together in the past years, which turn to be a triumph so far for us all.

Many thanks to the colleagues of River and Harbour Engineering Department of NHRI, Prof. Yu, Guohua, Prof. Liu, Jiaju, Dr. Lu, Peidong. Thank you for guiding me to this fascinating Coastal Engineering field. Thanks to Prof. Liu, heng, Prof. Lu, Yongjun, Dr. Zhang, Jinshan, etc., thank you for your directions and enlightening helps during the last a few years.

At the end, I should thank my parents and my wife, Wan, Taoping for your consistent support and love.

Table of Contents

List of symbols

c: suspended sediment concentration

$\bar{c}$: the depth-averaged concentration

c_b: near bed concentration (often $\bar{c}$ is set equal to c_b)

c_{gel}: gelling concentration of suspended sediments concentration at which a network structrue exists

c_v : consolidation coefficient of the soil

$c_x, c_y, c_\sigma, c_\theta$: propagation velocities in x, y and σ , θ space (*m/s*)

$c_b^{(a)}$: average sediment concentration in the near bottom computational layer of sediment fraction (a)

$c_\mu{}'$: a constant determined by calibration

$d_{m,n}^{\zeta}$: water level value at a water level point

$H_{m.n}^{U}$: water depth at the velocity point

D: the diameter of the sediment (in mm)

D: dissipation due to wave breaking (W/m^2)

D_d: deposition rate

D_H, D_V: Horizontal and vertical diffusion coefficients (m^2/s)

$D^{(a)}$: Deposition flux of sediment fraction (a) ($kg/m^2/s$)

E (σ, θ): energy density spectrum

$E^{(a)}$: erosion flux of sediment fraction (a) ($kg/m^2/s$)

f_{cor}: the Coriolis coefficient

F_{wave}: the wave force

F_x, F_y: horizontal Reynold's stresses terms, which is determined by eddy viscosity concept. For large scale, where the shear stress along closed boundaries may be neglected, it can be expressed by (the gradient is considered along σ plane)

HCMS: high-Concentration Mud Suspension

H_b: breaking wave height

k: the turbulent kinetic energy

$\vec{k}$: wave number vector (*rad/m*)

LCMS: low-Concentration Mud Suspension

L: the mixing length

M: erosion rate parameter

$M^{(a)}$: user specified erosion parameter EROUNI of sediment fraction (a) ($kg/m^2/s$)

M_x, M_y: the contributions due to external sources or sinks of momentum (by hydraulic structures, discharge or withdrawal of water, wave stress, etc.)

$\vec{M}$: The forcing due to radiation stress gradients (N/m^2)

$N(\sigma, \theta)$: the action density spectrum

p_e : hydrostatic pore water stress

Pe: Peclet number, is a measure to determine whether a deformation process should be regarded as drained or undrained

p^w : total pore water pressure

P_x, P_y : horizontal pressure terms, which is given by Boussinesq approximations

Re: Reynolds number

Re_e : effective Reynolds number

Re_y : yields Reynolds number

$\mathrm{Re}_{e,c}$: critical effective Reynolds

Ri: Richardson Number, is to determine whether (sediment-induced) buoyancy effects (stratification) on the turbulent properties of the flow are important.

s: specific gravity of sediments

S: a source or sink term per unit area (discharge, withdrawal of water, evaporation, precipitation,etc.)

S_s : Salinity

$S_{\max}$: SALMAX, maximal salinity at which WSM is specified

$S(\tau_{cw}, \tau_{cr,e}^{(a)})$: erosion step function of sediment fraction (^{a}):

$$S(\tau_{cw}, \tau_{cr,e}^{(a)}) = (\frac{\tau_{cw}}{\tau_{cr,e}^{(a)}} - 1) \quad \text{when } \tau_{cw} > \tau_{cr,e}^{(a)}$$

$$= 0 \qquad \text{when } \tau_{cw} \le \tau_{cr,e}^{(a)}$$

$S(\tau_{cw}, \tau_{cr,d}^{(a)})$: deposition step function of sediment fraction (^{a}):

$$S(\tau_{cw}, \tau_{cr,d}^{(a)}) = (\frac{\tau_{cw}}{\tau_{cr,d}^{(a)}} - 1) \quad \text{when } \tau_{cw} \le \tau_{cr,d}^{(a)}$$

$$= 0 \qquad \text{when } \tau_{cw} > \tau_{cr,d}^{(a)}$$

T : wave period

T_p : peak period

T_{mean} : Mean period

TR : spring tide range

x, y, σ : horizontal coordinate and vertical coordinate

U, V : GLM velocity components(*m/s*)

$\bar{U}, \bar{V}$: Depth averaged generalized Lagrangian Mean (GLM) velocity components (*m/s*)

u, v, ω : Eulerian velocity components in Cartesian coordinates (*m/s*)

u_s, v_s : the Stokes' drift components

u_* : shear velocity.

U_m : the mean velocity in the fluid mud layer with thickness δ_m

V_d : the velocity of the deformation process

W_s : settling velocity

^{a} is a length scale of the deformation process

γ : constant breaker parameter

ζ : Water surface elevation above reference datum (*m*)

β : Rouse Number, which define the vertical suspended sediment concentration profile

ε : dissipation rate of turbulent kinetic energy

$\varepsilon_S^{(a)}$: vertical sediment mixing coefficient of sediment fraction (^{a})

ε_f : vertical fluid mixing coefficient calculated by the selected turbulence closure model

ϕ : the fitness factor of sediments ($\phi = -\log_2 D$)

ρ_s : sediment density

ρ : fluid density

σ : externally applied stress

σ_c : the Prandtl-schmidt number given by: $\sigma_c = \sigma_{c0} F_\sigma(Ri)$, where σ_{c0} is purely a function of the substance being transported.

σ_T : the turbulent Prandtl-Schmidt number

τ_y : yield strength

τ_{bottom} : the bed shear stress

τ_{wind} : the wind stress

τ_{bx} , τ_{by} : bed shear stress components that include the effects of wave–current interaction.

τ_{cw} : mean bed shear stress due to current and waves as calculated by the wave-current interaction model selected by the user of sediment fraction (^{a})

$\tau_{cr,e}^{(a)}$: user specified critical erosion shear stress TCEUNI of sediment fraction (^{a}) (N/m^2)

$\tau_{cr,d}^{(a)}$: user specified critical deposition shear stress TCDUNI of sediment fraction (^{a}) (N/m^2)

κ : Von Karman constant

δ_m : thickness of mud

τ_B : Bingham strength of fluid mud

ν_m : viscosity of fluid mud

ν_H, ν_V : Horizontal and vertical kinematic viscosity coefficients (m^2/s)

ρ_m : density of fluid mud

τ_b : turbulent mean bed shear stresses

τ_d : critical shear stress for deposition, typical value is 0.05-0.1 Pa.

τ_e : critical shear stress for erosion

w_a : angular wave frequency (*rad/s*)

w_s : sediments fall velocity

$w_{s,0}^{(a)}$: the (non-hindered) settling velocity of sediment fraction (^{a})

$w_{s,\max}^{(a)}$: *WSM*, settling velocity of sediment fraction (^{a}) at salinity concentration SALMAX

$w_{s,f}^{(a)}$: *WS0*, fresh water settling velocity of sediment fraction (^{a})

$w_s^{(a)}$: Fall velocity (hindered) of sediment fraction (^{a}) (*m/s*)

Part 1 Introduction

1.1 Background

Coastal zones and estuaries, encountered with continents and oceans, rivers and seas, are characteristically multiform, infinitely complex, quasi-fractal, always changing and unpredictable in many aspects (Dronkers, 2005). They are valuable and unique systems to human beings. Knowledge of the behaviours of the systems is important. Managing authorities are therefore under strong pressure to develop and implement plans for the sustainable development and management of these systems, and to compensate for infrastructural and other measures. The sediment transportation in the coastal zone and estuaries governed by physical dynamics, tide, wave, wind etc. and corresponding current, and their mutual interactions, are very complicated.

Problems like the sediment transportation, especially cohesive sediment transport due to wave breaking in the surf zone, wave and wave-induced current, always appear during the aspects of coastal management, port waterway maintenance, and land reclamation etc. To satisfy the planning and design specification in engineering and to avoid the occurrence of undesirable effects, understanding the coastal processes, and corresponding sediment processes, is essential.

To improve the understanding of the physical dynamics and sediment environments along the Dutch coast, a lot of research has been carried out. Numerous efforts have been put into the development of sophisticated numerical models, which may couple flow dynamics and wave effects, sediment transportation and corresponding morphological changes. Examples are the 1D SOBEK and the 2D/3D modelling system Delft3D of WL | Delft Hydraulics and the MIKE series modelling system of Danish Hydraulics Institute.

1.2 Present State of Knowledge

In the Dutch coastal zone, where the marine environment is characterized by shallow depths and is well mixed with highly energetic hydrodynamic conditions, people have realized that the cohesive sediments, or mud, play an important role in the formation of morphological patterns and siltation of ports and the access channels. For instance, the mud deposits and high concentrations of suspended particulate matter (SPM) occur frequently, especially in extreme wave conditions, which lead to a great concern of transportation authorities and coastal managers.

Thus quite a lot of work has been carried out so far. Still, there are several different definitions of cohesive sediment, or mud, exist. Mehta (2002), for instance, defines mud as a sediment-water mixture composed of grains which are predominately less than 63 micron in size, exhibiting a rheological behaviour that is poro-elastic or visio-elastic

when the matrix is particle-supported, and is highly viscous and non-Newtonian when it is in a fluid-like state. One of the difficulties is that the cohesive sediments vary so much in composition and may appear in so many formations. It is still not possible to provide a generally applicable rule and recipe to analyze and predict the behaviour, transportation, suspension, deposition and resuspension of mud in the natural environments (Winterwerp, 2004).

On the key processes in the cohesive sediment dynamics, such as settling and deposition, interaction between cohesive sediments and turbulent flow at high-concentrated sediments, consolidations, erosion and entrainment of fresh and consolidated deposits etc., some distinguished work has been carried out as well. For instance, Manning (2002) presents floc data sets collected during neap and spring tidal condition in the upper reaches of the Tamar estuary in the south-western England and concludes the flocculation was enhanced by spring tide with high carbonhydrate concentration and settling velocities of the macroflocs of 1.5mm in diameters can reach 16.6mm/s.

As to the cohesive sediments research along the Dutch coastal area, as early as the 1960's, De Groot analyzed the differences in the manganese content of the mud, the result of which has been verified by Terwindt (1967). Two kinds of mud, viz. river mud and marine mud had been defined in the Dutch coastal area in his study. He found that the mud found in the Haringvliet Mouth, the sea area between the Haringvliet and the Rotterdam Waterway and in the Waterway itself was almost exclusively river mud before the construction of DELTA works. Some of the mud in the mouth of the Haringvliet was carried seawards through the Brouwershavense Gat, some of it continued to circulate in the mouth and some of it was carried to sea, where it was transported northwards to the Waterway by the current in the North Sea running parallel to the coast and by the flood tide surplus close inshore (Terwindt, 1967). After the construction of the Haringvliet sluice in 1970, the river supplied only a very little amount of mud (Molen, 2000). Thus the mud supply of Haringvliet mouth is mainly from sea side nowadays.

The mud deposits and the high turbidity in the Belgian–Dutch coastal zone, southern part of the North Sea from the Dover strait to the Zeebrugge, were examined with integrated 2D hydrodynamic and sediment transport model. It was found that the processes responsible for the high turbidity zone formation were the currents and the influx of SPM through the Dover Strait. Mainly because of the decreasing magnitude of residual transport and the shallowness of the area, the SPM is concentrated in the Belgian–Dutch coastal waters and forms a turbidity maximum in front of Zeebrugge. Mud was found continuously deposited and re-suspended. Significant variations occur during tidal cycles and during neap-spring cycles. Also seasons and meteorological conditions have an influence on the mud behaviours. Because of the many processes involved, it remained still difficult to compare quantitatively model output to measurement data (Fettweis, 2003).

In 1999, the Netherlands government decided to study the possibilities and impact of a new airport on an artificial island in the Dutch coastal zone. In this extensive research programme called Flyland (http://www.wldelft.nl/cons/area/mse/edm/flyland), a large number of aspects related to a possible location are being investigated. One of them is focused on the transport and fate of dissolved and suspended matter, the sea bed composition, nutrient transport, underwater light climate and primary production in the southern North Sea in order to assess the effects of the construction and presence of the

island on the ecology in the Dutch coastal zone and in the Wadden Sea. Intensive model studies show that the suspended sediment concentrations in the southern North Sea are small in general, ranging from a few mg/l in the northern part to a few 10 mg/l further south. In the coastal zones larger concentrations are measured up to 50 to 100 mg/l under mild weather conditions, and up to 20 g/l near the bed under storm conditions. In-situ measurements as well as remote sensing images show a clear seasonal variation of the SPM levels throughout the year. The strong spatial and temporal variability in SPM is not yet properly understood, but is most likely to be affected by the variations in hydro-meteo forcing, meteo-induced variations in the supply of sediment. From the performed sensitivity simulations it is concluded that the model results are sensitive to the applied concentration in the English Channel (as northern boundary), the settling velocity, critical shear stresses and, to a lesser extent, to the sediment supply originating from the Belgian coast (Johan Boon, 2001).

For the port of Rotterdam, the access channel and harbour basin need to be maintained by frequent dredging, especially during and after the rough weather periods, when rapid siltation are observed and large amount of cohesive sediments (mud) are deposited in short time intervals. A 1DV POINT MODEL, which is a fully 3D sediment transport model omitting horizontal gradients, except for pressure gradient along the longitude direction, was applied and salinity-induced and sediment-induced stratification effects / hinder settling effects, wave-induced mixing is represented. The result is that the collapse of concentration profile is not a sufficient condition to form a high-concentrated near-bed suspension and it is hypothesized that the collapse of suspension triggers the generation of a sediment-driven density current causing the rapid siltation through the transport and accumulation of fluid mud into the channel and harbour basins (Winterwerp, 1998). Bhattacharya (2005) examined the sedimentation problem in the port of Rotterdam and built a data-driven model that predicts transport rates of cohesive sediments. This work implies that there could be some new strategies that can be used in the mud-related research.

In summary, a lot of research on the cohesive dynamics along the Dutch coast had been carried out and fruitful results had been achieved. Nevertheless, due to the complexity of the problem, the mechanism of cohesive sediment transportation, deposition and resuspension, especially due to wave effects, still need further studies and careful formulation. Research on this topic is necessary in order to gain insight into the temporal and spatial variability of morphological processes.

1.3 Objectives of the study

1.3.1 Main Objectives

The main objective of this study is to increase the understanding of the complex patterns of cohesive sediments transportation, deposition and resuspension due to wave effects with tide, wind, density-driven flow in the Dutch coastal area.

The study will focus on the case studies of areas adjacent to the approach channel of the

port of Rotterdam and Haringvliet mouth, which are characterized by complex interactions between hydrodynamics and sedimentation (See Fig 1.1).

This study will try to reproduce the hydrodynamics and cohesive sediment processes in the Haringvliet Mouth and to delineate the cohesive sediment transportation, deposition and resuspension pattern mainly due to wave effects in meso-temporal and spatial scale.

1.3.2 Specific Objectives

1. The study will extend the existing ZUNO model with wave module and get the pattern of sediment movement under wave dynamics in macro space scale.

2. The study will utilize domain decomposition technology to generate detailed grid to cover the studied area with simultaneous simulation (which is termed as ONLINE simulation in Delft 3D's terminology, refer to Part 1.5.1) of flow, wave, sediments, morphological change models.

3. Due to the models complexity, a schematized model will be built and its efficiency, effectiveness and abilities to reproduce the cohesive sediments transportation, deposition and resuspension pattern mainly due to the wave effect will be tested.

4. The computational architecture allowing for the distributed simulation solution will be tested.

Fig 1.1 Location of study area—Haringvliet estuary (after Google Earth)

1.4 Methodology

1.4.1 Philosophy of research methodology

As de Vriend (1991) enlightened on the scales theory, the influence of bigger scaled processes act as boundary conditions for the smaller scaled processes, where influences from smaller scaled processes are considered 'noise' to the bigger scales. Processes on the same scale can have dynamic interactions. And similar to Odum (1996), he also argued that the increasingly detailed process knowledge and modelling capabilities on the small scale will not inevitably lead to correct the prediction of processes on a larger scale, due to emerging non-linearity, unpredictable events and omission of processes that were not relevant at the smaller scale.

This scale-based philosophy is followed in this thesis: bigger scale model provides the boundary conditions for the smaller scale model, while smaller scale model provides detailed process description for larger scale model.

A hydrodynamic model in mega scale covering the entire continental Shelf, up to the 2000m depth contour, provides boundary to the ZUNO coarse grid model. And the ZUNO coarse grid model, which covers bigger area with longer temporal scale processes (refer to Part 3), describes the dynamics in the macro scale and provides boundary conditions for smaller scaled refined grid model (refer to Part 4) and schematized model (refer to Part 5), while the schematized model, which is in meso-spatial and meso-temporal scale, provides a more detailed demonstration in physical processes (Fig 1.2).

In this study, the objective to understand the complex interaction between the flow dynamics, wave, wind and cohesive sediments, and cohesive sediment transportation, deposition and resuspension, mainly caused by waves in the Haringvliet Mouth, and adjacent coastal line of central and western part is classified as a meso-scaled problem with spatial scale of 10-100 km and temporal scale of months.

1.4.2 Research methodology

To meet the objectives of the study, the following methodology is adopted:

Literature review

The literature review aims at understanding the cohesive sediments characteristics, the processes of the overall coastal system and underlying theories on topics, such as, the flow model, the wave model, the cohesive sediment transportation model implemented in Delft3D systems.

Physical based process modelling

The model system simulation needs specified setup and proper boundary conditions. Different model systems have been setup and were utilized for various cases.

Experiments

With the same parameter sets, different scenarios have been tested and the results have been analyzed to find the mechanisms underneath.

Tools involved in this study are outlined as follows:

Delft3D distributed by WL | Delft Hydraulics

Matlab® distributed by Mathworks, Inc.

RCMI (Remote control manager interface) developed by Ye,Qinghua

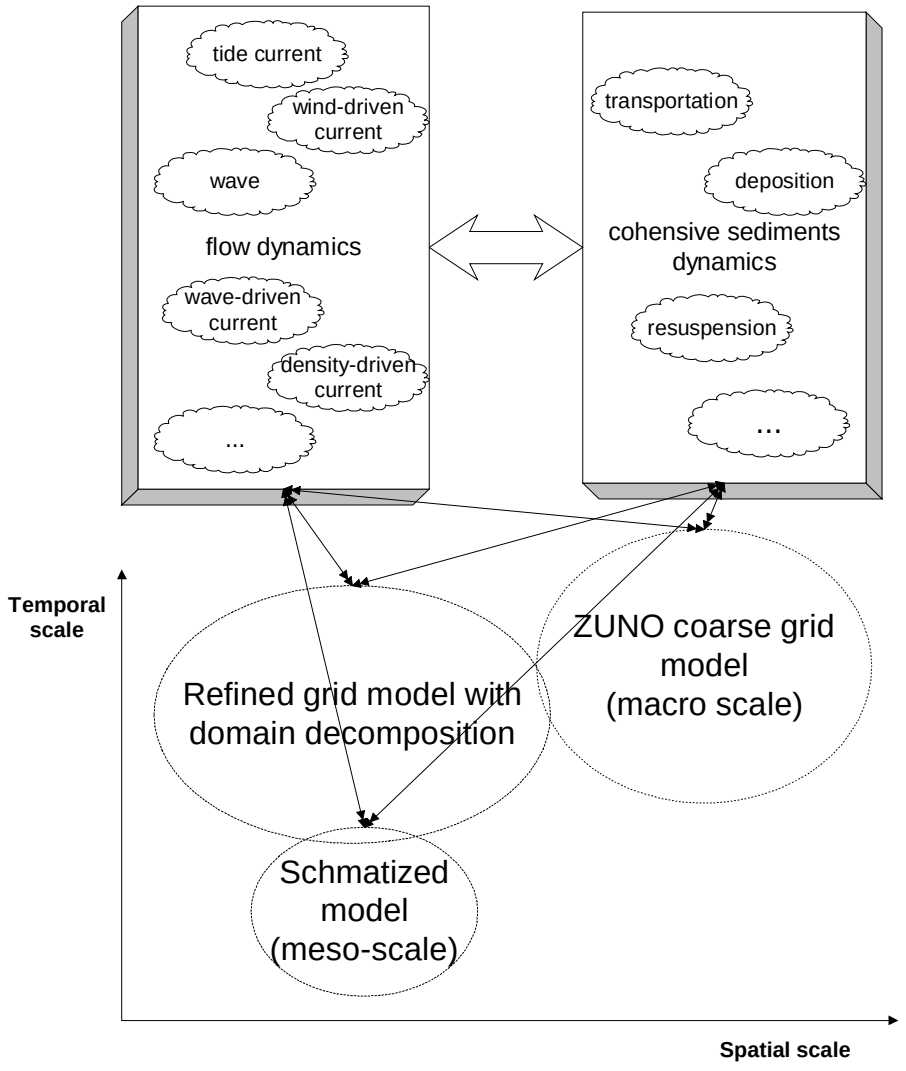

Fig 1.2 The schematization of the research methodology is based on scale linkage

1.5 Definitions used in this study

The basic methodology is to use physically based process models with some specializations, which are listed in the following as a limitation of this study.

ZUNO coarse grid model

This study starts from a coarse grid which covers the area from the south Dover Strait to the north of Scotland and most northern points of Denmark with about 9,000 elements. The grid is originally provided by the Dutch Ministry of Public Works and then to WL| Delft Hydraulics. The model setup based on the ZUNO grid, which is named ZUNO model in this thesis, is helpful in the beginning to simulate the overall tidal flow and wave pattern in macro scale.

Refined grid model with domain decomposition

Domain decomposition is a technique in which a model domain is subdivided into several smaller model domains, which are called *sub-domains*. The subdivision is based on the horizontal and vertical model resolution required for adequately simulating physical processes. Then, the computations can be carried out separately on these sub-domains. The communication between the sub-domains takes place along internal open boundaries, or so called *dd-boundaries*. If these computations are carried out concurrently, which is termed as parallel computing, it reduces the turn around time of multiple domain simulations (WL|Delft Hydraulics, 2005).

Due to the characteristics of cohesive sediments transportation, the ZUNO coarse grid is too rough to simulate the movement of cohesive sediments, while using a global finer grid is also not so suitable for such a big area. Thus, a locally finer grid with global coarser grids is combined and used as the computational grid inside the Delft3D flow/wave/sediment/morphology model, which is called as a domain decomposition model. The benefit of decomposition model is that not only the flow pattern in the wider area with coarser grid is taken into consideration, but also the minor, small scaled dynamics can be involved with the computation. Domain decomposition is widely recognized as an efficient and flexible tool for the simulation of complex physical processes, especially when coupling of different models, or coupling of models of different dimension, or coupling of models with different, independently generated sub-grids happens. It is supposed to be one of the most economic with high efficiency approaches of computation in the future, on the one hand, because the interested area in specific research is always not so big while the wider flow patterns are always needed to make similar with the real condition, on the other hands, it can be helpful to reduce memory demands by decomposition into smaller sub-domains, parallel execution of sub-domains, better software engineering and maintenance due to modular approach.

In this study, four sub-domains have been divided and computed (refer to Part 4).

Schematized model

With this objective, there is a paradox in the practical study. That is, the physical based process models which are supposed to simulate all the processes are extremely time-consuming, particularly with a large research area. It may happen sometimes that the computing time is one week for a simulation time of one week.

In the study, a numerical model with the schematized boundary conditions is used into simulation. The boundary here includes wave, tide wave, wind and discharge of rivers. Due to the main purpose of this study, the linear sinusoidal tidal wave is used in the model, where the periodic vibrations were smoothed and dominated dynamics characters were left. The open boundary uses a model determine the correct solution at the boundary by imposing the alongshore water level gradient (a so-called Neumann boundary condition) (refer to Part 5.2.1.3.1). Measured wave condition at Europlatform, which located around 60km offshore of Georee, and discharge data from Niuewe Waterweg and Haringvliet Sluice are used as wave and discharge boundaries.

For the schematized method, the computation time drops dramatically. However, the schematized model needs a deliberate setting of boundary, which is highlighted in this study, thus its usefulness depends fully on the expertise understanding of the physical dynamics in the research area.

Model with nested grid / Nested model

Grid nesting is a relatively older technology in computational hydraulics. In case the boundary conditions of a model are generated by a larger (overall) model we speak of a nested model. Nesting in Delft3D-FLOW is executed in three steps, using two separate utilities and the Delft3D-FLOW program, which can be referred to the manual of Delft-3D flow module.

In this study, the wave module of the schematized model used the larger grid as a boundary provider for a finer grid to cover the interested area.

Coupled model / Online simulation

In the latest version used in this study, the flow / wave / sediment / morphology model is simulated in a coupled way, which is also termed as online simulation.

Delft3D modelling system

Delft3D modelling system is the unique, fully integrated modelling framework for a multi-disciplinary approach and 3D computations for coastal zone, river, lake and estuarine areas provided by WL | Delft Hydraulics. The Delft3D framework is composed of several modules, including Delft3DFLOW for 2D/3D hydrodynamics, salinity, temperature, transport and online sediment transport and morphology, WAVE (SWAN) for short wave propagation, SED for cohesive and no-cohesive sediment transport, and MOR for morphodynamic simulations, etc.

1.6 Outline of the thesis

The basic structure is comprised of the following (Fig 1.3):

Part 1 gives some background knowledge about the system along with the objectives and methodology used in the study.

Part 2 is dedicated to the principles of numerical modelling after a generic introduction of the properties of cohesive sediments and cohesive sediment dynamics.

Part 3 describes the calibration and verification of models, which includes the verification of ZUNO coarse grid model for the wide range flow dynamics, the calibration and verification of domain decomposition model, the calibration and verification of schematized flow/wave/sediments/morphological coupled online simulation model.

Part 4 deals with the refined grid model with domain decomposition technology.

Part 5 is devoted to the schematized model and experiments design with result analysis. It shows the detailed simulation results and analysis with a real case study.

Part 6 carries out the conclusions based on the present studies.

Part 7 lists several recommendations for further work.

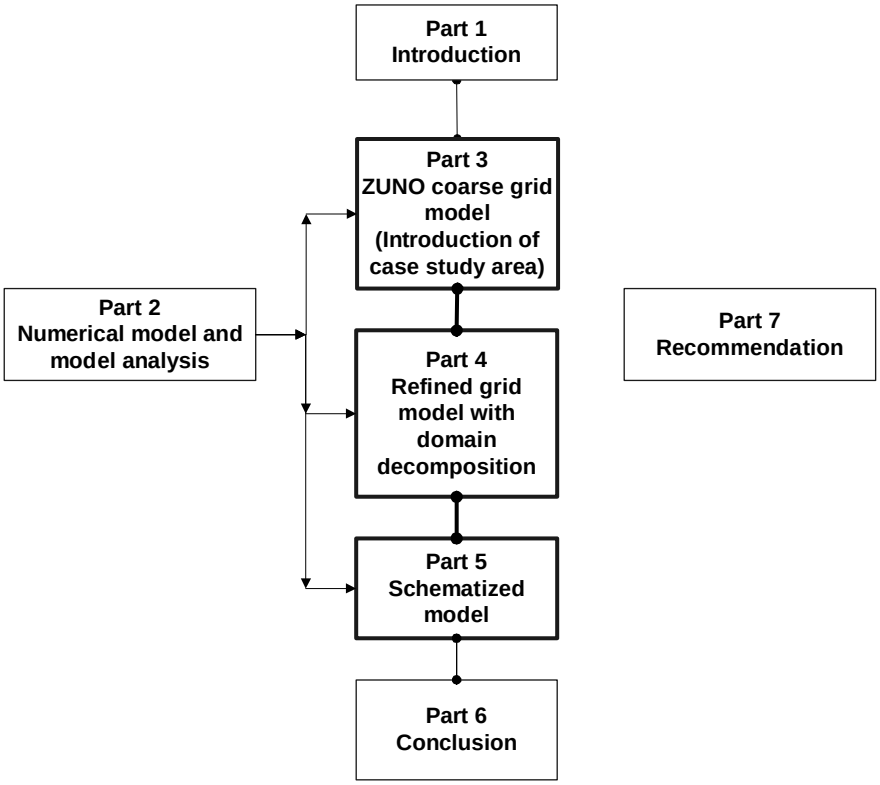

Fig 1.3 Outline of this thesis

Part 2 Numerical model and model analysis

Physically-based process models have three basic approaches: scaled model, numerical model, and in situ monitoring and measurements, of which the numerical model is the main approach in this study. Due to the complicated characteristic of cohesive sediment dynamics in the coastal zone, hydrodynamics models, cohesive sediment transport models, etc. are involved.

In the following parts, the basic concepts of flow, wave and sediment (mud) models are introduced and the implementations in Delft3D are described.

2.1 Basic concepts of cohesive sediments

2.1.1 Cohesive sediment (mud) properties

The term sediment, originated from disintegration or decomposition of rock, is defined as granular material that can settle in water by gravity. The size distribution and components are of main importance for the mechanical behaviour. The cohesive sediment, or mud, as encountered in the marine environment, consists of a mixture of clay, silt, fine sands, organic matter, water and sometimes gas. Thus its behaviour varies in space and time and is governed by the availability of the sediment and its compositions, the meteo-hydrodynamic condition, and biological activities (Winterwerp, 2004).

Usually the sediments are referred to as gravel, sand, silt and clay. These terms refer to the size of the sediment particle. In this thesis the grain size scale of the American Geophysical Union is used (Table 2.1).

In sedimentology, the particle diameter is often given in terms of the fitness factor ϕ, defined as:

$$\phi = -\log_2 D \tag{2.1}$$

where D is the diameter of the sediment (in mm) (Krumbein, 1941).

The density of most sediment particles ($<4mm$) varies between narrow limits. Since quartz is the predominant natural sediment the average density can be assumed to be (Tchouani, 2004):

$$\rho_s = 2650 kg/m^3 \tag{2.2}$$

Table 2.1 Grain size model of American Geophysical Union (Van Rijn, 1993)

Class Name	Millimeters	micrometers	Phi Values
Boulders	>256		<-8
Cobbles	256-64		-8 to -6
Gravel	64-2		-6 to -1
Very coarse sand	2.0-1.0	2000-1000	-1 to 0
Coarse sand	1.0-0.5	1000-500	0 to +1
Medium sand	0.5-0.25	500-250	+1 to +2
Fine sand	0.25-0.125	250-125	+2 to +3
Very fine sand	0.125-0.062	125-62	+3 to +4
Coarse silt	0.062-0.031	62-31	+4 to +5
Medium silt	0.031-0.016	31-16	+5 to +6
Fine silt	0.016-0.008	16-8	+6 to +7
Very fine silt	0.008-0.004	8-4	+7 to +8
Coarse clay	0.004-0.002	4-2	+8 to +9
Medium clay	0.002-0.001	2-1	+9 to +10
Fine clay	0.001-0.005	1-0.5	+10 to +11
Very fine clay	0.0005-0.00024	0.5-0.25	+11 to +12
Colloids	<0.00024	<0.24	>+12

The specific gravity s is defined as the ratio of the sediment density ρ_s and the density of water ρ :

$$s = \rho_s / \rho = 2.65 \tag{2.3}$$

The sediment, which is smaller than 62 micron, is regarded as the main ingredient of cohesive sediment. Due to the complicated characteristics of cohesive sediment, the particles bigger than 4 micron and smaller than 62 micron, which is termed as silt, is focused in this study.

The classification will help us to understand and quantify the behaviours and properties of cohesive sediments in microscopic scales. However, as we know, the behaviour and appearance of cohesive sediments on a large scale is not only dependent on the physical and chemical properties, but also on a number of environmental parameters, which should be kept in mind.

A variety of terminology is used to classify the mode of appearance of cohesive sediments under different hydrodynamic-environmental conditions (See Table 2.1.2).

Table 2.1.2 Classification of cohesive sediment modes in the marine environment (Winterwerp, 2004)

	Concentr.	Flow Characteristics		Governing scale numbers					
LCMS	$c << c_{gel}$	Turbulent	Newtonian	Re	β				
HCMS	$c < c_{gel}$	Turbulent	Newtonian	Re		Ri			
Turbidity current	$c \approx c_{gel}$	Turbulent	Non-Newt.	Re_e		Ri			
Mobile fluid mud	$c \approx c_{gel}$	Trans./lam.	Non-Newt.	Re_e		Ri		Pe	
Stationary fluid mud	$c \approx c_{gel}$	Trans./Creep	Non-Newt.				p^w/p_e	Pe	
Consolidating bed	$c > c_{gel}$	Creep	Non-Newt.				p^w/p_e	Pe	σ/τ_y
Consolidated bed	$c >> c_{gel}$	Stationary	Non-Newt.						σ/τ_y

where:

LCMS: low-Concentration Mud Suspension
HCMS: high-Concentration Mud Suspension
c: suspended sediment concentration
c_{gel}: gelling concentration
Re: Reynolds number
Re_e: effective Reynolds number
β: Rouse Number
Ri: Richardson Number
p^w: total pore water pressure
p_e: hydrostatic pore water stress
Pe: Peclet number
σ: externally applied stress
τ_y: yield strength

Hereby the c_{gel} is defined as a concentration at which a network structrue exists, i.e. when flocs are in direct contact with each other and yield strength is developing. The Rouse number β determines the vertical suspended sediment concentration profile, such as:

$$\beta = \sigma_T W_S / \kappa u_* \tag{2.4}$$

where:
σ_T: the turbulent Prandtl-Schmidt number
W_S: settling velocity
κ: Von Karman constant

u_* : shear velocity.

The Reynolds number Re defines whether the flow is laminar or turbulent. For non-Newtonian, Bingham plastic flow, the effective Reynolds number Re_e is defined as:

$$\frac{1}{\mathrm{Re}_e} = \frac{1}{\mathrm{Re}} + \frac{1}{\mathrm{Re}_y}, \text{ where } \mathrm{Re} = \frac{4U_m\delta_m}{\nu_m} \text{ and } \mathrm{Re}_y = \frac{8\rho_m U_m^2}{\tau_B} \quad (2.5)$$

U_m is the mean velocity in the fluid mud layer with thickness δ_m, τ_B is the Bingham strength of fluid mud, and ν_m and ρ_m are the viscosity and density of fluid mud. The critical effective Reynolds amounts to about $\mathrm{Re}_{e,c}$= 2-3*10^3 according to Liu and Mei (1989) and Van Kessel (1997).

The Richardson number is to determine whether (sediment-induced) buoyancy effects (stratification) on the turbulent properties of the flow are important.

The difference between the total pore water stress p^w and the hydrostatic pore water stress p_e is called the water over-pressure or excess pore water pressure. It is non-zero in a consolidating bed.

The Peclet number *Pe* is a measure to determine whether a deformation process should be regarded as drained or undrained, and is defined as:

$$Pe = V_d{}^{\mathrm{a}} / c_v \quad (2.6)$$

where V_d is the velocity of the deformation process, $^{\mathrm{a}}$ is a length scale of the deformation process, and ^{c_v} is the consolidation coefficient of the soil.

The ratio of the externally applied stresses σ and the yield strength $^{\tau_y}$ determines whether the soil may flow under the influence of the stress. Some examples are listed as followings:

- LCMS can be found in majority of natural systems, viz., rivers, large parts of estuaries and coastal areas, etc. when the concentrations are too low to affect the flow field.
- HCMS is for instance found in estuaries, in particular near their turbidity maxima, and above mud banks in coastal waters, when the turbulent flow field is largely affected by the suspended sediment.
- Turbidity currents may be found on the slopes of the deep sea, such as the slope of continental shelves.
- Fluid mud is found in many navigation channels and harbour basins.

§ Consolidating and consolidated beds are found everywhere where cohesive sediments are found (Winterwerp, 2004).

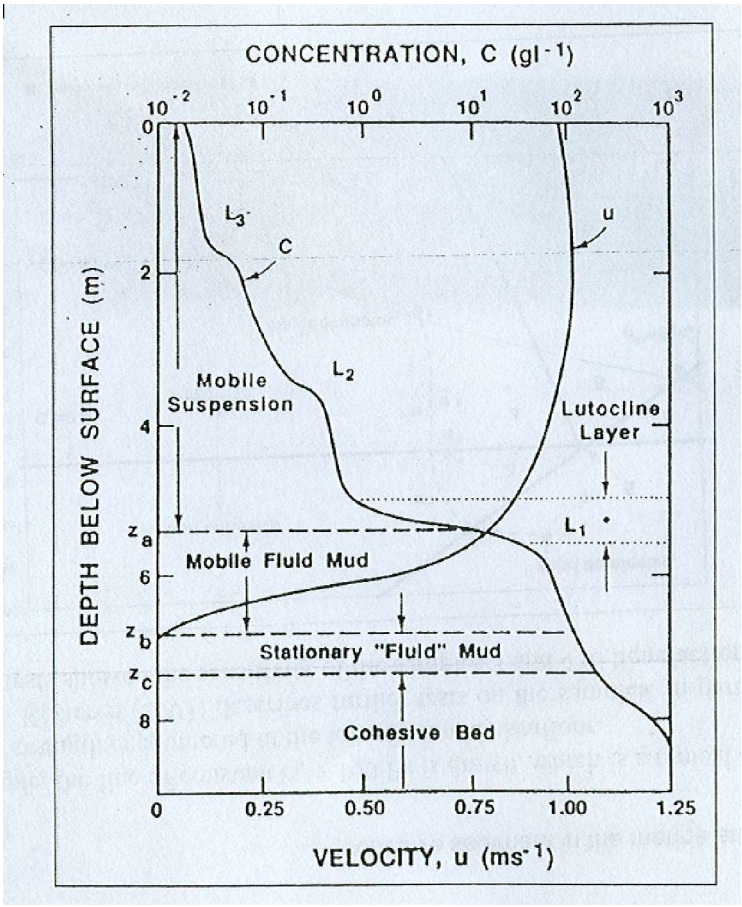

Fig 2.1 Typical vertical profiles of suspended sediment concentration and velocity of high concentration conditions (Ross, 1989)

The vertical concentration profile, such as demonstrated in Fig 2.1, is determined by a number of processes, some of them are significant and will be described more detailed in the following:

§ Flocculation: because of the cohesive, sticky nature of mud, flocs are formed, whose effect of settling velocity and bed structure can not be neglected.

§ Settling and mixing: mud particles fall through the water column due to gravity, opposed by mixing processes generated by the turbulent water movement.

§ Deposition: settling mud particles may become parts of the bed.

§ Resuspension: During the accelerating of flow and shear stress, particles deposited on the bed may be re-entrained into the water column by the turbulent flow.

- Entrainment: Turbulent flow over or underneath the less turbulent fluid entrains water and matter from this less turbulent layer.

- Erosion: the bed is eroded by turbulent flow or waves.

The processes may act simultaneously or successively. Often, however, only some of these play a role, depending on the prevailing conditions. In the following parts, some brief descriptions are reviewed.

2.1.2 Cohesive sediments (mud) settling and sedimentation

The most characteristic property of cohesive sediments is that it can form flocs when the sediment is brought in contact with a fluid, like water. And the reversible flocculation process is governed by three factors: Brownian motion cause the particles to collide, resulting in the formation of aggregates, particles with a larger settling velocity will overtake those with a smaller settling velocity, and turbulent motion will cause particles carried by turbulent eddies to collide and form flocs. The uniquely defined settling velocity for the cohesive sediments does not exist. However, it is often possible to define a characteristic settling velocity to describe the transport and fate of a cohesive sediment suspension, which should be a function of the scale of the problems to be addressed (near field, far field, seasonal variation, etc.)

Winterwerp (2004) circumvented the difficulties and defined three types of settling velocity with cohesive sediments: characteristic settling velocity, settling velocity of a single mud floc in still water, and effective settling velocity of a particle in a suspension of cohesive sediment. He also presented some formulas the settling velocity and floc size in still water, hindered settling and subsequently, the deposition and sedimentation.

In Delft3D system, not all the influence of flocs to the cohesive sediment is included so far. For instance, turbulence induced flocculation or the break-up of sediment flocs is not yet implemented (refer to Part 2.1.3 and Part 2.4).

The settling velocity of cohesive sediment flocs does not directly yield the deposition rate from the suspension, which is required as a bed boundary condition to the mass balance equation (Part 2.1.5). The deposition rate is the focus of quantifying cohesive sediment dynamics in the marine environment. After experiments data, Krone (1984) carried out his worldwide used deposition formula:

$$\frac{dh\bar{c}}{dt} = -D_d = -W_s c_b (1 - \frac{\tau_b}{\tau_d}) \tag{2.7}$$

where:

D_d : deposition rate

$\bar{c}$: the depth-averaged concentration

c_b : near bed concentration (often $\bar{c}$ is set equal to c_b)

τ_b : turbulent mean bed shear stresses

τ_d : critical shear stress for deposition, typical value is 0.05-0.1 Pa.

In this study, it is assumed that the erosion and deposition can occur simultaneously (Winterwerp, 2004). The deposition rate *D* is given by the sediment flux at the bed:

$$D = W_{s,b} c_b \tag{2.7a}$$

where c_b and $W_{s,b}$ are the suspended sediment concentration and settling velocity of the sediment at the bed, accounting for vertical concentration gradients on c_b and possible flocculation effects on $W_{s,b}$. The equation 2.7a is equivalent to the equation 2.7 by setting the τ_d as a large number.

2.1.3 Cohesive sediments (mud) erosion and resuspension

The transportation and fate of cohesive sediment in the marine environment is governed to a large extent by water-bed exchange processes, i.e. erosion, deposition and resuspension.

In this study, the bottom layer thickness of cohesive sediments is set as 0mm initially, which is due to the objective of the study focused on the mud transported from the south boundary, but not from the old, well-consolidated deposits.

It is not so difficult to understand that the erosion rates of such deposits as a function of the local hydrodynamics conditions (flow, wave, density-driven flow etc.) may vary by orders of magnitude. Often only thin layers of a few mm to a few cm of the bed are eroded in one tidal cycle. Yet, when mixed over the water column, the eroded sediments may increase the local suspended sediment concentration by tens to hundreds mg/l.

The basic formula of erosion is carried out by Partheniades (Partheniades, 1965) and parameterized by Ariathurai (Ariathurai, 1974) as:

$$E = M\left(\frac{\tau_b - \tau_e}{\tau_e}\right) \tag{2.8}$$

where:
M: erosion rate parameter
τ_b : turbulent mean bed shear stresses
τ_e : critical shear stress for erosion

The formula is combined with Krone's deposition formula (2.7) to compute the water-bed exchange rate in a numerical model for the transport of cohesive sediments. This description of water-bed exchange processes is known as the Krone-Partheniades bed-boundary condition (refer to Part 2.4).

2.2 Flow model

The hydrodynamic module Delft3D-FLOW simulates two-dimensional (2D, depth-averaged) or three-dimensional (3D) unsteady flow and transport phenomena resulting from tidal and/or meteorological forcing, including the effect of density differences due to a non-uniform temperature and salinity distribution (density-driven flow). The flow model can be used to predict the flow in shallow seas, coastal areas, estuaries, lagoons, rivers and lakes. It aims to model flow phenomena of which the horizontal length and time scales are significantly larger than the vertical scales.

If the fluid is vertically homogeneous, a depth-averaged approach is appropriate. Delft3D FLOW is able to run in two-dimensional mode (one computational layer), which corresponds to solve the depth-averaged equations. Examples in which the two-dimensional, depth-averaged flow equations can be applied are tidal waves, storm surges, tsunamis, harbour oscillations (seiches) and transport of pollutants in vertically well-mixed flow regimes.

Three-dimensional modelling is of particular interest in transport problems where the horizontal flow field shows significant variation in the vertical direction. This variation may be generated by wind forcing, bed stress, Coriolis force, and bed topography or density differences. Examples are dispersion of waste or cooling water in lakes and coastal areas, upwelling and downwelling of nutrients, salt intrusion in estuaries, fresh water river discharges in bays and thermal stratification in lakes and seas (WL|Delft Hydraulics, 2005).

2.2.1 Basic equations

The basic equations are presented as the following parts (Lesser, 2004).

2.2.1.1 Vertical σ - coordinate system

The vertical σ coordinate is scaled as ($-1 \le \sigma \le 0$):

$$\sigma = \frac{z - \zeta}{h} \tag{2.9}$$

The flow domain of a 3D shallow water model consists of a number of layers. In a σ - coordinate system, the layer interfaces are chosen following planes of constant σ. Thus, the number of layers is constant over the horizontal computational area (Fig. 2.2). For each layer, a set of coupled conservation equations is solved. The partial derivatives in the original Cartesian coordinate system are expressed in r-coordinates by use of the chain rule. This introduces additional terms (Stelling, 1994).

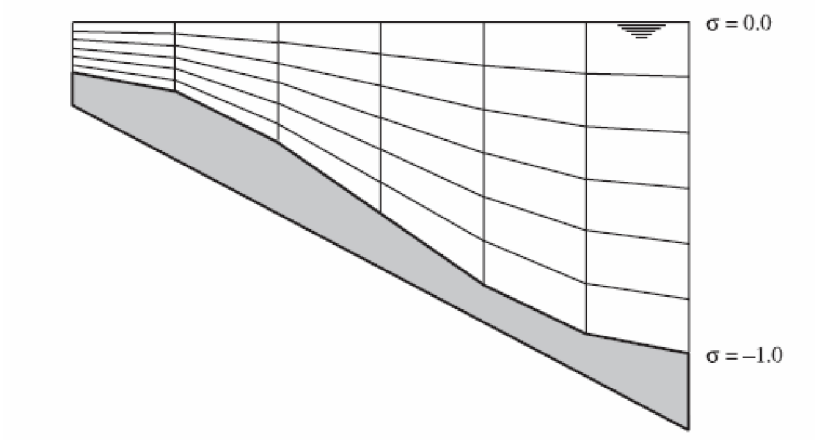

Fig 2.2 An example of a vertical grid consisting of six equal thickness σ -layers

2.2.1.2 Generalized Lagrangian Mean (GLM) reference frame

In simulations including waves, the hydrodynamic equations are written and solved in a GLM reference frame (Andrews, 1978; Groeneweg, 1999; Groeneweg, 1998). In GLM formulation, the 2DH and 3D flow equations are very similar to the standard Eulerian equations; however, the wave-induced driving forces averaged over the wave period are more accurately expressed. The relationship between the GLM velocity and the Eulerian velocity is given by

$$U = u + u_s \tag{2.10}$$

$$V = v + v_s \tag{2.11}$$

where U and V are GLM velocity components, u and v are Eulerian velocity components, and u_s and v_s are the Stokes' drift components. For details and verification results, we refer to Walstra et al (2000).

2.2.1.3 Hydrostatic pressure assumption

Under the so-called "shallow water assumption", the vertical momentum equation reduces to the hydrostatic pressure equation. Under this assumption, vertical acceleration due to buoyancy effects or sudden variations in the bottom topography is not taken into account. The resulting expression is

$$\frac{\partial P}{\partial \sigma} = -\rho g h \tag{2.12}$$

2.2.1.4 Horizontal momentum equations

The horizontal momentum equations are:

$$\frac{\partial U}{\partial t}+U\frac{\partial U}{\partial x}+V\frac{\partial U}{\partial y}+\frac{\omega}{h}\frac{\partial U}{\partial \sigma}-fV=-\frac{1}{\rho_0}P_x+F_x+M_x+\frac{1}{h^2}\frac{\partial}{\partial \sigma}(\nu_V\frac{\partial u}{\partial \sigma}) \quad (2.13)$$

$$\frac{\partial V}{\partial t}+U\frac{\partial V}{\partial x}+V\frac{\partial V}{\partial y}+\frac{\omega}{h}\frac{\partial V}{\partial \sigma}-fU=-\frac{1}{\rho_0}P_y+F_y+M_y+\frac{1}{h^2}\frac{\partial}{\partial \sigma}(\nu_V\frac{\partial v}{\partial \sigma}) \quad (2.14)$$

where:

U,V: Generalized Lagrangian Mean (GLM) velocity components (m/s)
u,v,ω: Eulerian velocity components in Cartesian coordinates (m/s)
x,y,σ : horizontal coordinate and vertical coordinate
P_x,P_y: horizontal pressure terms, which is given by (Boussinesq approximations):

$$\frac{P_x}{\rho_0}=g\frac{\partial \zeta}{\partial x}+g\frac{h}{\rho_0}\int_\sigma^0(\frac{\partial \rho}{\partial x}+\frac{\partial \sigma^\circ}{\partial x}\frac{\partial \rho}{\partial \sigma^\circ})d\sigma^\circ \quad (2.15)$$

$$\frac{P_y}{\rho_0}=g\frac{\partial \zeta}{\partial y}+g\frac{h}{\rho_0}\int_\sigma^0(\frac{\partial \rho}{\partial y}+\frac{\partial \sigma^\circ}{\partial y}\frac{\partial \rho}{\partial \sigma^\circ})d\sigma^\circ \quad (2.16)$$

F_x,F_y: horizontal Reynold's stresses terms, which is determined by eddy viscosity concept. For large scale, where the shear stress along closed boundaries may be neglected, it can be expressed by (the gradient is considered along σ plane):

$$F_x=\nu_H(\frac{\partial^2 U}{\partial x^2}+\frac{\partial^2 U}{\partial y^2}) \quad (2.17)$$

$$F_y=\nu_H(\frac{\partial^2 V}{\partial x^2}+\frac{\partial^2 V}{\partial y^2}) \quad (2.18)$$

M_x,M_y: the contributions due to external sources or sinks of momentum (by hydraulic structures, discharge or withdrawal of water, wave stress, etc.)
ν_H,ν_V: Horizontal and vertical kinematic viscosity coefficients (m2/s)

2.2.1.5 Continuity equation

The depth averaged continuity equation is given by:

$$\frac{\partial \zeta}{\partial t}+\frac{\partial(h\bar{U})}{\partial x}+\frac{\partial(h\bar{V})}{\partial y}=S \quad (2.19)$$

where:

$\bar{U},\bar{V}$: Depth averaged generalized Lagrangian Mean (GLM) velocity components (m/s)
ζ : Water surface elevation above reference datum (m)

S: a source or sink term per unit area (discharge, withdrawal of water, evaporation, precipitation,etc.)

2.2.1.6 Transport equation

The advection-diffusion equation reads:

$$\frac{\partial(hc)}{\partial t}+\frac{\partial(hUc)}{\partial x}+\frac{\partial(hVc)}{\partial y}+\frac{\partial(wc)}{\partial \sigma}=h[\frac{\partial}{\partial x}(D_H\frac{\partial c}{\partial x})+\frac{\partial}{\partial y}(D_H\frac{\partial c}{\partial y})]+\frac{1}{h}\frac{\partial}{\partial \sigma}(D_V\frac{\partial c}{\partial \sigma})+hS \tag{2.20}$$

where:

D_H, D_V : Horizontal and vertical diffusion coefficients (m^2/s)
w: vertical velocity of sediment particles in the σ - coordinate system

To solve the equations listed above, the horizontal and vertical viscosity (ν_H, ν_V) and diffusivity (D_H, D_V) need to be prescribed.

In Delft3D, the horizontal viscosity and diffusivity are assumed to be a superposition of three parts:

- Molecular viscosity, to fluid (water), it is a constant of $10^{-4} \sim 10^{-6}$
- 3D turbulence, in 3D simulation, it is computed by a selected turbulence closure model, which will be described later.
- 2D turbulence, is a measure of the horizontal mixing that is not resolved by advection on the horizontal computational grid. It is computed either by users as a constant or by a subgrid model for Horizontal Large Eddy Simulation (HLES).

The vertical eddy diffusivity is scaled from the vertical eddy viscosity:

$$D_V=\frac{\nu V}{\sigma_c} \tag{2.21}$$

where

V: Generalized Lagrangian Mean (GLM) velocity components (m/s)
σ_c: the Prandtl-schmidt number given by: $\sigma_c=\sigma_{c0}F_\sigma(Ri)$, where σ_{c0} is purely a function of the substance being transported. If algebraic turbulence model is used, $F_\sigma(Ri)$ is a damping function that depends on the amount of density stratification present by the gradient Richardson number. If the $k-\varepsilon$ turbulence model is used, $F_\sigma(Ri)$ is set to 1.0. And vertical effect is treated as the buoyancy term in the model automatically accounts for turbulence damping effect caused by the vertical density gradients.

2.2.2 Boundary conditions

To solve the systems of equations, the following boundary conditions are required.

2.2.2.1 Bed and free surface boundary conditions

In the σ -coordinate system, the bed and the free surface correspond with σ -planes.

Therefore, the vertical velocities at these boundaries are simply
$w(-1) = 0$ and $w(0) = 0$

Friction is applied at the bed as follows:

$$\frac{\nu_V}{h}\frac{\partial u}{\partial \sigma}\Big|_{\sigma=-1} = \frac{\tau_{bx}}{\rho} \text{ and } \frac{\nu_V}{h}\frac{\partial v}{\partial \sigma}\Big|_{\sigma=-1} = \frac{\tau_{by}}{\rho} \qquad (2.22)$$

where:

τ_{bx} , τ_{by} : bed shear stress components that include the effects of wave–current interaction.

2.2.2.2 Lateral boundary conditions

Along closed boundaries, the velocity component perpendicular to the closed boundary is set to zero (a free-slip condition). At open boundaries, one of the following types of boundary conditions must be specified: water level, velocity (in the direction normal to the boundary), discharge, or linearised Neumann invariant, which is a new type of boundary condition by setting water level gradient applied at lateral boundaries in this study (Roelvink, 2005b). Additionally, in the case of 3D models, the user must prescribe the use of either a uniform or logarithmic velocity profile at inflow boundaries. For the transport boundary conditions, it is assumed that the horizontal transport of dissolved substances is dominated by advection. This means that at an open inflow boundary, a boundary condition is needed. During outflow, the concentration must be free. DELFT3D-FLOW allows the user to prescribe the concentration at every σ -layer using a time series. For sand / mud sediment fractions, the local equilibrium sediment concentration profile may be used.

2.2.3 Solution Procedure

DELFT3D-FLOW is a numerical model based on finite differences. To discretize the 3D shallow water equations in space, the model area is covered by a rectangular, curvilinear, or spherical grid. It is assumed that the grid is orthogonal and well structured. The variables are arranged in a pattern called the Arakawa C-grid (a

staggered grid). In this arrangement, the water level points (pressure points) are defined in the centre of a (continuity) cell; the velocity components are perpendicular to the grid cell faces where they are situated (see Fig. 2.3).

For the simulations presented in this paper, an alternating direction implicit (ADI) method is used to solve the continuity and horizontal momentum equations (Leendertse, 1987). The advantage of the ADI method is that the implicitly integrated water levels and velocities are coupled along grid lines, leading to systems of equations with a small band width. Stelling (Stelling, 1984) extended the ADI method of Leendertse with a special approach for the horizontal advection terms. This approach splits the third-order upwind finite-difference scheme for the first derivative into two second-order consistent discretizations, a central discretization, and an upwind discretization, which is successively used in both stages of the ADI scheme. The scheme is denoted as "cyclic method" (Stelling, 1991). This leads to a method that is computationally efficient, at least second-order accurate, and stable at Courant numbers of up to approximately 10 (Roelvink, 2005b).

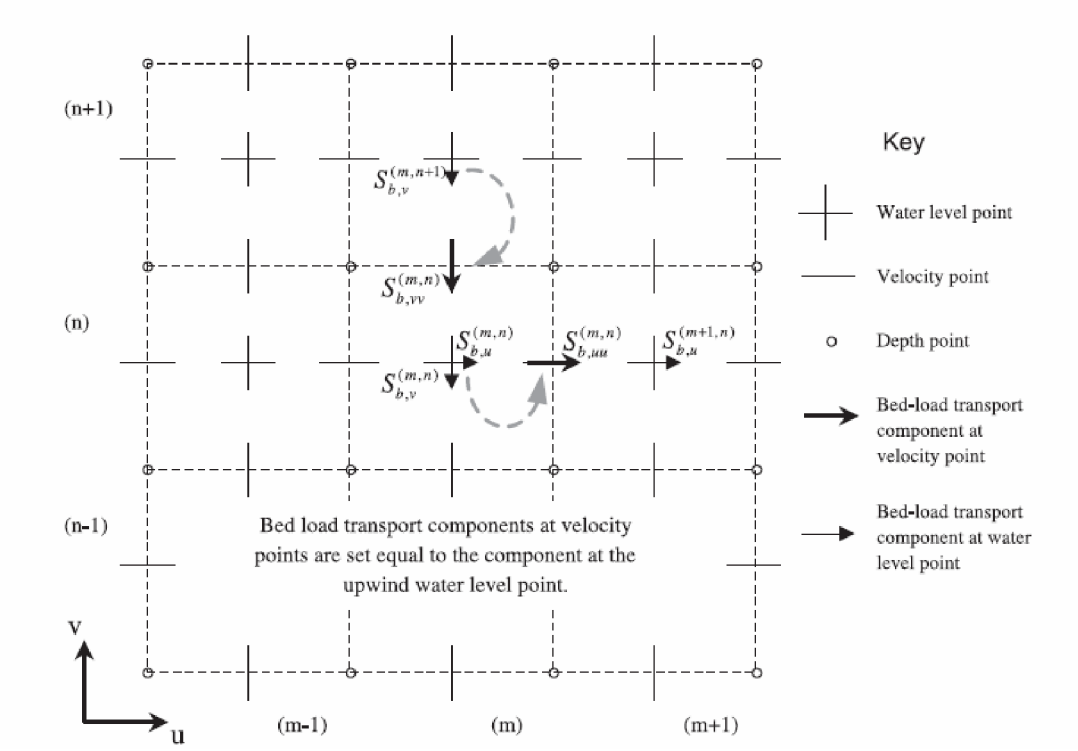

Fig 2.3 A Delft3D staggered grid showing the upwind method of setting bed load sediment transport components at velocity points. Water level points are located in the centre of the sediment control volumes (Lesser, 2004)

2.3 Wave model

The purpose of using wave model is twofold. First of all, the wave model provides wave force for the flow model, which enables the flow model to simulate the wave-driven current. Secondly, the wave parameters will be provided to the sediment transport model to account for the stirring effect of wave motion on the sediments which is one of the objectives to obtain in this study.

To simulate the evolution of wind-generated waves in coastal waters, the Delft3D-WAVE module (WAVE-INPUT 40.31) was used in which the SWAN (Simulating WAves Nearshore) third generation numerical wave model is implemented. The SWAN model is driven by wind and wave boundary conditions and is based on a discrete spectral balance of action density that accounts for refractive propagation of random, short-crested waves over arbitrary bathymetry and current fields (Booij, 1999; Ris, 1999). In SWAN, the processes of wave generation, whitecapping, nonlinear triad and quadruplet wave–wave interaction, bottom dissipation and depth-induced wave breaking are represented explicitly (refer to Booij, 1999 for a complete description). The numerical scheme for wave propagation is implicit and therefore unconditionally stable at all water depths. To model the energy dissipation in random waves due to depth-induced breaking, a spectral version of the bore-based model of Battjes and Jansen (1978) is used, here applied with a time-independent constant breaker parameter γ =0.73, and to model bottom-induced dissipation, the JONSWAP formulation (Hasselmann, 1973) is applied to compute bottom friction. The formulation for wave-induced bottom stress is modelled according to Fredsøe (1984).

2.3.1 Basic equations

In SWAN the waves are described with the two-dimensional wave action density spectrum, even when non-linear phenomena dominate (e.g., in the surf zone). The rational for using the spectrum in such highly non-linear conditions is that, even in such conditions it seems possible to predict with reasonable accuracy this spectral distribution of the second order moment of the waves (although it may not be sufficient to fully describe the waves statistically). The spectrum that is considered in SWAN is the action density spectrum $N(\sigma, \theta)$ rather than the energy density spectrum $E(\sigma, \theta)$ since in the presence of currents, action density is conserved whereas energy density is not (Whitham, 1974). The independent variables are the relative frequency σ (as observed in a frame of reference moving with the current velocity) and the wave direction θ (the direction normal to the wave crest of each spectral component). The action density is equal to the energy density divided by the relative frequency: $N(\sigma, \theta) = E(\sigma, \theta) / \sigma$. In SWAN this spectrum may vary in time and space.

In SWAN the evolution of the wave spectrum is described by the spectral action balance equation which for Cartesian co-ordinates is (Hasselmann, 1973; Holthuijsen, 2005):

$$\frac{\partial}{\partial t} N + \frac{\partial}{\partial x}(c_x N) + \frac{\partial}{\partial y}(c_y N) + \frac{\partial}{\partial \sigma}(c_\sigma N) + \frac{\partial}{\partial \theta}(c_\theta N) = \frac{S}{\sigma} \qquad (2.23)$$

where:

$c_x, c_y, c_\sigma, c_\theta$: propagation velocities in *x*, *y* and σ , θ space (m/s)

The first term in the left-hand side of this equation represents the local rate of change of action density in time, and the second and third term represent propagation of action in geographical space. The fourth term represents shifting of the relative frequency due to variations in depths and currents. The fifth term represents depth-induced and current-induced refraction. The expressions for these propagation speeds are taken from linear wave theory (Dingemans, 1997; Mei, 1983; Whitham, 1974). The term $S(S(\sigma,\theta))$ at the right-hand side of the action balance equation is the source term in terms of energy density representing the effects of generation, dissipation and non-linear wave-wave interactions.

The following processes are accounted for in SWAN:

- Generation by wind
- Dissipation by whitecapping, bottom friction and depth-induced breaking
- Non-linear wave-wave interaction (quadruplets and triads)

In addition wave propagation through obstacles and wave-induced set-up of the mean sea surface can be computed in SWAN.

2.3.2 Wave effects on flow

In coastal seas, wave action may influence flow for a number of reasons, which is especially important for the accurate modeling of sediment transport in a near shore coastal zone. The following processes are presently available in DELFT3D-FLOW:

- Wave forcing due to breaking (by radiation stress gradients) is modeled as a shear stress at the water surface (Stive, 1986; Svendsen, 1985). This radiation stress gradient is modeled using the implified expression of Dingemans et al. (Dingemans, 1987), where contributions other than those related to the dissipation of wave energy are neglected. This expression is as follows:

$$\vec{M} = \frac{D}{w_a}\vec{k} \tag{2.24}$$

  where:
  $\vec{M}$: The forcing due to radiation stress gradients (N/m^2)
  D : dissipation due to wave breaking (W/m^2)
  w_a : angular wave frequency (rad/s)
  $\vec{k}$: wave number vector (rad/m)

- The effect of the enhanced bed shear stress on the flow simulation is accounted

for by following the parameterizations of Soulsby et al. (1993). Of the several models available, the simulations presented in this paper use the wave–current interaction model of Fredsoe (1984).

§ The wave-induced mass flux is included and is adjusted for the vertically nonuniform Stokes drift (Walstra and Roelvink, 2000).

§ The additional turbulence production due to dissipation in the bottom wave boundary layer and due to wave whitecapping and breaking at the surface is included as extra production terms in the $k-\varepsilon$ turbulence closure model (Walstra and Roelvink, 2000).

§ Streaming (a wave-induced current in the bottom boundary layer directed in the direction of wave propagation) is modeled as additional shear stress acting across the thickness of the bottom wave boundary layer (Walstra and Roelvink, 2000).

2.4 Cohesive sediment dynamics implemented in Delft3D

2.4.1 Cohesive sediment settling velocity implement in Delft3D

As mentioned in part 2.1.2, cohesive sediment tends to flocculate in salt water to form sediment "flocs", with the degree of flocculation depending on the salinity of the water. These flocs are much larger than the individual sediment particles and settle at a faster rate. In order to model this salinity dependency two settling velocities are supplied and a maximum salinity. The first velocity, *WS0*, is taken to be the settling velocity of the sediment fraction in fresh water (salinity = 0). The second velocity, *WSM*, is the settling velocity of the fraction in water having a salinity equal to *SALMAX*. The settling velocity of the sediment flocs is calculated as follows in Delft3D:

$$w_{s,0}^{(a)} = \frac{w_{s,\max}^{(a)}}{2}\left(1-\cos\left(\frac{\pi S}{S_{\max}}\right)\right)+\frac{w_{s,f}^{(a)}}{2}\left(1+\cos\left(\frac{\pi S_s}{S_{\max}}\right)\right) \qquad \text{when } S_s \le SALMAX$$

$$w_{s,0}^{(a)} = w_{s,\max}^{(a)} \qquad \text{when } S_s > SALMAX \tag{2.25}$$

where:

$w_{s,0}^{(a)}$: the (non-hindered) settling velocity of sediment fraction (^{a})

$w_{s,\max}^{(a)}$: *WSM*, settling velocity of sediment fraction (^{a}) at salinity concentration SALMAX

$w_{s,f}^{(a)}$: *WS0*, fresh water settling velocity of sediment fraction (^{a})

S_s: Salinity

$S_{\max}$: SALMAX, maximal salinity at which WSM is specified

Remarks:

- Modelling turbulence induced flocculation or the break-up of sediment flocs is not yet implemented
- The influence of flocculation is disregarded by setting *WSM = WS0*

2.4.2 Cohesive sediment dispersion

The vertical mixing coefficient for sediment is equal to the vertical fluid mixing coefficient calculated by the selected turbulence closure model, i.e:

$$\varepsilon_S^{(a)} = \varepsilon_f \tag{2.26}$$

where:

$\varepsilon_S^{(a)}$: vertical sediment mixing coefficient for sediment fraction

ε_f : vertical fluid mixing coefficient calculated by the selected turbulence closure model

2.4.3 Cohesive sediment erosion and deposition

For cohesive sediment fractions the fluxes between the water phase and the bed are calculated with the well-known Partheniades-Krone (1965) formulations.

$$E^{(a)} = M^{(a)} S(\tau_{cw}, \tau_{cr,e}^{(a)}) \tag{2.27}$$

$$D^{(a)} = w_s^{(a)} c_b^{(a)} S(\tau_{cw}, \tau_{cr,d}^{(a)}) \tag{2.28}$$

$$c_b^{(a)} = c^{(a)}(z = \frac{\Delta z_b}{2}, t) \tag{2.29}$$

where:

$E^{(a)}$: erosion flux ($kg/m^2/s$)

$M^{(a)}$: user specified erosion parameter *EROUNI* ($kg/m^2/s$)

$S(\tau_{cw}, \tau_{cr,e}^{(a)})$: erosion step function:

$$S(\tau_{cw}, \tau_{cr,e}^{(a)}) = (\frac{\tau_{cw}}{\tau_{cr,e}^{(a)}} - 1) \quad \text{when } \tau_{cw} > \tau_{cr,e}^{(a)} \tag{2.30}$$

$$= 0 \qquad \text{when } \tau_{cw} \le \tau_{cr,e}^{(a)}$$

$D^{(a)}$: Deposition flux ($kg/m^2/s$)

$w_s^{(a)}$: Fall velocity (hindered) (m/s)

$c_b^{(a)}$: average sediment concentration in the near bottom computational layer

$S(\tau_{cw},\tau_{cr,d}^{(a)})$: deposition step function:

$$S(\tau_{cw},\tau_{cr,d}^{(a)}) = (\frac{\tau_{cw}}{\tau_{cr,d}^{(a)}} - 1) \quad \text{when } \tau_{cw} \le \tau_{cr,d}^{(a)} \tag{2.31}$$

$$= 0 \qquad \text{when } \tau_{cw} > \tau_{cr,d}^{(a)}$$

τ_{cw} : mean bed shear stress due to current and waves as calculated by the wave-current interaction model selected by the user

$\tau_{cr,e}^{(a)}$: user specified critical erosion shear stress *TCEUNI* (N/m^2)

$\tau_{cr,d}^{(a)}$: user specified critical deposition shear stress *TCDUNI* (N/m^2)

Superscript (^{a}): implies that this quantity applies to sediment fraction(^{a})

2.5 Conclusions

In this chapter, the basic concepts of cohesive sediments have been reviewed. Some crucial parts of flow model and wave model applied in Delft3D are listed as well. At the end, the implication of settling velocity, dispersion, erosion and deposition of cohesive sediment in Delft3D is listed. It shows that Delft3D can be a generic tool, which covered quite a part, but not all the known processes, to study the cohesive sediments, of which the thorough understanding of the underlying physical process is not so clear yet.

In the following chapters, a ZUNO coarse grid model which covered the most part of North Sea is applied first to get the flow dynamics and cohesive sediments transportation with waves in a macro scale. It also acts as the boundary condition for the coming refined grid model.

Part 3 ZUNO Coarse grid model

To increase the understanding of the complex interactions between the flow dynamics, wave, wind and cohesive sediment transportation etc. in a specific area, a model of macro scale, which covers bigger area, is necessary to get a reasonable flow and sediment transportation pattern in wide range. Accordingly, ZUNO coarse grid model, which covered south part of North Sea, is setup first as a macro scale model. The model helps the modellers to get a generic description of the flow and wave fields in the large area, which provides boundary conditions for the smaller scale models in the coming parts.

The result expected in this chapter is: Firstly, a right pattern of fluid movement is obtained by running the existing ZUNO coarse grid model and the analysis of measured data. The flow field pattern is reproduced with various verifications and sensitivity tests. Secondly, wave dynamics is introduced by the Delft3D WAVE module to extend the existing ZUNO coarse model coupling with the flow model.

Though the Haringvliet Mouth is described by only one single element in the model, the ZUNO coarse model can offer a generic background to modellers and provide boundary conditions for the schematized models introduced in Part 5.

3.1 Introduction of case study area – Haringvliet Mouth

3.1.1 General information of Dutch coast

For 82% of its total length (432 km) the Dutch coast consists of sandy shores. This coast is part of the sandy coast system of the North Sea extending from Cap Blanc Nez in France as far as Northern Jutland in Denmark. The Dutch coast can be divided into three physically different parts: the Wadden Sea islands in the north, the Schelde delta in the south, and in between, the central and western coasts with a sand barrier system fronted by beach and surf zones containing 2 or 3 bars. The Dutch beaches can be described using Dean's dimensionless parameter (Ω) and the relative tidal range (RTR), which are defined as (Dean, 1973; Short, 1996; Short, 2006):

$$\Omega = \frac{H_b}{w_s T} \qquad \text{and} \qquad RTR = \frac{TR}{H_b} \tag{3.1}$$

where:

H_b : breaking wave height
w_s : sediments fall velocity
T : wave period
TR : spring tide range

According to this classification system, the Dutch beaches are mesotidal and dissipative ($5 < \Omega < 9$, for Dutch beaches, Ω = 2.6-7), and geomorphology of these beaches is not tide-dominated (the threshold value of tide dominated is RTR > 12, while for Dutch coast, RTR = 8.5-10). And based on McLachlan's beach state index (BSI), which is denoted as Ω multiplied by tide range and indicates the ability of waves and tides to move sand, it ranges from 1.4 to 1.1 for the northern Wadden Sea and the southern estuaries (McLachlan, 1993). However, there are some local differences, for instance, the north part, the Wadden Sea area is ultra-dissipative (Ω =11.5), while the west coast part is dissipative (Ω =6.6).

The seemingly considerable difference between the high and low-water levels (1.4–3.8 m) contributes little to the variation in beach morphology. In fact, this is influenced mainly by breaker height, which ranges from 1.0 m (summer mean) to 1.7 m (winter mean) along the Dutch coast. Dunes, beaches and surf zones have always protected the land against flooding by the sea. Compared with the coastal zone of Belgium, Dutch beaches are influenced more by wind and wave action than by tide (Janssen, 2005).

The origin of the mud and suspended particulate material of Dutch coast remains controversial yet. McManus and Prandle (1997) showed that only the Dover Strait, the northern boundary (56˚ N), the Wash and the Suffolk coast of UK are statistically significant sources of suspended sediments in the Southern North Sea. The smectite content in the fine-grained surface sediment in the Belgian coastal zone is high, which points to the Cretaceous formations in the Dover Strait as a source area. It is reported that the erosion and resuspension of Tertiary clay, Holocene mud and peat layers along the Flemish Banks served as a local source of suspended material in the Belgian/Dutch coastal area, although quantities are not provided (Fettweis, 2003).

The suspended material and mud layer are carried by the residual current from south to north along the Belgian/Dutch coast. On the way of transportation northwards, the complex coastal hydrodynamics, consisting of gyres, divergences or convergence's of currents, mixing of the freshwater, or geological trap, lead to the accumulation of cohesive sediments along the coastal zone. The Haringvliet Mouth is chosen as a case study area, not because of serious cohesive sedimentation problems happened in the area, but for the reasons that it is a typical area involved by all the hydrodynamics, such as, tide, wave, wind, controlled fresh water discharge, with complicated morphological patterns, consisting of a number of channels and active sandy shoals etc.

3.1.2 Description of Haringvliet Mouth

Along the Dutch coast line, Haringvliet Mouth is chosen as the case study area, not because of serious sedimentation problem happened in the area, but because of the characteristic of hydro-dynamics of this area. Due to the complicated hydrodynamics pattern, the Haringvliet Mouth area is a sedimentation dominant area and is still active till nowadays.

The Haringvliet estuary (Fig. 3.1) is part of the Dutch Delta Coast and is situated just south of the port of Rotterdam. Before the closure in 1970, the Haringvliet was a large river mouth and estuary. The tidal range and salinity intrusion reached approximately

50 km landwards (measured from the present location of the dam) into the area called Biesbosch (Tonis, 2002). The estuary itself was formed of channels up to 15 m in depth and sandy shoals. The tidal volume (i.e. the sum of ebb and flood volumes during a tidal cycle) before closure was in order of 530×10^6 m^3 (Tonis, 2002). Throughout the 14th century dykes were built along the river causing a decrease in estuary area (Tonis, 2002). These were, however, relatively small and gradual changes compared to the change after the constructions of Delta Works. The construction works completely closed the river at two locations: one 30 km upstreams with the Volkerak dam (1969) and one at the river mouth with the Haringvliet dam (1970). The area landwards from the Haringvliet dam slowly turned into a fresh water zone. Seaward of the dam a reduced estuary remained.

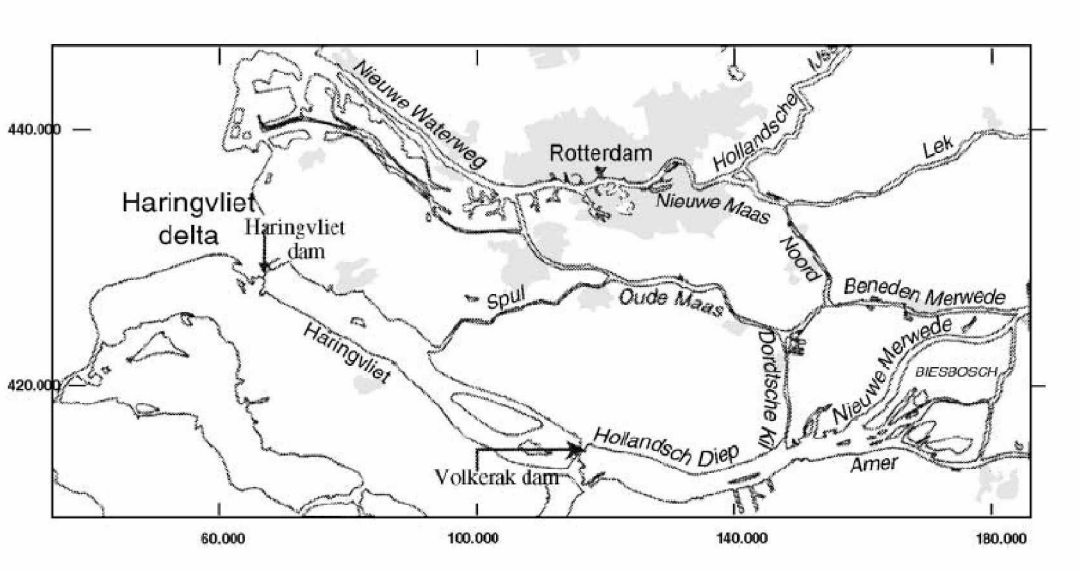

Fig 3.1 Haringvliet estuary before closure (Tonis, 2002)

The present estuary covers an area of more than 100 km^2 and the coastline along the estuary has a length of approximately 26 km. In the north, the estuary is bounded by the dikes, built for the land reclamation of the Maasvlakte and the Slufter. Further clockwise, the Brielsche Gat dam and the sandy coast Voorne are found. In the southeast lies the Haringvliet dam with sluices. The rest of the boundary of the estuary consists of the wide sandy beaches of Goeree in the south.

Table 3.1 gives the average wave height for different directions, measured from a point located approximately 20 km from the coast at 21 m water depth (known as Goeree Platform). The wave energy fluxes from southwest to west dominate, but frequently waves with relatively long periods arrive from the northwest. The tidal currents run parallel to the coast: northward during flood and southward during ebb. The tide is semi diurnal, with a mean range 2.4 m. After closure of Haringvliet Sluice, the tidal volume became in the order of 22,106 m^3 which is due to river discharge (Tonis, 2002). Since 1957, coastal engineering structures and human interventions have changed the morphology of the estuary. Land reclamation has taken place north of the estuary to expand the port of Rotterdam (the Maasvlakte, 1964–1976). A dam with sluices has been built (1957–1970) in a narrow seaward part of the original river mouth

(see Fig. 3.2). Most of the interventions, at least the interventions with the largest impact on the hydrodynamic situation and the morphology, were finished in 1970. However, from 1986 until 1987, smaller land reclamation (the Slufter project) was carried out in the north part of the estuary. The present estuary consists of a number of channels and sandy shoals. The sluices in the dam have been built at the south side of the dam. At low tide water is discharged into the sea. One of the channels is the entrance channel to the small harbour of Stellendam near the dam. The largest part of the river discharge follows this channel, yet the channel has to be dredged frequently. Large-scale adaptations to the new hydrodynamic situation occurred. Most channels became shallower, while the sandy shoals extended.

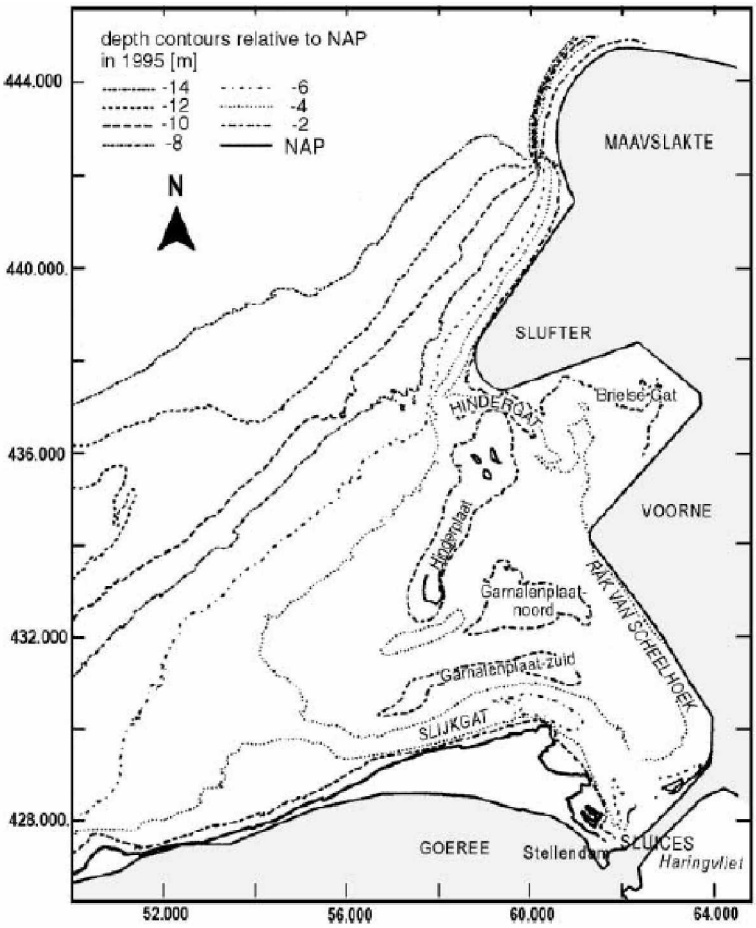

Fig 3.2 Haringvliet estuary after closure (Tonis, 2002)

Table 3.1 Average wave height for different directions, measured from Goeree Lightvessel (a measurement point located approximately 20 km from the coast at 21 m water depth) (Tonis, 2002)

Direction Range (°)	Occurrence (%)	Averg. Wave Height (m)
338– 22	10.3	1.05
22–67	11.2	1.09
67–112	4.2	0.93
112– 157	2.7	0.78
157– 202	5.8	1.05
202– 247	27.8	1.49
247– 292	13.5	1.41
292– 337	24.6	1.28
000– 360	100.0	1.27

At this moment, new projects in this area are under discussion, namely the Maasvlakte 2 (MV2) project, which has been approved by the Dutch government as the Outline Zoning Procedure Plus (Planologische Kernbeslissing Plus, PKB-Plus) on Sept 2, 2005, is mainly focused on the reclamation to extend the south part of the Port of Rotterdam based on the existing area. The reclamation will produce approximately 1000 hectares of new industrial sites, which are intended mainly for deep-sea-related container handling, storage & distribution, chemicals and new industry (Port Of Rotterdam, 2005). Nevertheless, the MV2 reclamation will influence the existing morphological processes. The reclamation will create a physical barrier for waves and tidal flow along the coast and that in turn influences the transport of sand and silt in the sea. In the long term, this process can change morphology (See Fig 3.3a, Fig 3.3 b).

Fig 3.3a MV1 and Slufter from southwest

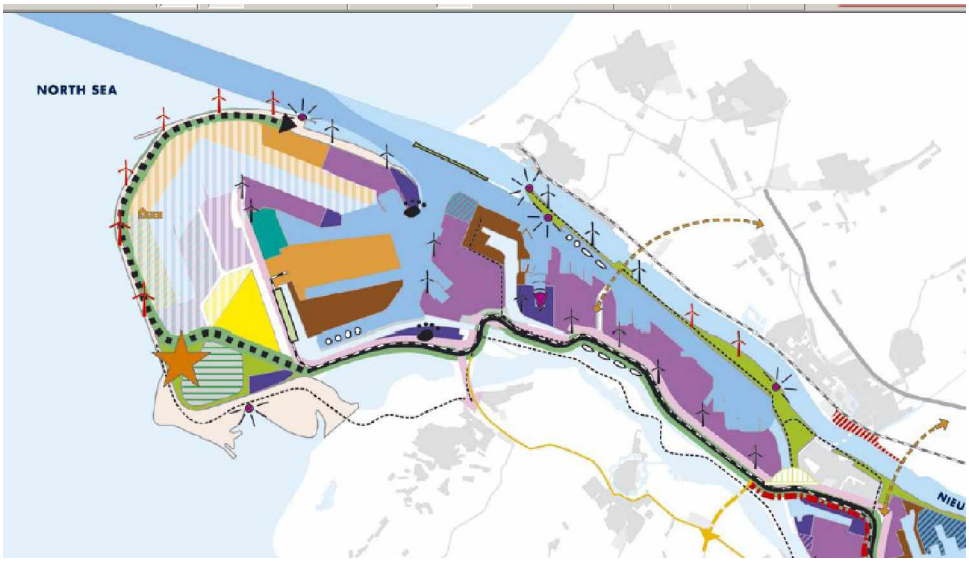

Fig 3.3b Plan view of MV2 (after Port of Rotterdam)

3.2 Models setup

The aim of the hydrodynamic models is to access the flow and wave field of southern North Sea in a macro scale. In addition, the suspended sediment transportation is also simulated in the flow and wave field.

A coarse grid, which covered the large area of south part of North Sea, provided by WL | Delft Hydraulics has been applied for the simulation with the hydrodynamic simulation

program Delft3D-FLOW to solve the shallow water equations in 2D or 3D including the impact of salinity and temperature effects.

3.2.1 Grid

To compromise between the cover area and computation time, the ZUNO grid is relatively coarse. It is a rectilinear or a curvilinear, boundary fitted grid which contains 8,710 computational elements to cover about 1,000 km×800 km area with cell size around 8 km by 6 km (Fig 3.4).

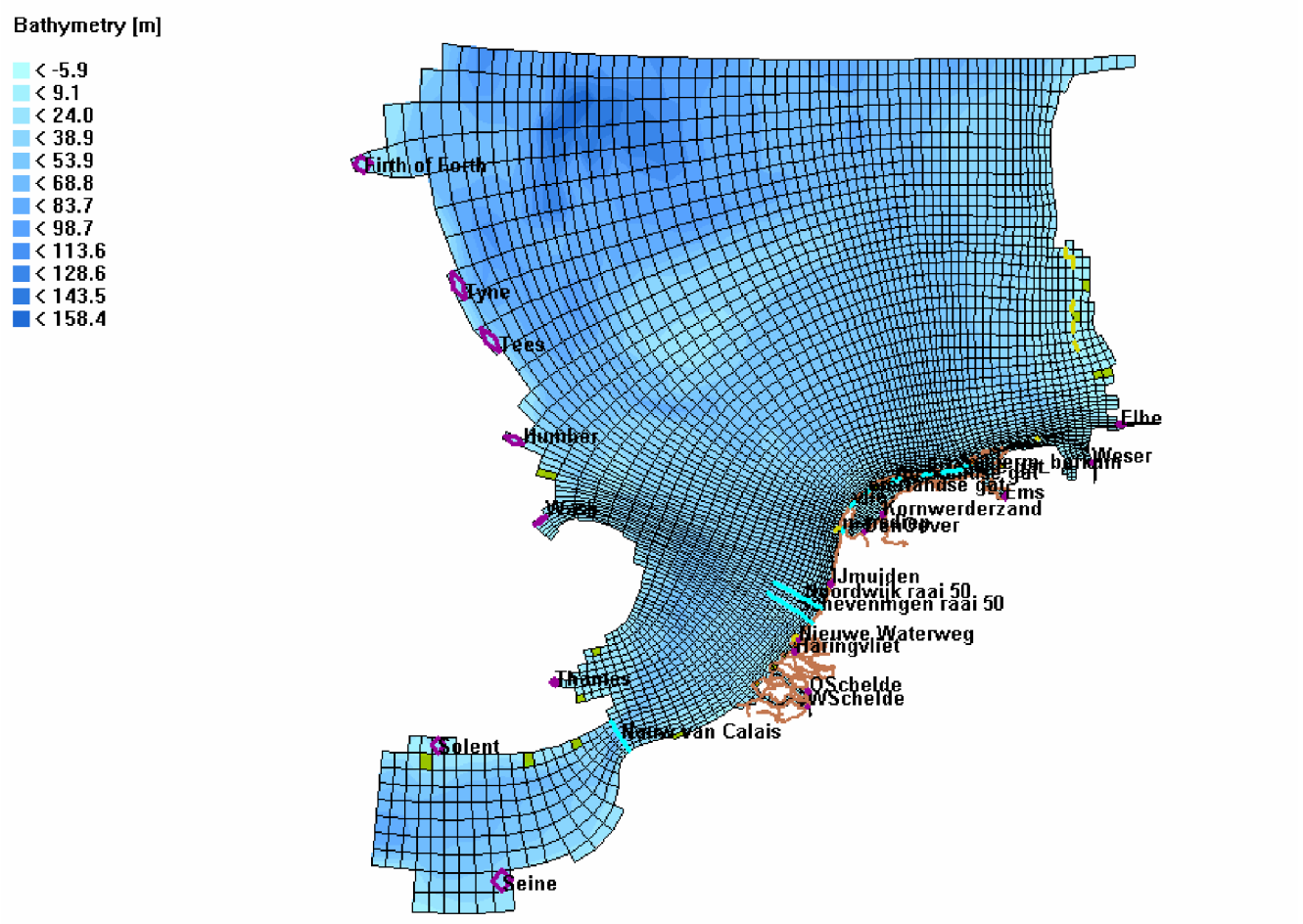

Fig 3.4 ZUNO Coarse Grid and bathymetry

In vertical direction, Delft3D uses a so-called “Sigma grid”. This means that the total water depth is divided into a number of layers each covering a percentage of the total water depth. These sigma layers results in the same vertical solution in the entire model domain regardless of the local water depth. For 3D computations with this grid, 10 computational layers were defined. The layer distribution and thickness of layer is listed in Table 3.2:

Table 3.2 The vertical layer distribution of model

Layer	1	2	3	4	5	6	7	8	9	10
Relative thickness of total depth (%)	4.0	5.9	8.7	12.7	18.7	18.7	12.7	8.7	5.9	4.0

The logarithmic layer distribution provides relatively high resolution near the surface and near the bed. Near the surface a high resolution is required to include the impact of wind on velocity profiles, while near bed, a high resolution is needed in view of sediment transport computation within the model (Roelvink, 2001a).

3.2.2 Bathymetry

The bathymetry is provided with ZUNO grid by WL | Delft Hydraulics and is modified to some extent.

3.2.3 Open boundary condition

The model has two open boundaries. A southern open boundary located just at the south of the Dover Strait and a northern open boundary located between Scotland and the most northern part of Denmark. Each open boundary is divided in a number of boundary conditions, which need to be prescribed.

Through the open boundary, the behaviour of mega scale system can transport inside the macro scaled ZUNO coarse grid model domain. The water levels, specified by means of tidal constant, amplitudes and phases of tidal constitutes, in every element of the open boundaries, are generated from a larger scale hydrodynamic model covering the entire continental Shelf, up to the 2000m depth contour (Roelvink, 2005a; Roelvink, 2001a). The water levels in two grid elements which combine of different tide components in both boundaries are showed as examples in Fig3.5. And the wind effect is reported to be not included inside the boundary water level, i.e. the water level reflects only the tidal effect.

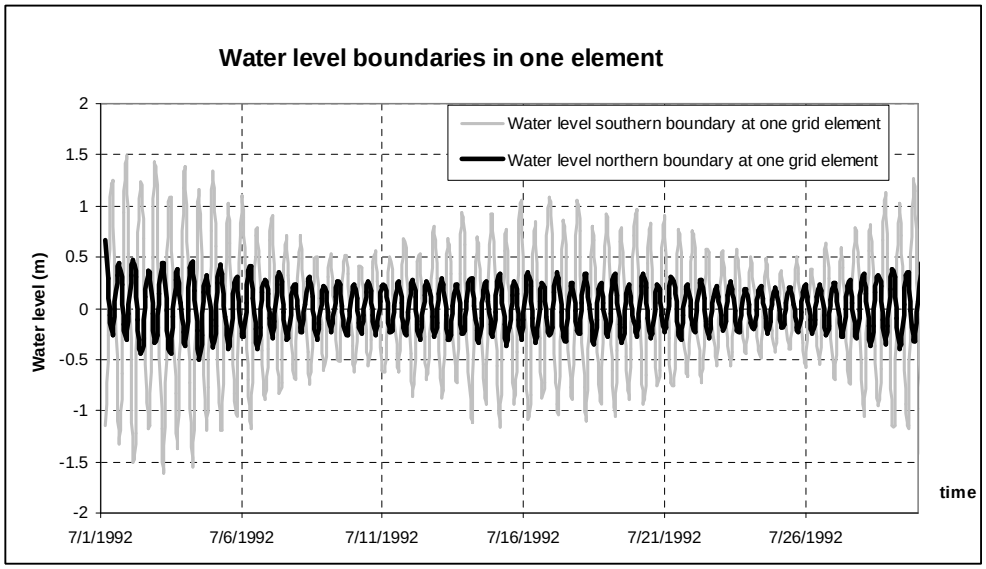

Fig 3.5 Example water levels in two grid elements which combine of different tide components in both boundaries

3.2.4 River discharges

A large amount of rivers discharge fresh water into the saline North Sea, which contributes significantly to density difference which, in turn, affects the hydrodynamics and then affects the fine suspended sediment transportation consequently.

For model simulations covering the actual measurement period, actually measured discharges of each river are used in this model. The measured data time interval is 10 days. However, for the model simulation aims to represent the typical discharge pattern, the long term averaged river discharge are applied in the model.

3.3 Verification on 1992 Noordwijk dataset

The model is given with well calibration. Hence, no further calibration work has been done.

The verification simulation setting is:

- Simulation period: 1 July 1992- 1 Aug 1992
- Time step: 5mins
- Turbulence model: $k-\varepsilon$ model
- Number of vertical layers: 10 layers
- Layer spacing: Logarithmic
- Wind data: every hour measurement data of Noordwijk (from The Royal Netherlands Meteorological Institute (KNMI) website, www.knmi.nl)

3.3.1 Flow field pattern

As we know, the North Sea is the interface where the continental shelf of north-west Europe opens to the Atlantic Ocean to the north, via the English Channel to the south-west (Fig 3.6).

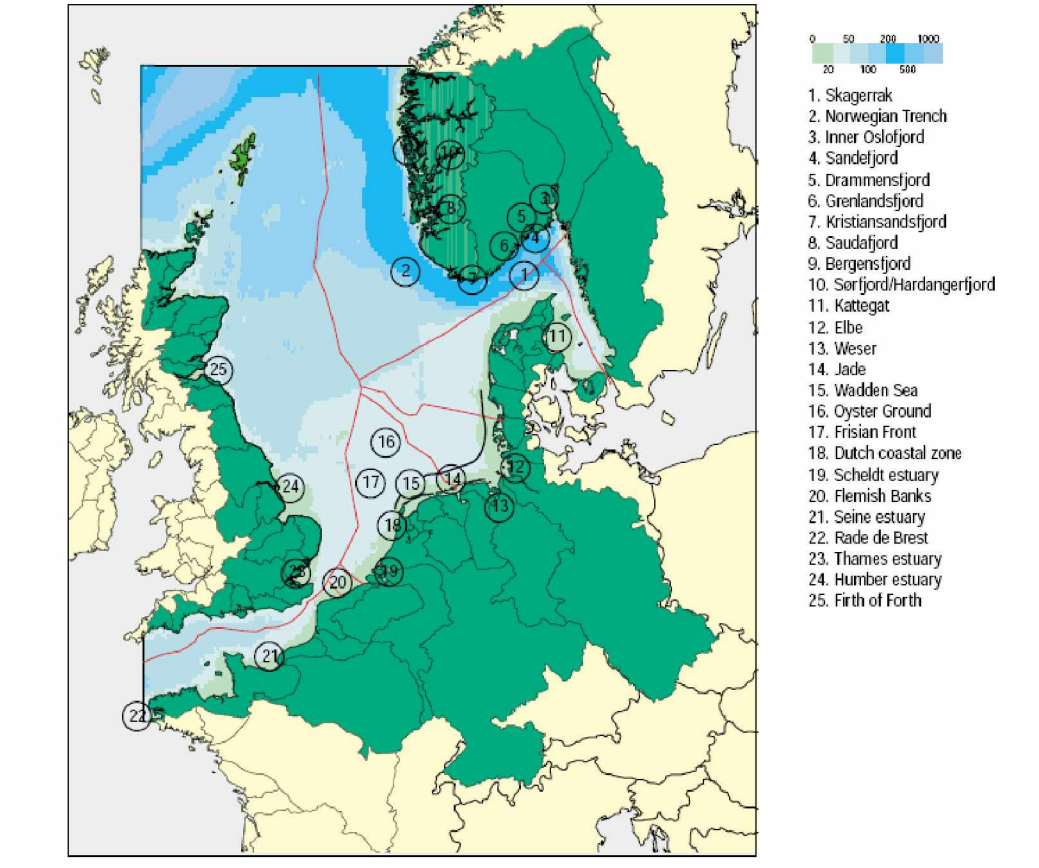

Fig 3.6 The bottom topography of North Sea (OSPAR Commission, 2004)

The Dutch coast zone located at the southern part of North Sea and the water depth is relatively small as about 30m. Tidal duration of this area is about 12.00- 12.30, which is a typical semi dual type.

From 00:00 of each day, when the water level is the lowest water at about -2m, to 06:00 about 0.6-1m, the highest level, it is the flood rising period. And then it turns to ebb falling period, to 12:00, at noon of each day, when the water level is the second lowest, at about –1.8m to -2m. Consequently, the water level increases again till 18:00 to the second highest level of that day, after when it turns down again till 00:00 of the next day. In such a way the tidal cycle continues eternally.

The tidal flow pattern of Dutch coastal zone in the model is described as the following: The flooding currents start from the south boundary of the model at 00:00 and arrive at Dover Strait after 1.5 hour. At that time, current outside of the area of Rotterdam harbour is still during its ebb falling period, directed to south at about 1m/s. At 03:00, the flooding currents pass by the estuary of Scheldt, which cause current flow towards

inland, and then arrive at the Hoek van Holland, where some eddy flow exists during the slack time. At 4:30, the flooding currents go northwards at about 1.5m/s and the front of flood currents arrives at the outlet of the Wadden Sea. Till 6:00 in the evening, the water level at Noordwijk raise to the highest (HHWS) in that day.

After that, the ebb tides dominate the main area. At 7.30, the flow tends to be slack while the flow direction still point to north. At 9:00 the northwest part of North Sea begin to flow to south while the flow near the northeast part, along the Dutch and Danish, still are slack to north. To 10:30, the ebb flow turns stronger and diverse in the middle of the North Sea. Part of the flow join the previous flood current northwards, while other part turns to be ebb flow towards south. The outlet of Wadden Sea locate at the diverse point and part of flow current flows inside the tidal channel. The current along the Dutch coast turns southwards now. At the same time, the flow in Scheldt River directs outwards. Till 12:00 flow ebb flow increase and the flow current causes eddy at the estuary again and flow towards inland at Scheldt.

Then the flow current keep going southwards till the flood tide increase at 13:30. To 15:00 the balance of flood current and ebb tide concurs at the estuary of Scheldt estuary. To 16:30, the fronts of flood tide move to the middle part of Dutch coast. Then, till 18:00 the water level at Noordwijk raise to the second highest of that day (HLWS).
The flood tide current turns weak after 18:00 and till the 21:00 in the evening, the tide outside of Noordwijk still point to north and the flow in the Scheldt river points outside. Flow current will change direction to south at 22:30 and then keep increasing. To 1:30 of the second day, the flow in the Scheldt River change direction towards inland again. Another tide cycle comes from the Dover Strait.

In summary, The tidal current along the Noordwijk is quite regular (Fig 3.7) while the inlet of Wadden Sea and middle part of North sea is quite complex. For instance, the tide currents along the Scotland keep flow towards southeast at all the time at relatively high speed of 2m/s, which is quite impressive.

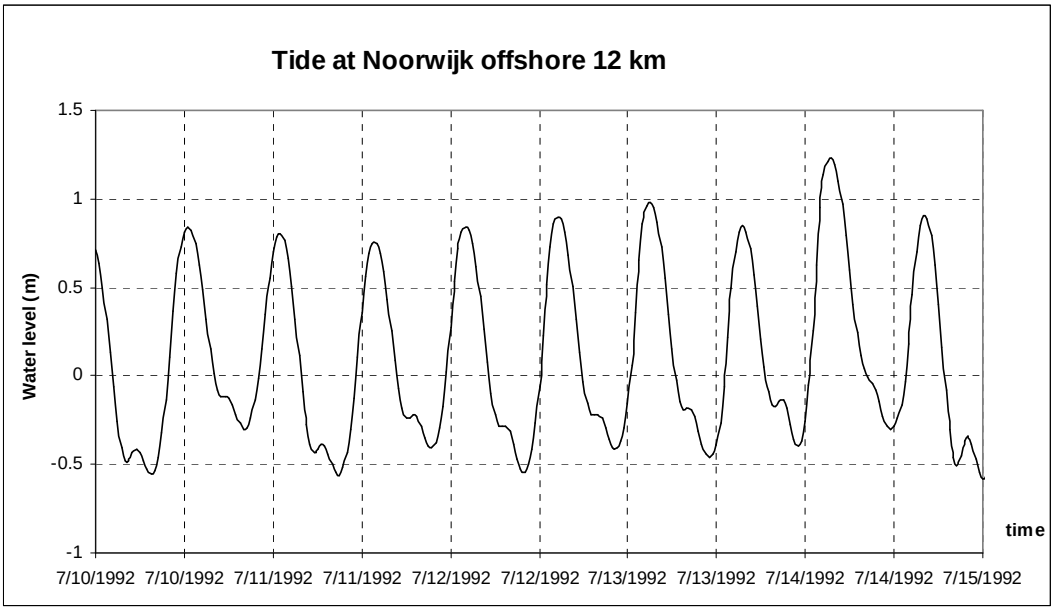

Fig 3.7 The tide curve at Noordwijk offshore 12 km

3.3.2 Verification with data at Noordwijk

Verification includes the flow current velocity magnitude and water level compared with the measured data at Noordwijk 12 km offshore.

3.3.2.1 Current velocity magnitude

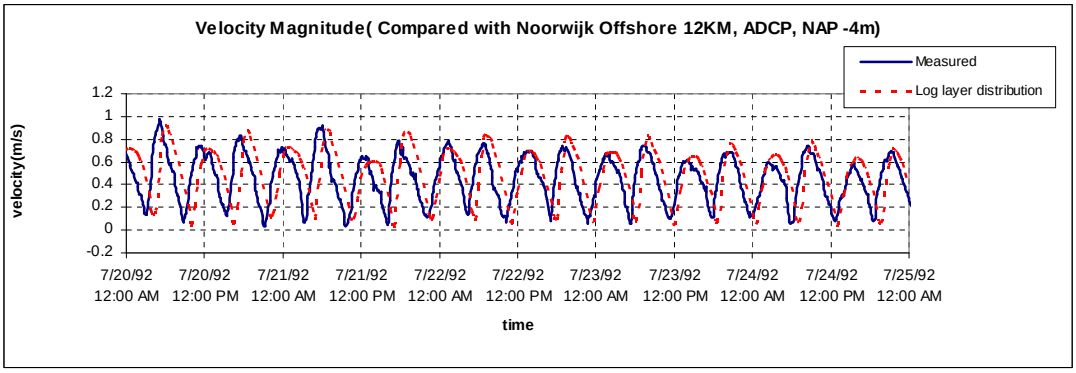

Fig 3.8 Velocity magnitude in the upper layer

The velocity magnitude value extracted from the simulation velocity on the 3rd layer at the Noordwijk offshore 12km of the 3D model is compared with the ADCP (refer to http://www.coastalresearch.nl) measured data at NAP -4m level in the figure 3.8. It can be seen that there is one hour time lag between the simulation and measured data. The error in reproducing the magnitude value is acceptably low. It maybe happens because of the boundary condition time lag.

3.3.2.2 Water level

As to the water level comparison, in one tide cycle, the high water level of simulation is about 30-40% higher in some places and the low water is better (Fig 3.9). Some comments on that will be depicted in the sensitivity tests part.

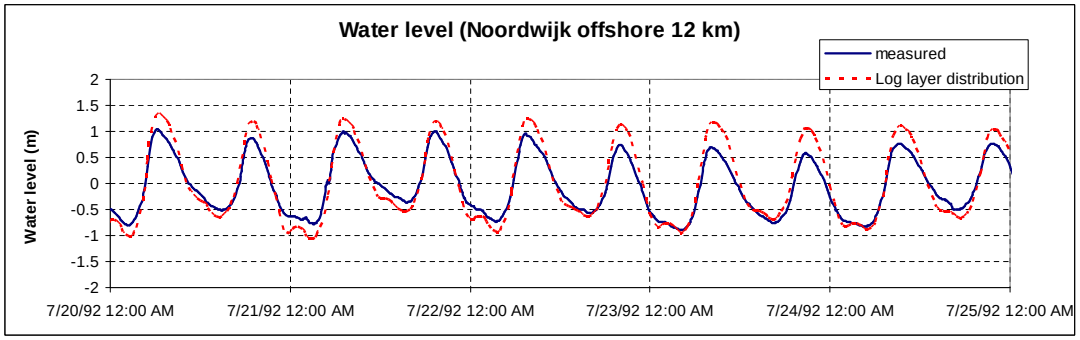

Fig 3.9 Water level in the upper layer

3.3.2.3 Alongshore residual currents

Residual currents were computed for a time series of alongshore and cross-shore current velocities using a Doodson-Godin filter (1972), which involves the application of eliminate the dominant M2 tidal components in the observed and simulation data.

The residual current computed from data collected in 1988-1989 at Noordwijk is analyzed extensively by Van der Giessen et al (Roelvink, 2001a). With the new ADCP measured data at Noordwijk in 1992 is analyzed in this study. The half-year averaged residual currents are showed as Fig 3.10. Alongshore residual currents over the entire water volume are positive, that is, in the northward direction. In the lower half of water column, the residual current is relatively weak, less than 0.01m/s. Near the NAP z = -12m, a break in slope can be observed, with the mean residual currents increasing to about 0.05m/s northwards.

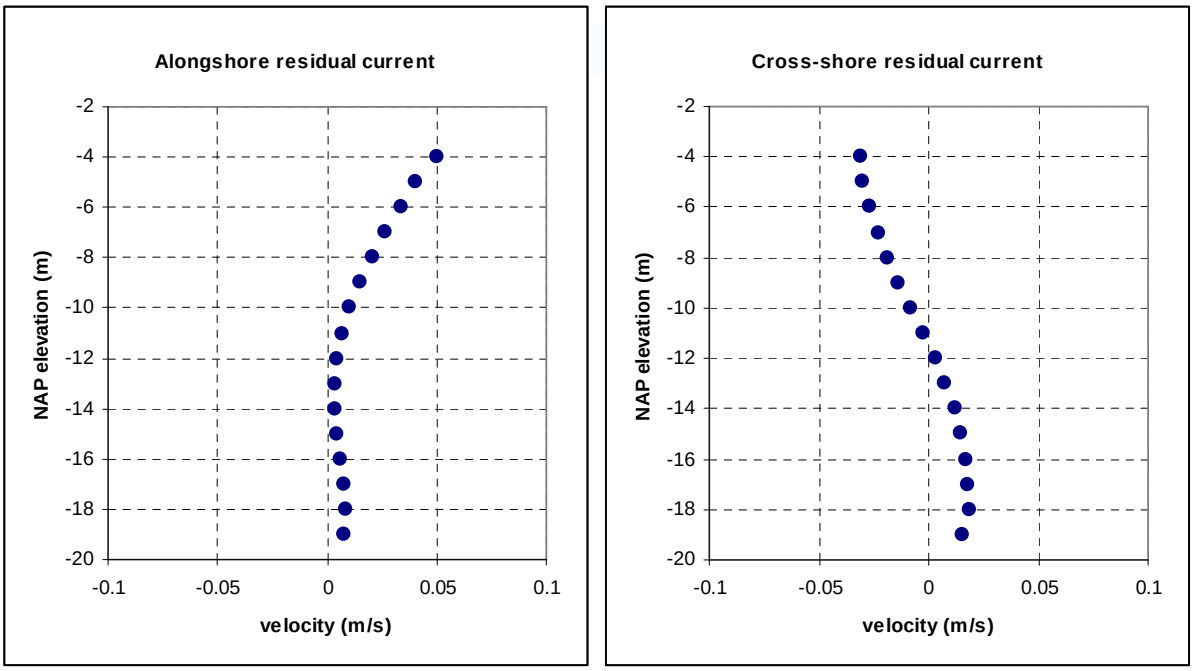

Fig 3.10 Vertical profile of alongshore and cross-shore residual current at Noordwjik offshore 12km by ADCP measured data for June, 1992 to Dec., 1992

As to the cross-shore residual current, the half-year averaged value is offshore at the magnitude of 0.03m/s and under NAP z = -12m, it changes shoreward as a magnitude of 0.01m/s. The trends are exactly the same as Roelvink analyzed on the dataset for 1988-1989 (Roelvink, 2001a).

As Roelvink et al.(2001a) mentioned, the temporal variability in the alongshore residual currents in all the depths appears to be well related to the alongshore component of the wind stress, which has been verified in this study as well. The measured data shows that the long-shore wind stress pointed to north accompanied with residual currents

northwards (Fig 3.11).

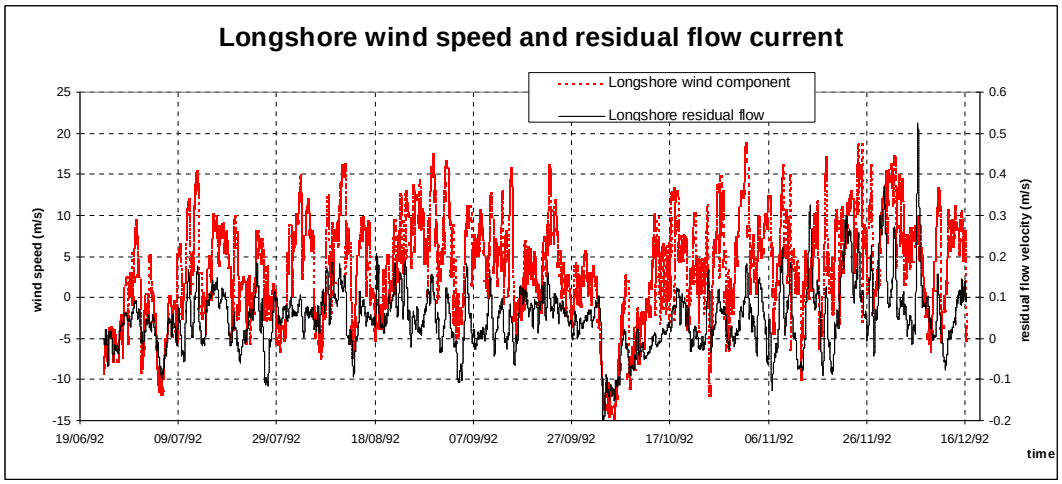

Fig 3.11 Alongshore measured residual current and alongshore wind component in the surface layer (velocity measured at Noordwjik offshore 12km by ADCP measured data for June, 1992 to Dec., 1992, wind data is measured at 10m height over open water with roughness length 0.002m from KNMI)

Correlation coefficient between alongshore residual flow current and longshore wind potential velocity is examined further at each measured ADCP measured layers and varied from about 0.6-0.65 in the lower part of water column to the surface.

The simulation result reproduced the correlation between alongshore wind component and flow residual flow quite acceptable. However, it is still distinguishable that flood-ebb periodical characters of the residual flow current, which implied that not only the M2 and S2 components are the main tidal components in that area as showed in the follow figure (Fig 3.12).

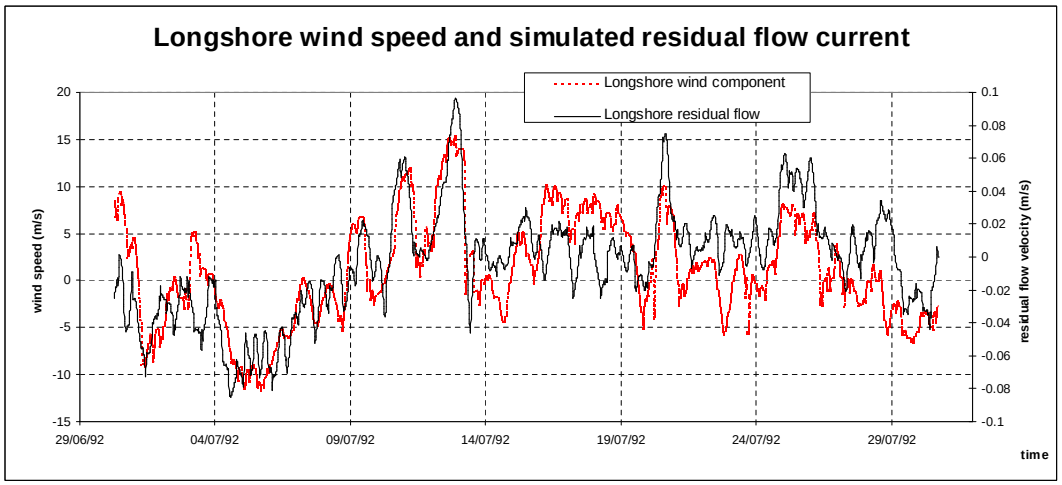

Fig 3.12 Alongshore simulated residual current and alongshore wind component in the surface layer (velocity simulated at Noordwjik offshore 12km by 3D model for July 1992, wind data is measured at 10m height over open water with roughness length 0.002m from KNMI)

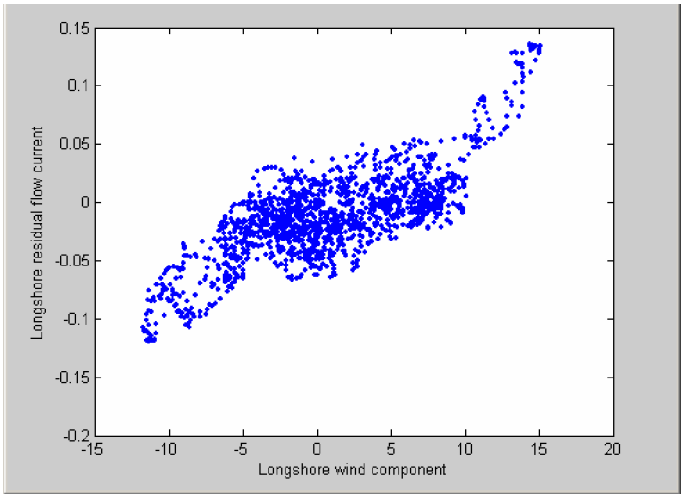

Fig 3.13 Correlation between longshore wind component and longshore simulated residual flow current in the surface layer

Correlation coefficient between alongshore residual flow current and longshore wind potential velocity is examined further at surface layer is as high as 0.76 (Fig3.13).

The analytical solution for the coefficient between the long shore component and longshore flow is a hyperbolic curve, which is estimated as the equilibrium status longshore velocity(Roelvink, 2005a):

$$\tau_{wind} = \rho_{air} C_d |w_{10m}| w_{10m} \quad (3.2)$$

$$\tau_{water} = \rho_{water} C_f |v| v \quad (3.3)$$

where: τ_{wind} is the wind shear stress, τ_{water} is the bed shear stress, ρ_{air} is the density of air, C_d is the wind drag coefficient, normally 0.001-0.003, w_{10m} is the measured alongshore wind velocity component, ρ_{water} is the density of water, C_f is the friction coefficient, which is prescribed by:

- A prescribed value of C_f or Chézy coefficient *C*, where: $C_f = g / C^2$ (3.4)
- A prescribed Manning value n, where: $C_f = gn^2 / h^{1/3}$ (3.5)
- A prescribed Nikuradse roughness height ks, where: $C_f = 0.03(\log \frac{12h}{k_s})^{-2}$ (3.6)

At the equilibrium status, the wind shear stress is balanced the bed shear stress,

$$\rho_{water} C_f |v| v = \rho_{air} C_d |w_{10m}| w_{10m} \quad (3.7)$$

which can be demonstrated as a hyperbolic curve as Fig 3.13.

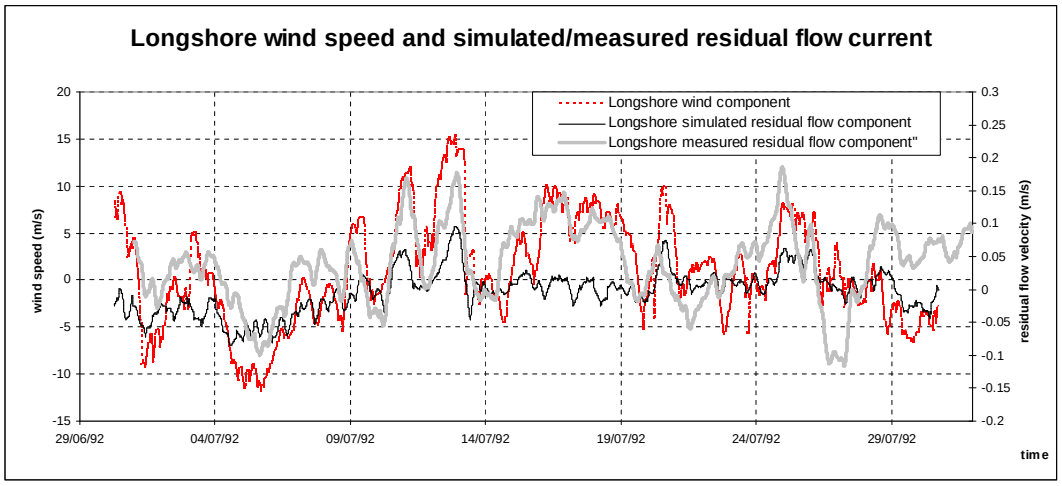

Fig 3.14 Alongshore wind component, alongshore measured residual flow and alongshore simulated residual flow current in the surface layer

The comparison (Fig 3.14) shows that the simulation of residual flow is quite acceptable, although there appears to be a southwards bias.

3.3.2.4 Cross-shore residual currents

As to the cross shore residual currents, the long-term averaged residual current has a onshore directed component of about 0.01m/s magnitude, while at the surface the cross-shore residual is significantly offshore at about 0.03m/s (Fig 3.10).

Compared to the temporal variations in the alongshore direction residual flow currents, the temporal variability in the cross-shore direction is rather small (Fig 3.15). Currents near bed are nearly always directed onshore, where as those higher up are almost always directed offshore. This suggests that the estuarine-like density driven circulation is a persistent feature. In more detail, some of the observed variations appear to be related to the cross-shore wind stress. For instance, the few situations with offshore directed near-bed residual currents (e.g., mid November) coincided with strong onshore winds, consistent with down welling during these periods.

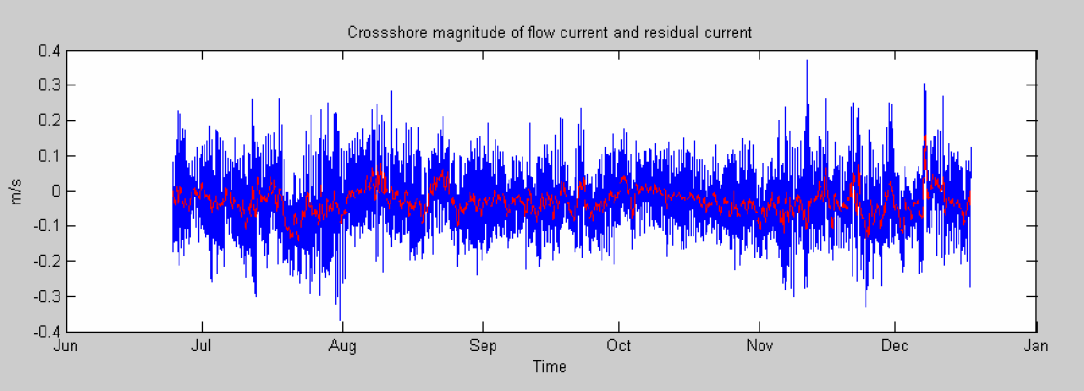

Fig 3.15 the temporal variations in the cross-shore direction residual flow currents is not so remarkable (-0.01m/s to 0.01m/s)

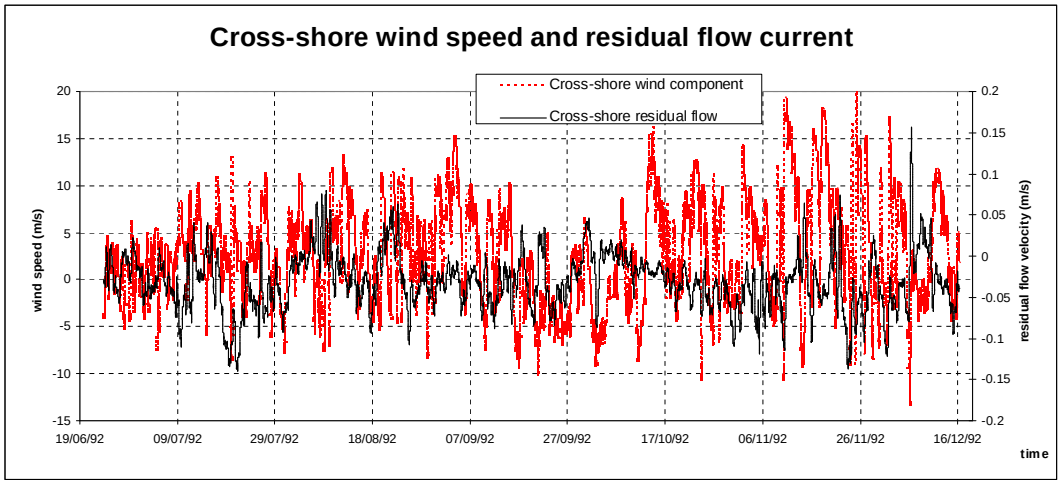

Fig 3.16 Cross-shore residual current and Cross-shore wind component in the surface layer (velocity measured at Noordwjik offshore 12km by ADCP measured data for June, 1992 to Dec., 1992, wind data is measured at 10m height over open water with roughness length 0.002m from KNMI)

To examine the relation between cross-shore direction wind component and cross-shore residual flow current, the relations has been calculated to be -0.008 (Fig 3.16), which indicated that the relation of wind component effect on the surface cross-shore residual flow current is not so remarkable. But, that correlation coefficient is about -0.5 at the bottom, rapidly reducing when higher up. The effect of cross-shore wind is thus most notably in the lower parts of the water column.

The simulation of cross-shore is also quite underestimated (Fig3.17), which needs further study.

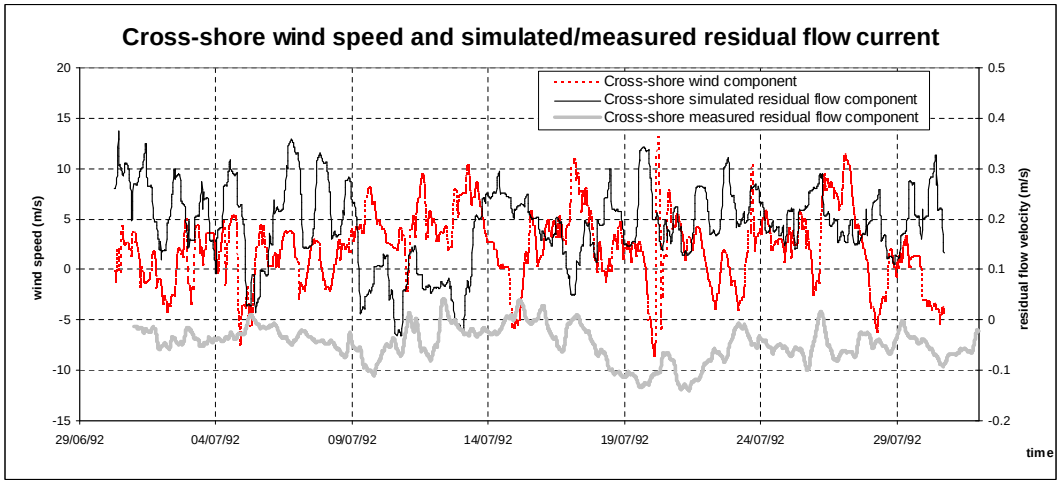

Fig 3.17 Cross-shore wind component, cross-shore measured residual flow and cross-shore simulated residual flow current in the surface layer

In summary, the vertical distribution of the cross-shore residual currents appears to be controlled largely by the estuarine-like density-driven circulation. It is modified to some extent by the cross-shore wind stress, consistent with down welling patterns.

3.3.3 Conclusion

Based on the analyses on the measured data and simulation result, some conclusion about the ZUNO coarse grid model can be obtained:

- The model reproduces the flow dynamic pattern, even though there is a 1 hour time lag between the simulation and measured velocity magnitude, which may be caused by the given boundary condition time lag, and some discrepancies of the higher water level and lower water level appears. The further study shows that it may be caused numerical processes parameter settings.

- Analyses on the measured ADCP data, near the bottom, the long-term residual current has a significant onshore directed component, with values of 0.025 - 0.035 m/s, while near the surface, the long-term residual current is offshore directed. This pattern is ascribed to an estuarine-like cross-shore circulation due to horizontal and vertical variation in the density field related to the outflow of the system. The effect of onshore wind on the cross-shore residual currents shows a characteristic down welling pattern. Near-bottom currents are offshore directed, whereas near-surface currents are onshore directed, both opposite to the persistent density-driven cross-shore pattern.

- Near the surface, long-term residual currents are larger, 0.07 - 0.11 m/s, and are mainly in the alongshore direction with an onshore component increasing with distance from shore. Variability in the alongshore residual current is correlated to variations in the alongshore wind stress, particularly for the near-bottom currents.

- The simulation roughly reproduced the alongshore residual flow and cross residual flow pattern.

3.4 Sensitivity tests

The sensitivity test in this study is mainly focused on two topics, one is the effects of the turbulence closure model, and the other is a numerical coefficient DPSOPT and DPUOPT, which is delineated in detail in the following parts.

3.4.1 Effects of different turbulence closure models

Delft3D-FLOW solves the Navier-Stokes equations for an incompressible fluid. Usually the grid (horizontal and/or vertical) is too coarse and the time step too large to resolve the turbulent scales of motion. The turbulent processes need appropriate closure assumptions to achieve space- and time-averaged quantities.

3.4.1.1 Background (WL|Delft Hydraulics, 2005)

For 3D shallow water flow the stress and diffusion tensor are anisotropic. The horizontal eddy viscosity coefficient ν_H and eddy diffusivity coefficient D_H are much larger than the vertical coefficients. The horizontal coefficients are assumed to be a superposition of three parts: a part due to "2D-turbulence", a part due to "3D-turbulence" see (Uittenbogaard, 1992) and a part due to molecular viscosity (refer to Part 2.2.1.6). The 2D part is associated with the contribution of horizontal motions and forces that cannot be resolved ("sub-grid scale turbulence") by the horizontal grid (Reynolds averaged or eddy-resolving computations). The 3D part is referred to as the three-dimensional turbulence and is computed following the turbulence closure model, described in this part. For 2D depth-averaged simulations, the horizontal eddy viscosity and eddy diffusivity coefficient should also contain a contribution due to the vertical variation of the horizontal flow (Taylor shear dispersion).

The horizontal coefficients are an order of magnitude larger than the vertical coefficients determined by the turbulence closure model specified by users. In Delft3D-FLOW, four turbulence closure models have been implemented to determine ν_V and D_V:

- Constant coefficient
- Algebraic eddy viscosity closure model
- k-L turbulence closure model
- k-ε turbulence closure model

The turbulence closure models differ in their prescription of the turbulent kinetic energy k, the dissipation rate of turbulent kinetic energy ε, and/or the mixing length L.

The first turbulence closure model is the simplest closure based on a constant value which has to be specified by you. A constant eddy viscosity will lead to parabolic vertical velocity profiles (laminar flow). The other three turbulence closure models are based on the so-called eddy viscosity concept of Kolmogorov and Prandtl (Kolmogorov, 1942; Prandtl, 1945). The eddy viscosity is related to a characteristic length scale and

velocity scale. The eddy viscosity has the following form:

$$\nu_V = c_\mu' L\sqrt{k} \tag{3.8}$$

where:

c_μ' : a constant determined by calibration
L: the mixing length
k : the turbulent kinetic energy

The "algebraic" turbulence closure model uses algebraic / analytical formulas to determine k and L and therefore the vertical eddy viscosity. No transport equation is involved for the turbulent quantities. This so-called zero order closure scheme is a combination of two algebraic formulations, i.e. the model uses analytical (algebraic) formulas to determine k and L. The turbulent kinetic energy k depends on the (friction) velocities or velocity gradients and for the mixing length, L, a function of the depth is taken.

The third closure model for the eddy viscosity involves one transport equation for k and is called a first order turbulence closure scheme. The mixing length L is prescribed analytically and the same formulation, including damping functions, is used as for the Algebraic Eddy viscosity closure Model. However, to find the kinetic energy k, a transport equation is solved, which is known as the k-L model, or "single equation model".

The fourth is the $k-\varepsilon$ turbulence closure model in which both the turbulent energy k and the dissipation ε are produced by production terms representing shear stresses at the bed, surface, and in the flow. The "concentrations" of k and ε in every grid cell are then calculated by transport equations. The mixing length L is determined from k and ε according to:

$$L = c_D \frac{k\sqrt{k}}{\varepsilon} \tag{3.9}$$

where:

c_D : a constant determined by calibration

3.4.1.2 Result

The tests are carried out in two topics: with/without sediments and algebra/k-ε models to see how these setting will influence the water level and velocity magnitude at the measurement point at Noordwijk offshore 12km.

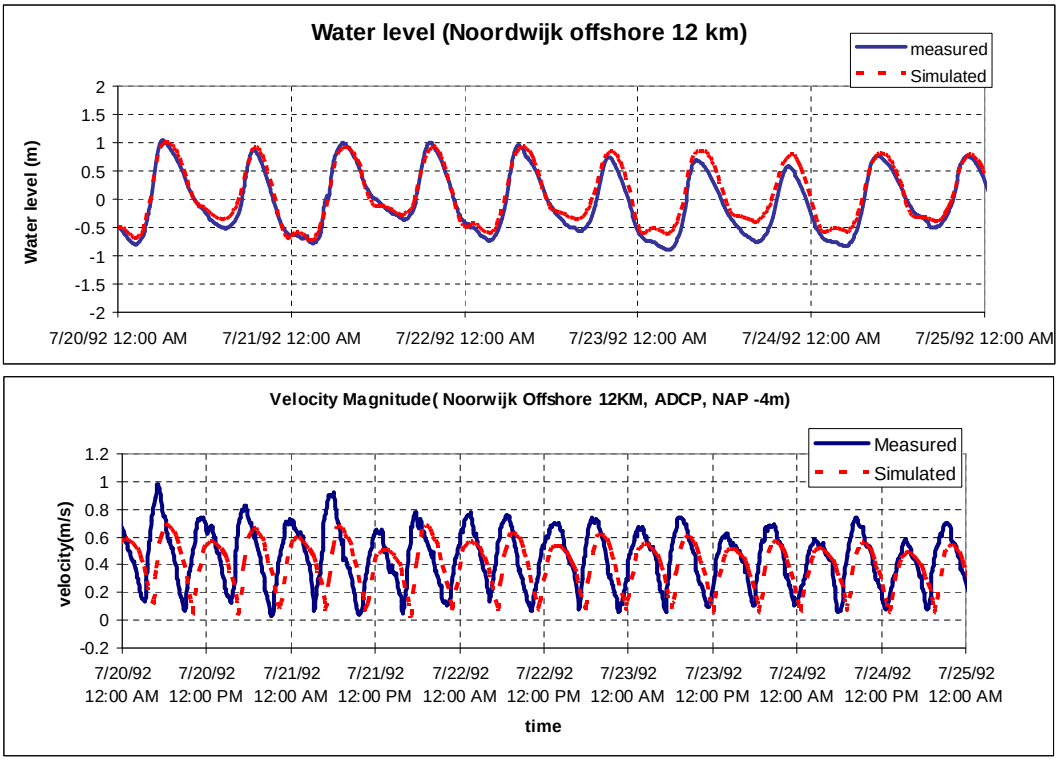

Fig 3.18 Water level and velocity magnitude without sediment process and with Algebraic Eddy Viscosity Closure Model

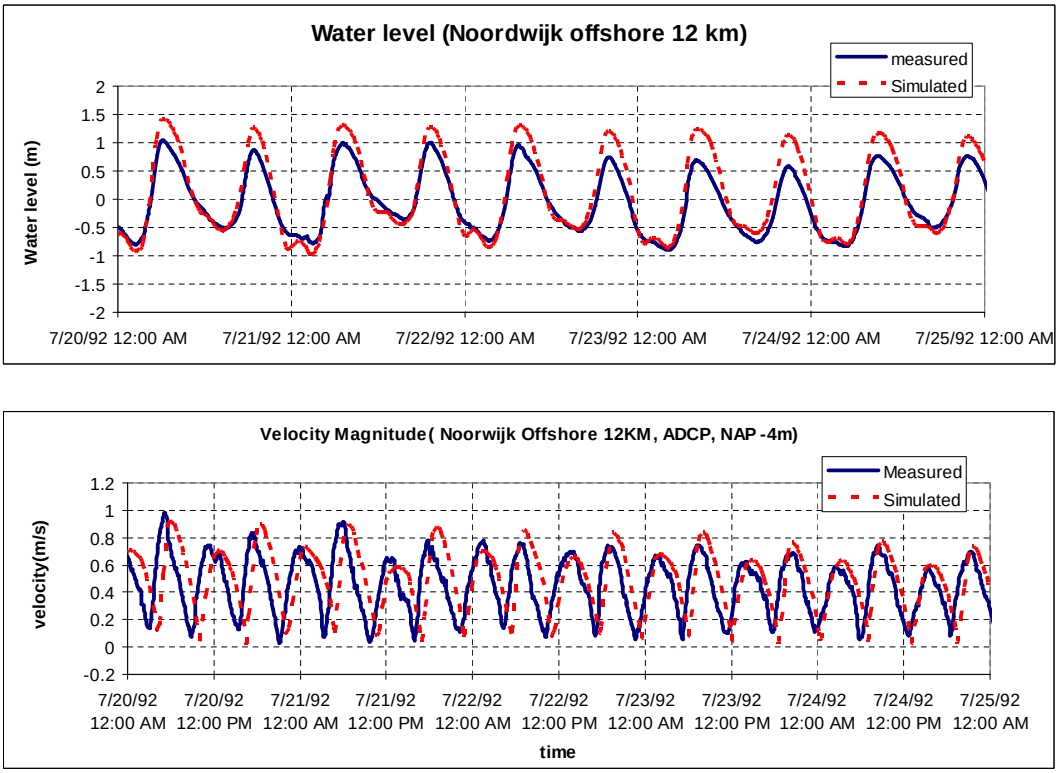

Fig 3.19 Water level and velocity magnitude without sediment process and with k-ε Turbulence Closure Model

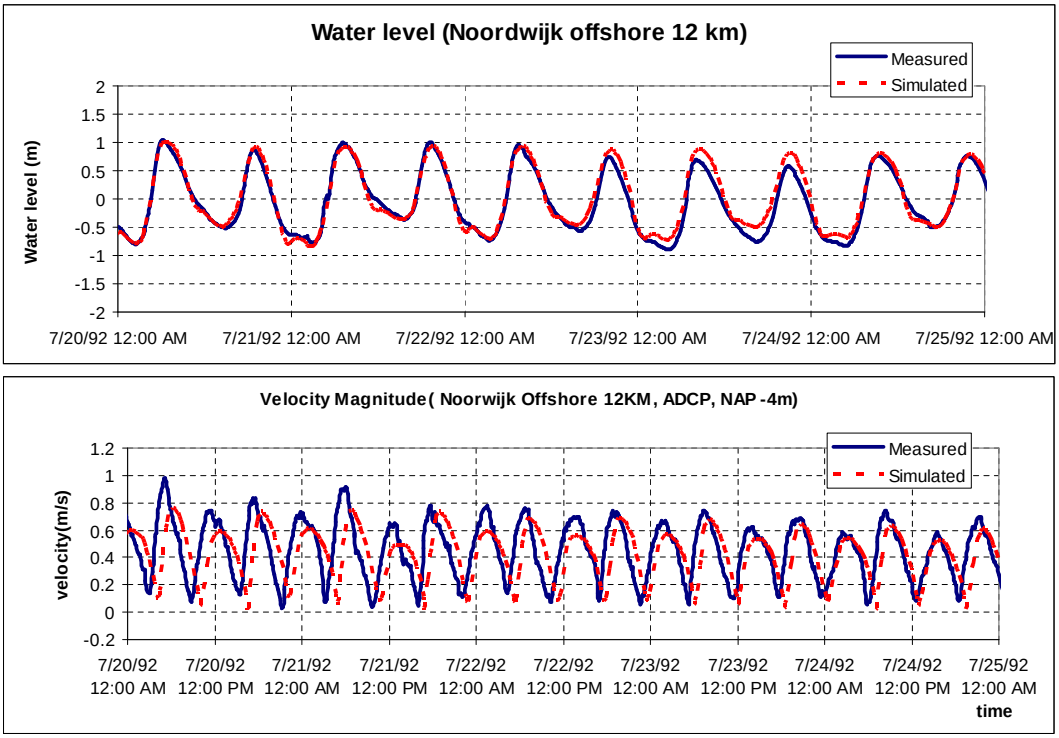

Fig 3.20 Water level and velocity magnitude with sediment process and with Algebraic Eddy Viscosity Closure Model

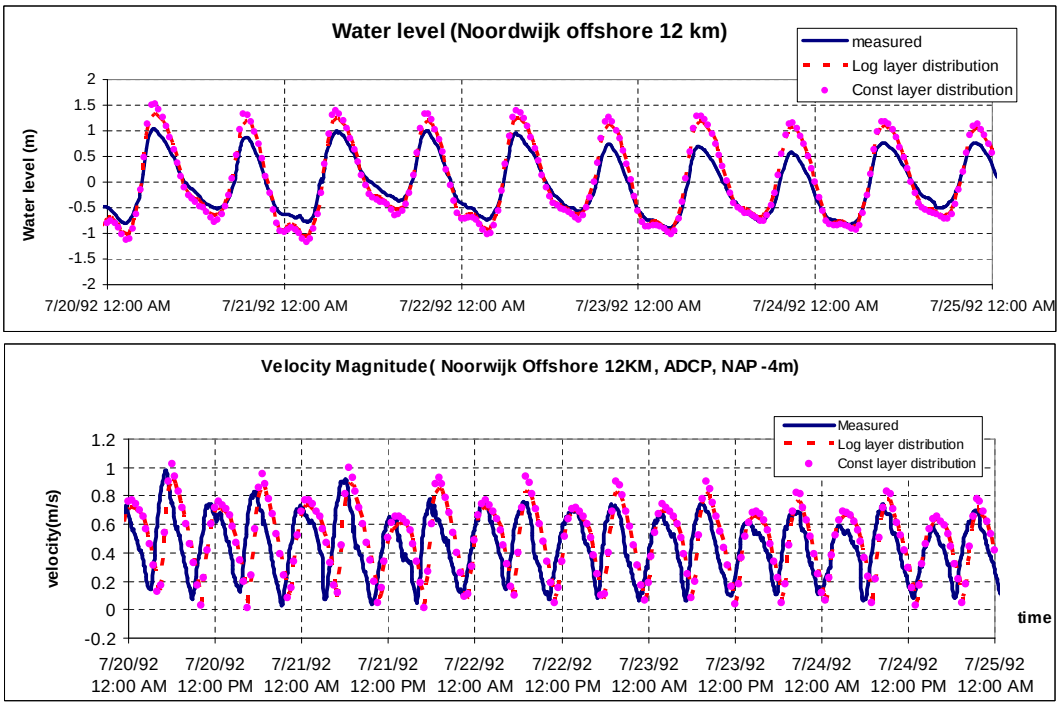

Fig 3.21 Water level and velocity magnitude with sediment process and with k-ε Turbulence Closure Model (with different 3D layer setting: 10 equal thickness layers / logarithmic layer distribution refer to Part 3.2.1)

From the figures list above, the conclusion is:

1. The k-ε closure model did influence the hydrodynamic computation in this 3D case. Fig 3.18 and Fig 3.19 shows the k-ε model overrates the water level and velocity magnitude as well, while the algebraic eddy viscosity closure model underestimates the water level and velocity magnitude, especially during the high water level period.

2. The sediment transportation process hardly effects the hydrodynamic computation in this case. Fig 3.18 and Fig 3.20, Fig 3.19 and Fig 3.21 demonstrate the same shape of water level and velocity magnitude.

3. The vertical layer distribution has positive effect on the accuracy of result. The logarithmic vertical layer distribution provides less discrepancy between the measured water level and velocity magnitude than the averaged vertical layer thickness distribution does. However, the effect is rather limited.

4. The discrepancy of the computed value and measured data in this measurement point may happen due to the coarse grid used for the model, which may be improved by refining the calculation grid.

3.4.2 Effects of the numerical coefficients

DPSOPT is a new numerical coefficient indicated the option for check the water level points, which has 4 options: Mean/Max/Min/From depth point (DP). DPUOPT is the option for the velocity points for choosing the depth at velocity point, which has 3 options: Mean/Min (Mor)/UPWind.

3.4.2.1 Background (WL|Delft Hydraulics, 2005)

Delft3D-FLOW uses a staggered grid (see Figure 2.3). At input the bottom depth can be specified by users at the vertices of a computational cell, the so-called depth points, or in the cell centre, the so-called water level point (DPSOPT=DP).

The DPSOPT=DP –option implies that the position of the depth points is shifted to the water level points. The user should consider this interpretation when generating the depth values with e.g. QUICKIN. To determine the total water depth at water level points, a bottom depth in the cell centre of the Control Volume is required. The bottom depth in a water level point $d^{\zeta}_{m,n}$ is not uniquely defined (Fig 3.22 and Fig 3.23). The algorithm used to determine this depth value from the four surrounding depth points depends on the choice over the four options by users: MEAN, MAX, MIN and DP.

The algorithms to determine the depth in a water level point from the four surrounding

depth points are given by (Fig 3.22):

MAX-option: $d^{\zeta}_{m,n} = \max\,(d_{m.n}, d_{m-1.n}, d_{m.n-1}, d_{m-1.n-1})$ (3.10)

MEAN-option: $d^{\zeta}_{m,n} = 0.25 * (d_{m.n} + d_{m-1.n} + d_{m.n-1} + d_{m-1.n-1})$ (3.11)

MIN-option: $d^{\zeta}_{m,n} = \min\,(d_{m.n}, d_{m-1.n}, d_{m.n-1}, d_{m-1.n-1})$ (3.12)

DP-option: $d^{\zeta}_{m,n} = d_{m.n}$ (3.13)

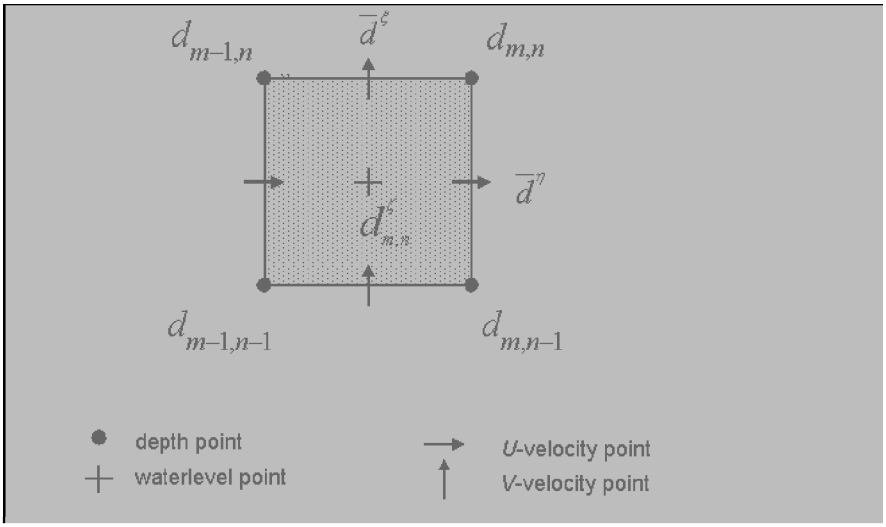

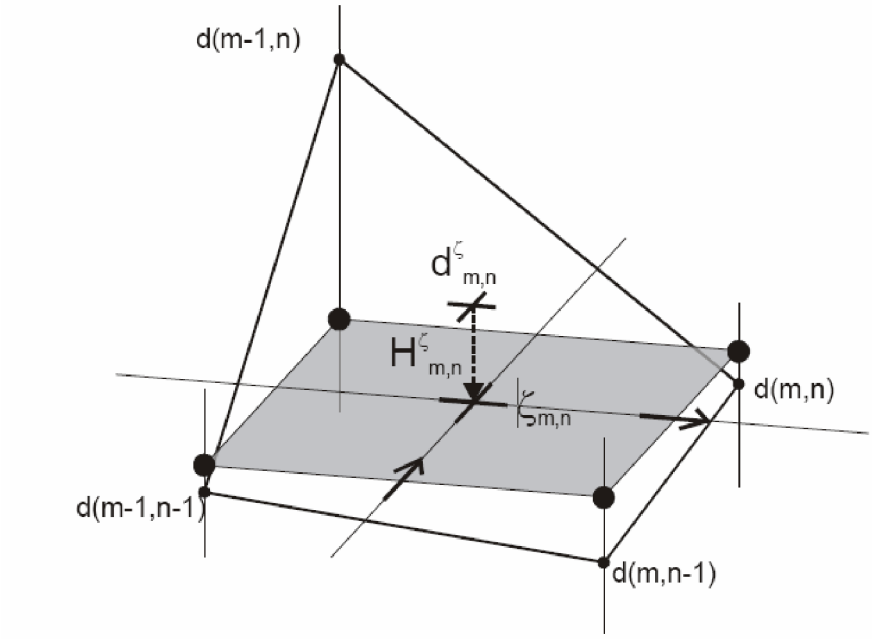

Fig 3.23 Definition bottom depth on FLOW grid in 3D

As to the DPUOPT option, which means the water depth at the velocity point, due to the staggered grid applied in Delft3D-FLOW, the total water depth at a velocity point for the computation of the discharge through a cell face is not uniquely defined. Usually (default option, the marginal threshold water depth at shallow area, DCO= - 999) it is

determined by the arithmetic average of the depth specified in the vertices of the cell face (side) plus the average of the water levels computed in the cell centres at each side of that cell face:

$$H^{U}_{m.n} = \overline{d}^{\eta} + \overline{\zeta}^{\zeta} \tag{3.14}$$

For the depth values at the cell interfaces, dh , you can now choose from the following three options by setting an appropriate value for the input parameter DPUOPT:

DPUOPT = MEAN (default option): $\overline{d}^{\eta} = \frac{d_{m.n} + d_{m.n-1}}{2}$ (3.15)

DPUOPT = MIN(imum): $\overline{d}^{\eta} = \min(d^{\zeta}_{m.n} + d^{\zeta}_{m+1.n})$ (3.16)

DPUOPT = UPW(ind): $$\overline{d}^{\eta} = \begin{cases} d^{\zeta}_{m.n} & if \quad U_{m.n} > 0 \\ d^{\zeta}_{m+1.n} & if \quad U_{m.n} > 0 \\ \min(d^{\zeta}_{m+1.n}, d^{\zeta}_{m.n}) & if \quad U_{m.n} = 0 \end{cases} \tag{3.17}$$

Remark: DPSOPT is DP and DPUOPT is MEAN should not be used together.

3.4.2.2 Result

The model was changed back to 2D to simplify and the result is quite constructive to practice.

Some experiments were carried out as the table listed in the following:

Filename	Dimension	With sediment process	DPSOPT	DPUOPT	Water level	Velocity
theo_origin_92_oneMonth_2d_nsed	2DH	NO	Max	Mean	Good	Good
theo_origin_92_oneMonth_2d_nsed_min	2DH	NO	Max	Min/Mor	Bad	Very good
theo_origin_92_oneMonth_2d_nsed_meanmin	2DH	NO	Mean	Min/Mor	Good	Not bad
theo_origin_92_oneMonth_2d_wsed	2DH	YES	Max	Min/Mor	Bad	Very good
theo_origin_92_oneMonth_2d_wsed_meanmor	2DH	YES	Mean	Min/Mor	Good	Not bad

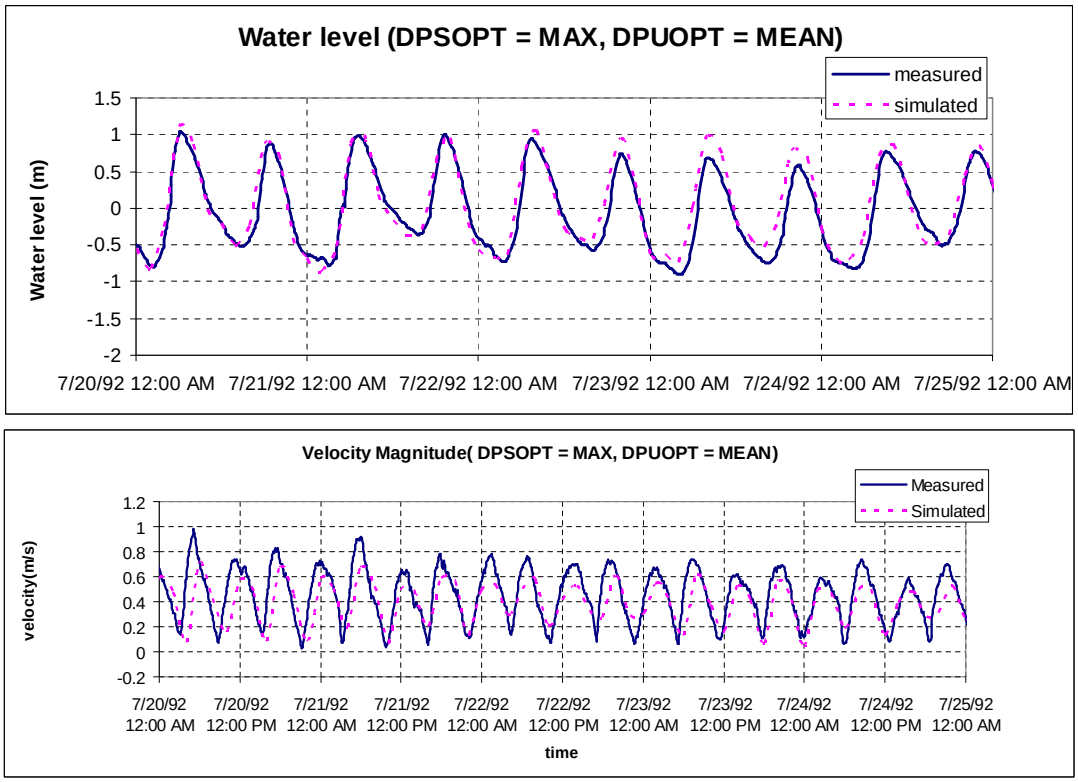

Fig 3.24 Water level and velocity magnitude at Noordwijk offshore 12 km WITHOUT sediment process (the measured velocity data is ADCP NAP -4m data)

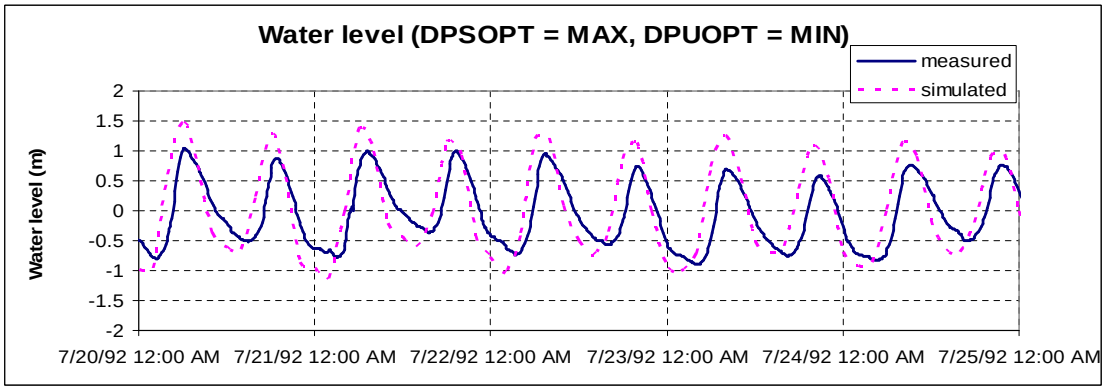

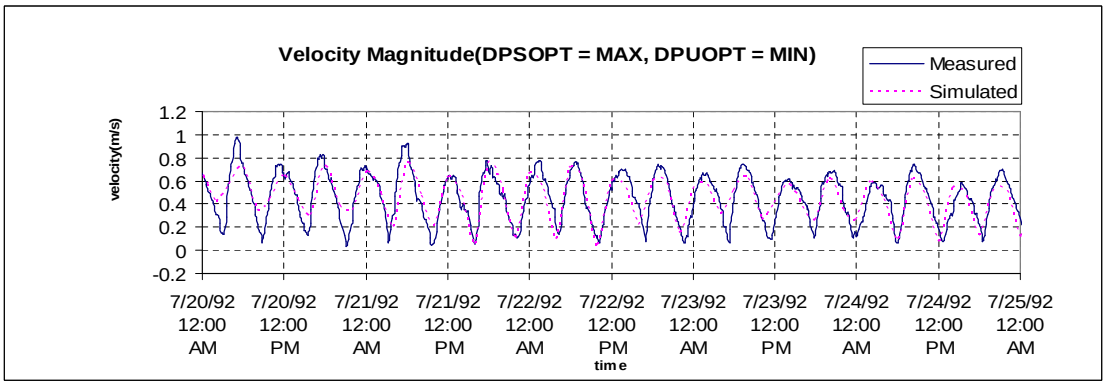

Fig 3.25 Water level and velocity magnitude at Noordwijk offshore 12 km WITHOUT sediment process (the measured velocity data is ADCP NAP -4m data)

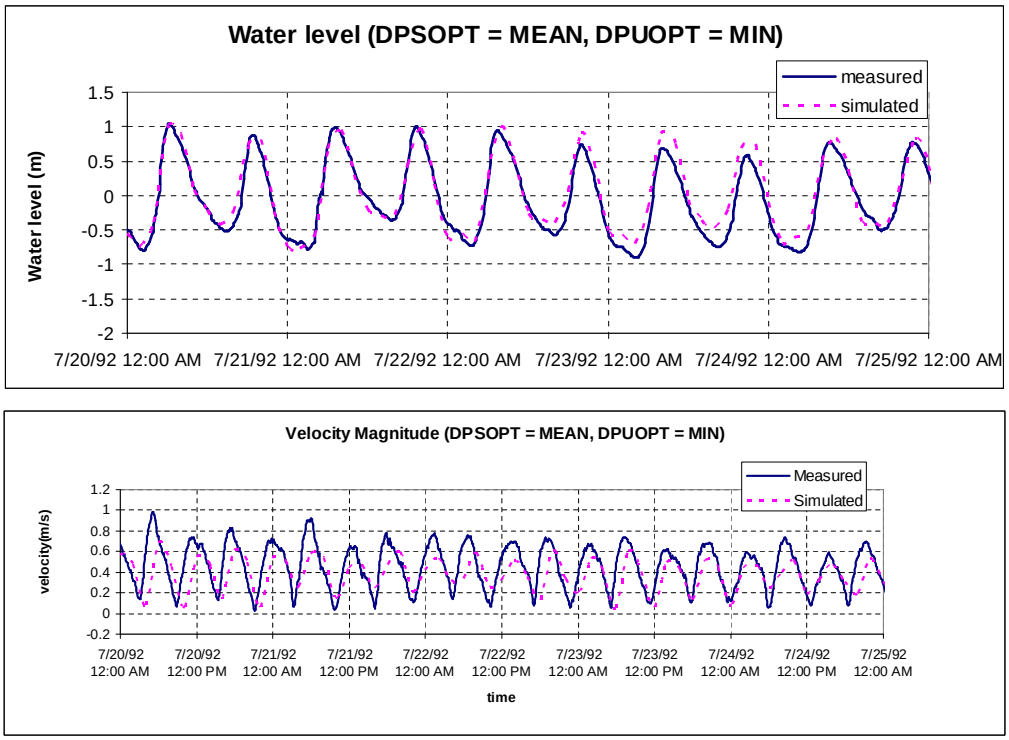

Fig 3.26 Water level and velocity magnitude at Noordwijk offshore 12 km WITHOUT sediment process (the measured velocity data is ADCP NAP -4m data)

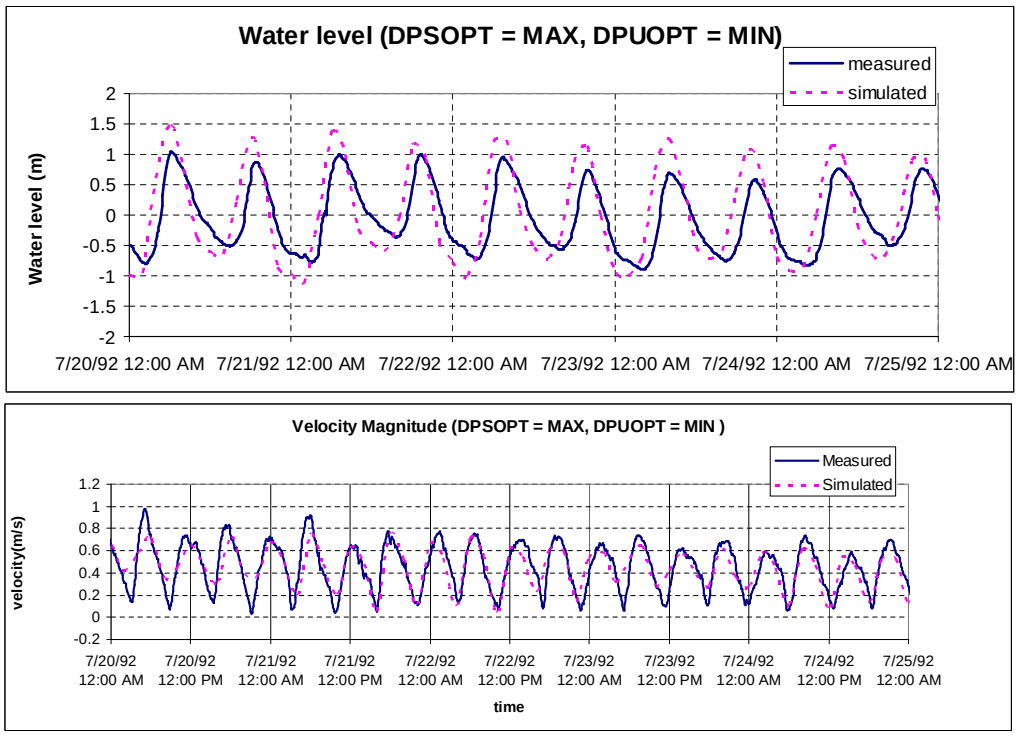

Fig 3.27 Water level and velocity magnitude at Noordwijk offshore 12 km WITH sediment process (the measured velocity data is ADCP NAP -4m data)

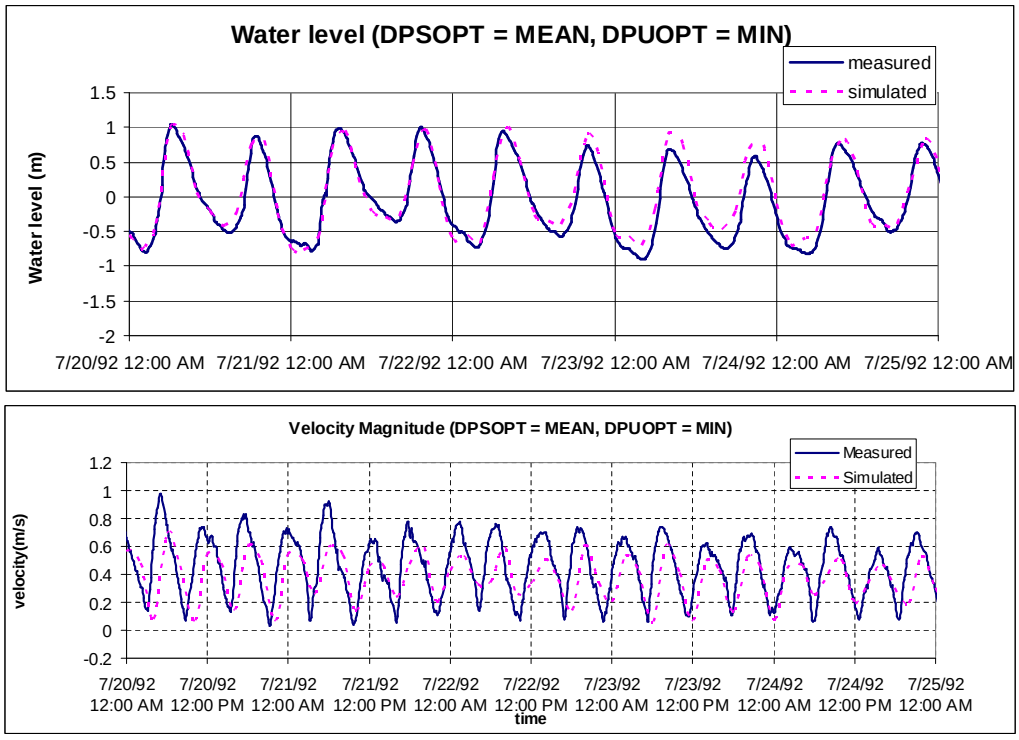

Fig 3.28 Water level and velocity magnitude at Noordwijk offshore 12 km WITH sediment process (the measured velocity data is ADCP NAP -4m data)

From the figures list above, the conclusion is:

It seems obvious that the combination of DPSOPT=MAX and DPUOPT=MIN or MOR leads to a general deepening at the velocity points (Fig 3.25, Fig3.27), whereas this is not the case with the combination of DPSOPT=MAX and DPUOPT=MEAN or with the combination DPSOPT=MEAN and DPUOPT=MIN/MOR (Fig 3.24, Fig 3.26, Fig 3.28). The effects, in a relatively coarse model such as ZUNO, are very severe (30-50% increase in water level amplitude), so it is clear that this combination should not be the default setting and should even produce a warning or error. Some modification of the original default setting for morphological runs to DPSOPT=MEAN and DPUOPT=MIN (Fig 3.26, Fig 3.28), or DPSOPT=DP and DPUOPT=MIN; the second option of course is to provide the parameter in combination with an instruction on how to create a correct bathymetry in water level points.

The sediments process doesn't influence much on the water level and velocity magnitude results (Fig 3.27, Fig 3.28).

3.4.3 Conclusion

Based on the analyses on the measured data and simulation result, some conclusion about the sensitivity test of the ZUNO coarse grid model can be obtained:

- The sensitivity tests on effects of different turbulence closure model shows that the k-ε model overrates the water level and velocity magnitude as well, while the algebraic eddy viscosity closure model underestimates the water level and velocity magnitude, especially during the high water level period in this 3D case. The discrepancies may happen due to the coarse grid used for the model, which may be improved by refining the calculation grid. This is the motivation of the coming study as following parts.

- The sediment transportation process hardly affects the computation result in this case.

- The vertical layer distribution has positive effect on the accuracy of result. The logarithmic vertical layer distribution provides less discrepancy between the measured water level and velocity magnitude than the averaged vertical layer thickness distribution does. However, the effect is rather limited.

- The sensitivity test on the effects of the numerical coefficients depicts that the selection of DPSOPT =MAX and DPUOPT=MIN or MOR leads to a general deepening at the velocity points, which may influence the result of simulation. This test implies that it is necessary to create a correct bathymetry in water level points may be essential to the calibration and verification of the model.

3.5 Wave modeling

The wave model with ZUNO coarse model is setup to simulate the general dynamics.

3.5.1 Grid

The wave modeling here is using the same grid as the flow model (refer to Part 3.2.1 and Fig 3.4).

3.5.2 Boundary condition

The wave model need boundary condition of wave period, significant wave, wave direction etc, which is given by a WAVECON.runid file. In this experiment, the boundary condition is schematized from wave information (significant wave, direction, mean period) at Station AUK-ALPHA (refer to AUKFIELD), having a geographical coordinates NB 56˚24’ OL 02˚04’, provided by Rijkswaterstaat (Mr. Koos Doekes).

At the SWAN model boundary wave period conditions were applied in terms of peak

period, T_p, which is computed as the following in this study (Roelvink, 2001b):

$$T_p = 1.3 * T_{mean} \tag{3.18}$$

Wave boundary conditions are applied as the northern boundary.

Wind boundary conditions from the station of Meetpost Noordwijk. The wind speed has been corrected to the wind speed at 10m height over with open water with roughness length 0.002m, provided by KNMI (http://www.knmi.nl/samenw/hydra)

3.5.3 Coupling with flow model

The wave model is coupled with flow model in this study. The hydrodynamics effects of bathymetry, water level and current have been included from the specified flow module input file. Moreover, some significant inputs are introduced from flow moduel.

3.5.3.1 Time frame

Calculation time point can either be specified by user explicitly or be extracted from the involved flow model implicitly. In case a flow input has been selected, the simulation start and stop time and the time step of the flow simulation are displayed, and then user can choose the calculation time point of wave explicitly. In this study, we choose the second option, which is controlled by the communication output file of flow module or controlled by the MOR module by a tree-like application illustrated in part 3.5.3.4.

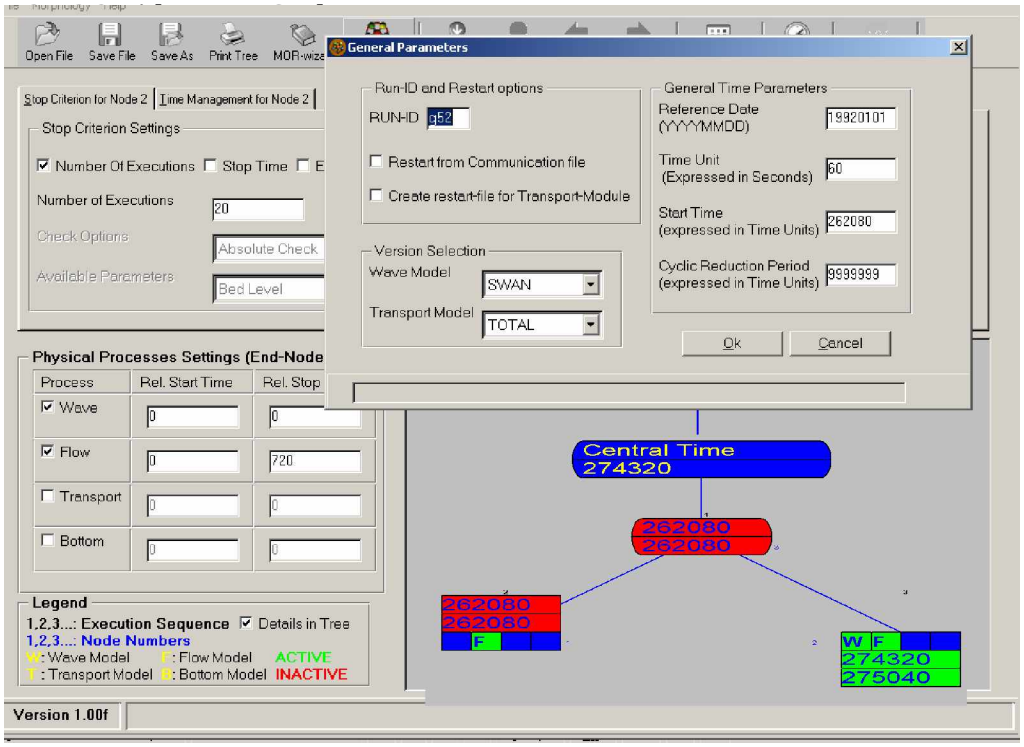

Fig 3.28 The tree-control of wave-tide cycle

The tidal-wave cycle is managed by the mor file, which reflected from in the work flow above. The reference time of tide-wave model is 1992-01-01, and the simulation starting time is from 262080 minutes and then flow will run once and then wave model run once at the calculation point 262080. Subsequently, the flow model will continue calculation for 20 times for another 720 mins, then the wave model will be waken up and calculate for another time point, and so on (Fig3.28). The tide-wave cycle is a simplification of the morphological loop (Roelvink, 1993; Vriend, 1993).

3.5.4 Result

The result shows the model can reproduce the wave pattern as we expected.

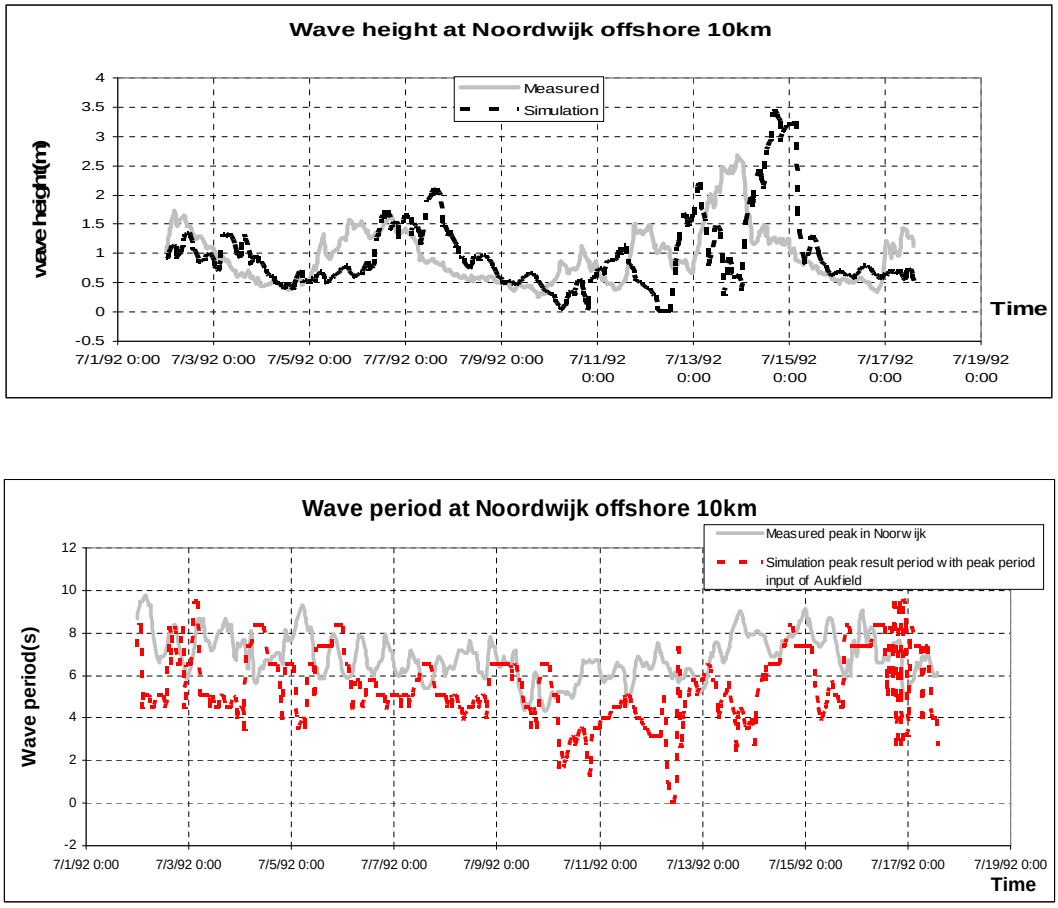

Fig 3.29 the comparison of significant wave height and peak wave period

It is obvious that the magnitude of significant wave height is reproduced, yet there are still some discrepancies of phase of peak wave height. The same characters happened to wave peak period as well (Fig 3.29).

3.6 Discussion and conclusions

As a start of the study, the calibrated model with ZUNO coarse grid provided by WL | Delft Hydraulics was validated with measured dataset of summer time of 1992.

- The wide area tide flow field pattern has been well reproduced. The detailed tidal water level and velocity magnitude has been selected to compare with the measured data in Noordwijk, which indicates that he model reproduced the flow dynamic pattern, even though there is a 1 hour time lag between the simulation and measured velocity magnitude, which may be caused by the given boundary condition time lag, and some discrepancies of the higher water level and lower water level appears. The further sensitivity test showed that may happen because of 2D/3D different numerical processes and different turbulence closure model. However, a constant roughness over the whole area was used in the model, which may be one of the reasons and needs further study.

- Analyses on the measured ADCP data, near the bottom, the long-term residual current has a significant onshore directed component, with values of 0.025 - 0.035 m/s, while near the surface, the long-term residual current is offshore directed. This pattern is ascribed to an estuarine-like cross-shore circulation due to horizontal and vertical variation in the density field related to the outflow of the system. The effect of onshore wind on the cross-shore residual currents shows a characteristic down welling pattern. Near-bottom currents are offshore directed, whereas near-surface currents are onshore directed, both opposite to the persistent density-driven cross-shore pattern.

- Near the surface, long-term residual currents are larger, 0.07 - 0.11 m/s, and are mainly in the alongshore direction with an onshore component increasing with distance from shore. Variability in the alongshore residual current is correlated to variations in the alongshore wind stress, particularly for the near-bottom currents.

- The simulation accurately reproduced the alongshore residual flow and cross residual flow pattern.

- Sensitive test showed that the effects on difference turbulence closure model is quite remarkable, which will introduced arguments on the benefit of 3D model, and need further proof. The tests on the numerical coefficients show that some of the default setting of Delft3D needs detailed tuning under different conditions, which can cause significant difference between the simulation and reality.

- Wave modeling coupled with the model showed the wave period and significant wave height at the verified point are acceptable. Apparently, there are some discrepancies which show that, to such a big area, the wave field is affected by so many factors.

The ZUNO grid model reproduced the flow and wave pattern over such a big area, though there are some discrepancies exist and need further study.

The following chapters listed two solutions to study the area and the wave force and mud transportation in detail. One is to use the finer grids to cover the interest area and coarser grid to cover surrounding area, which is termed as Domain Decomposition technology (Chapter 4). The other is to use a schematized model to formulate the main dynamics in the field and the responding mud dynamics (Chapter 5).

Part 4 Refined grid model with domain decomposition

The right flow pattern and wave dynamics has been verified with coarse ZUNO grid model, while the model is not accurate model to study the detailed information of sediments transportation pattern in the specific small area. For instance, the Haringvliet Mouth only occupies one single element in the coarse ZUNO model. There appears a problem obviously that a coarse grid model can not be used to study such a small area, such as the Haringvliet Mouth.

To model the flow dynamics and cohesive sediments in the relatively small area, the Haringvliet Mouth, a model with finer grid is needed. There are two approaches to achieve this objective: one is to use the refined grid technology, termed as domain decomposition in Delft3D framework, which is studied in this part, the other is to use a schematized model, which has a smaller model domain with finer grid, which is considered in the next part (Part 5).

The overall objective of this chapter is to get the right pattern of sediment movement under wave dynamics by refining the existing ZUNO model using domain decomposition technology. The first step is to setup the grids in the decomposition domain and setup the models to reproduce the flow field patterns with calibration and verification. The second step then is to add the wave model coupling with flow model.

4.1 Introduction of study area and data

4.1.1 General information of domain decomposition technology

Domain decomposition is a technique in which a model domain is subdivided into several smaller model domains, which are called *sub-domains*. The subdivision is based on the horizontal and vertical model resolution required for adequately simulating physical processes. Then, the computations can be carried out separately on these sub-domains. The communication between the sub-domains takes place along internal open boundaries, or so-called *dd-boundaries*. If these computations are carried out concurrently, we speak of parallel computing. Parallel computing will reduce the turn around time of multiple domain simulations (WL|Delft Hydraulics, 2005).

Domain decomposition is widely recognized as an efficient and flexible tool for the simulation of complex physical processes. The advantages of a multi-domain modeling approach for flow and transport problems can be summarized by:

- Flexibility

It can help to combine two or more different models by integrating the grids, which can be generated separately, or as shown in Fig 4.1, to combine models in different dimensions.

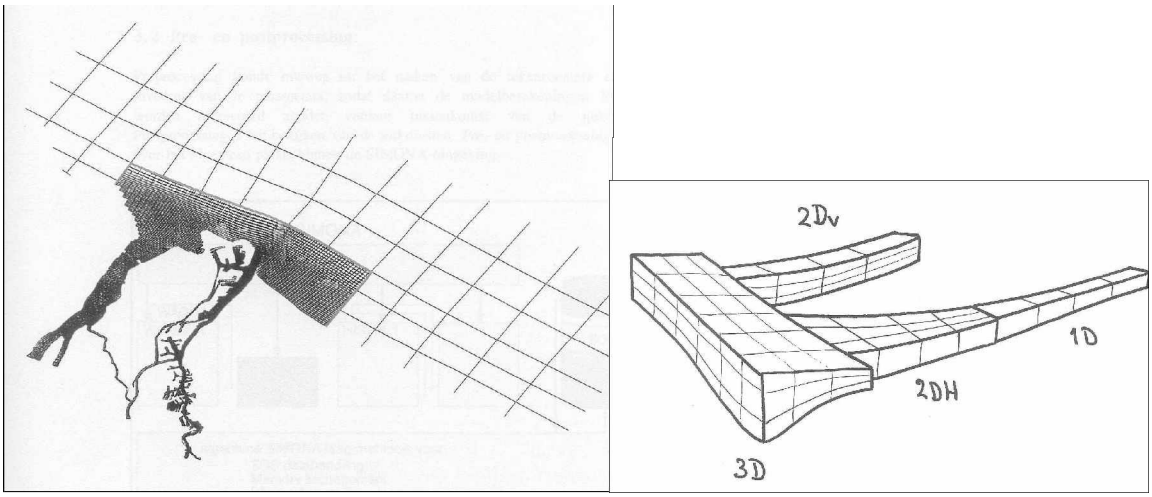

Fig 4.1 Examples of coupling with different grid size and dimensions

§ Accuracy

Because the area can be covered by different size grids and interested area can be covered with refined grid, the whole area can be covered smoothly, thus the model will represent the reality in higher accuracy.

§ Efficiency

During the computation of smaller sub-domains, memory demands will be reduced with smaller computation loads. In addition, the computation on the sub-domains can be carried out in parallel. Such a modular approach can be better from software engineering and maintenance point of view.

4.1.2 Study area and data

The study area covers ZUNO coarse grid area as well, i.e. the ZUNO grid is refined locally by the decomposition grids.

The area is refined based on the ZUNO coarse grid and RIJMAMO grid provided by WL | Delft Hydraulics, which is a very fine grid and need extremely high computational abilities that is not suitable for this study. Thus the computation grid is generated based on the RIJMAMO grid, and the grid covered the interest area - Haringvliet Mouth was refined with surrounding area covered by relatively coarse grid (Fig 4.2).

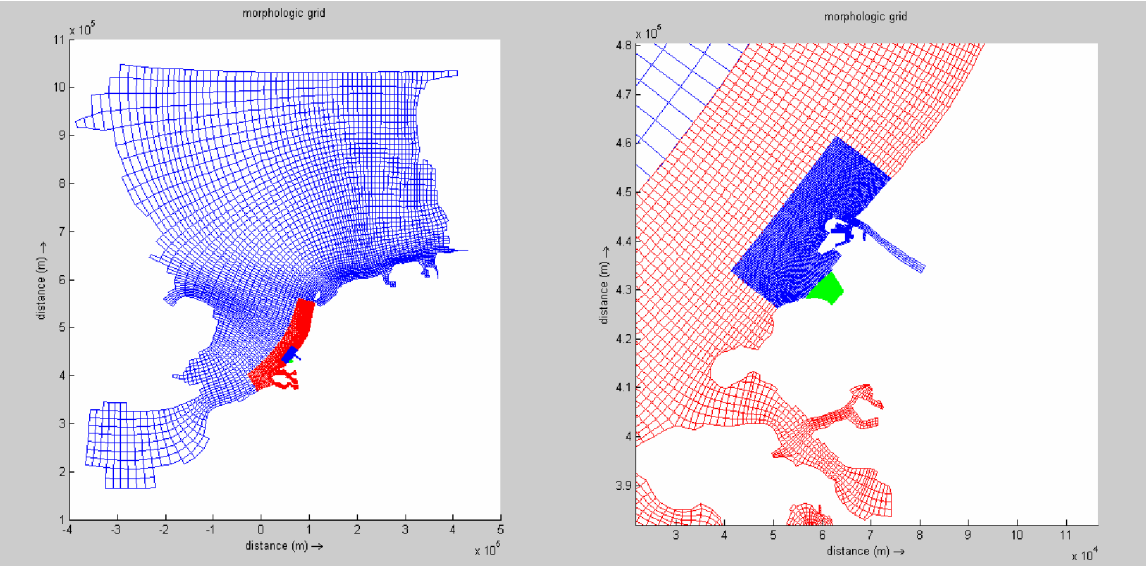

Fig 4.2 Four sets of grid covers the research area in this study.

4.2 Models setup

As mentioned above, the model, combined four models, can be set up separately.

4.2.1 Grid

The grids are generated based on ZUNO coarse grid and RIJMAMO fine grid. The grids are named CS0-CS3, where the CS0 grid is the coarsest with the element size of 6km*8km, subsequently, the element size of CS1 is about 3km*2km, and CS2 is 400*150m, CS3 is 120m*60m , which cover the Haringvliet Mouth area exactly.

4.2.2 Bathymetry

The bathymetry of CS0 set is using with the previous bathymetry given with ZUNO grid. In addition, the finer grid bathymetry CS1 and CS2 are provided by a even finer RIJMAMO grid by WL | Delft Hydraulics (Winterwerp, 2005). The finest grid is provided by RIJMAMO grid and is modified following paper map manually.

There are also some other limitations for the bathymetry at the boundary where the decomposed domains meet each other. First of all, the depth values at sub-domain interfaces in corresponding depth points should be identical in both domains. Furthermore, for the refined model, it is proposed that the depth values in the intermediate points are determined by linear interpolation.

4.2.3 Boundary conditions

The boundary conditions of the CS0 grid model, which covers the open boundary of all the other sub-domains, is given by prescribed water level, by means of tidal constant, amplitudes and phases of tidal constitutes, in every element of the open boundaries (refer to Part 3.2.3).

The internal boundary conditions for the finer grid model are passed by the adjacent bigger grid model, which infer the computation of all the domains are computed in parallel.

4.2.4 Domain decomposition information

Some special demands like the following should be noticed (WL|Delft Hydraulics, 2005):

- Each model file (*.mdf) should satisfy the requirements for a single domain Delft3D-FLOW simulation.
- In all sub-domains the same simulation period and time step should be used.
- In all sub-domains the same processes for transport should be used (e.g., salinity and temperature). Nevertheless, that turbulence processes may vary (e.g. $k-\varepsilon$ in one domain and an algebraic turbulence model in another domain).
- No permanently dry points are allowed along sub-domain interfaces. And temporary dry points are allowed.
- Thin dams may be specified perpendicular to a sub-domain interface, but not parallel.
- Part of Delft3D-FLOW functionality does not work in combination with domain decomposition, for example, Real Time control (RTC), Online coupling with water quality module, Z-model (strictly horizontal layers), Internal Wave model, etc.
- It is strongly advised to avoid special points (hydraulic structures) at sub-domain interfaces.
- Though not strictly necessary it is advised to have the output timings the same in all sub-domain models.
- Online visualisation can be activated for each sub-domain.
- If users want to visualise all domains in the online visualisation, the menu: *Output – Refresh screen at each step* should be turned off.

An additional input configuration file (<model_id.ddb>) is required, which specifies all sub-domains couplings and the location of the interfaces (dd-boundaries).

In this study, four sub-domains are coupled in 7 boundary lines, and the file is edited as following:

cs1.grd 31 118 1 118 cs0.grd 45 71 35 71
cs0.grd 35 71 35 32 cs1.grd 1 118 1 1

```
cs0.grd   35   32   43   32  cs1.grd    1    1   25    1
cs2.grd   91   85    1   85  cs1.grd   31   59   16   59
cs1.grd   16   59   16   38  cs2.grd    1   85    1    1
cs1.grd   16   38   29   38  cs2.grd    1    1   79    1
cs2.grd   97   30   97   14  cs3.grd    1   65    1    1
```

And then the pre-process file, tdatom.exe, is used to process the grids based the coupling information listed above before the simulation.

4.3 Wave modelling

As mentioned, the processes with domain decomposition grids should be identical. The wave process is included in the model and the processes are called in the batch file as the following code:

```
// pre-process the grids
echo %runid% > runid
echo === start tdatom.exe for %runid% ===
%exedir%\tdatom.exe
echo === end tdatom.exe for %runid% ===

// simulation process of flow
echo === start trisim.exe ===
start %exedir%\trisim.exe %ddboundfile% >  tri-cs0.scr
echo === end trisim.exe ===

//simulation process of wave
echo === start waves.exe ===
%D3D_HOME%\%ARCH%\wave\bin\waves.exe cs0.mdw 1 >  wav-cs0.scr
echo === end waves.exe for %runid4% ===
```

The nested model is used for in the wave model in this case (Fig 4.3).

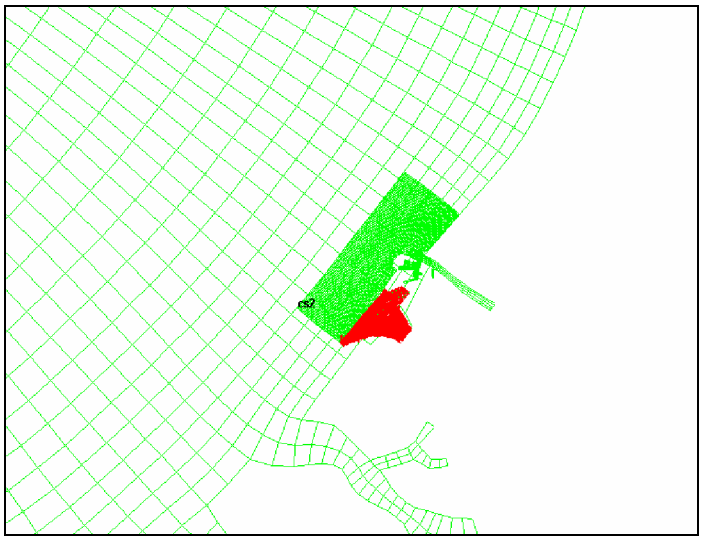

Fig 4.3 Three grids are nested used for wave simulation model

4.4 Discussion and conclusions

The refined grid model with domain decomposition has been setup and some runs have been carried out. The area is described with much more detailed results, as we expected. The problem caused by the ZUNO coarse model has been solved by imposing another problem for modellers: the simulation is quite time-consuming, which can be foreseen since more grids need more computational time for the finer grids model. A 5-days simulation need about 40 hours for wave and flow process.

Because of time limitation of the study, the refined grid model with domain decomposition is paused.

Nevertheless, it is a good try to use the domain decomposition to get a compromised between the simulation processes and simulation time. It allows modellers to refine the interest area only, which can save quite an amount of time.

Another possible approach is to use a schematized model which has a smaller model domain with finer grid, which is considered in the next part (Part 5). The model domain is relatively small, and the processes in the model are regarded meso-spatial and meso-temporal. Since the total number of computational elements is smaller, the schematized model needs shorter time with same physical processes.

Part 5 Schematized model

The modellers always have the difficult dilemma when they need to get compromise between the simulation time and the detailed physical processes. On one hand, if the time limitation is satisfied, the model may be non-realistic. On the other hand, modellers intend to involve processes as much as possible to expose the intrinsic rules underneath the phenomena, which means that a more complicated model will be introduced and more computational time is needed, which is always restricted.

A schematized model is just such a concession, with smaller area compared with coarse grid ZUNO model, which covers 70 km area along the middle and southern part of Dutch coast, and tide, wave and wind dynamics with cohesive sediment transportation and salinity processes in acceptable short time. As described above, the boundary conditions are provided by the macro scaled coarse grid ZUNO model.

With delicate setting of boundary conditions, the schematized model provides correct tide, wave and wind dynamics. Subsequently, the right pattern of suspended sediment movement under tide, wave and wind dynamics will be achieved.

The case study is carried out in two steps. The first step is to setup the schematized flow model in a relative small area, and wave model in a comparatively big area (Fig 5.1), then calibrate them with measured wave characters. The second step then is to calibrate the sediment model to get the reasonable transportation, deposition and resuspension pattern of cohesive sediments due to the wave effect. The measured suspended sediment concentration will be compared with the simulation result in some points in the Haringvliet Mouth.

5.1 Introduction of study area and data

Some researchers, De Vriend (1991), Odum (1996), and others, argued that the increasingly detailed process knowledge and modelling capabilities on the small scale will not inevitably lead to correct the prediction of processes on a larger scale, due to emerging non-linearity, unpredictable events and omission of processes that were not relevant at the smaller scale.

Roelvink et. al. (2005b) supported that the application of existing 2DH/3D models is hampered by the fact that they are considered to be difficult to setup, time-consuming to run, have unstable or unpredictable behaviour and are consequently difficult to calibrate to realistic solutions even with more processes. In other words, a consultant or modeller is better off using a simple, predictable model, other than doing an expensive exercise with a complex model if the results are unreliable or only cover weeks instead of years, which is needed for the model time scales.

This is exactly the case when the suspended sediment in Haringvliet Mouth area is

considered. For the complexity of the dynamics of the cohesive sediment and coastal zone area, the model needs quite a number of dynamic processes to be involved, even though, the model is quite simplified compared with the real conditions, which demands much on the computation capacity and no guarantee for better results.

A schematized model has some advantages, yet, the boundary condition should be manipulated deliberately to make the whole system behave close to reality. In this study, harmonic tidal forcing and real time wind, waves and discharge from the Haringvliet Sluice and the Nieuwe Waterweg is used for the flow field simulation.

5.2 Models setup

In this case, two coupling models are involved, flow model and wave model.

5.2.1 Flow model

5.2.1.1 Grid

The grid for the flow model is relatively finer in the Haringvliet area and coarser in the adjacent area.

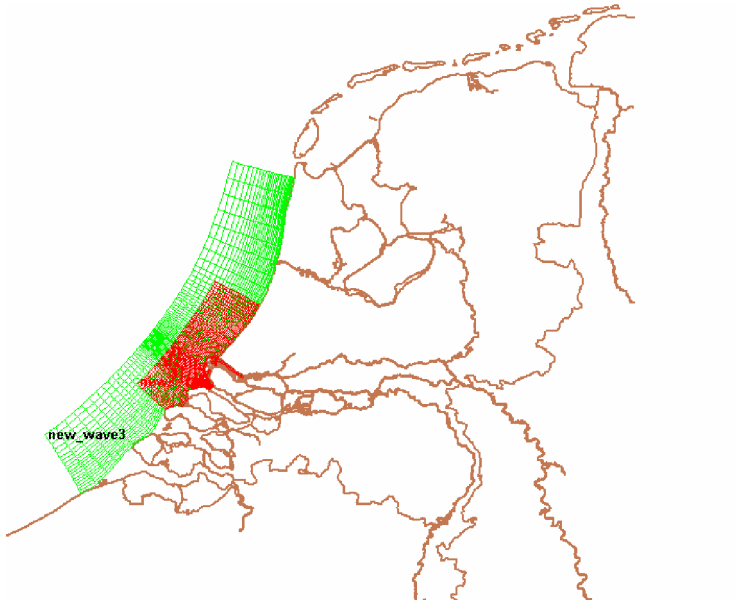

Fig 5.1 Wider wave grid and smaller flow grid

5.2.1.2 Bathymetry

The bathymetry of flow is using the previous bathymetry given with ZUNO grid. In addition, the detailed bathymetry in the Haringvliet Mouth is provided by a more finer RIJMAMO grid of WL | Delft Hydraulics (Winterwerp, 2005).

5.2.1.3 Boundary conditions

5.2.1.3.1 Open boundary

Some problems at lateral boundaries are caused by the specific model grid because, due to the combination of the processes in the domain, a certain water level or velocity distribution will develop in the cross-shore direction. If the boundary value is not known beforehand, the boundary disturbance will be introduced.

This kind of boundary condition can be solved in two ways. One is to predict the water level setup or the current velocity along the lateral boundary by solving a 1DH or 2DV problem along the boundary. In simple cases, it helps, however, while for more complex combinations, it is too cumbersome. Another simpler way is to let the model determine the correct solution at the boundary by imposing the alongshore water level gradient (a so-called Neumann boundary condition) (Roelvink, 2005b).

The alongshore gradient, which is very small when the cross-shore extent is limited, can be always assumed to be zero, except for the water level gradient, which is not negligible in case of tidal forcing.

So, the equations to solve the water level and velocity in alongshore and cross-shore directions are:

$$\frac{\partial \eta}{\partial n} = f(t) \tag{5.1}$$

$$\frac{\partial u_s}{\partial t} + u_s \frac{\partial u_s}{\partial s} + u_n \frac{\partial u_s}{\partial n} = -g \frac{\partial \eta}{\partial s} + f_{cor} u_n + \frac{\tau_{winds}}{\rho h} + \frac{F_{waves}}{\rho h} + \frac{R_s}{\rho h} - \frac{\tau_{bottoms}}{\rho h} \tag{5.2}$$

$$\frac{\partial u_n}{\partial t} + u_s \frac{\partial u_n}{\partial s} + u_n \frac{\partial u_n}{\partial n} = -g \frac{\partial \eta}{\partial n} - f_{cor} u_s + \frac{\tau_{windn}}{\rho h} + \frac{F_{waven}}{\rho h} + \frac{R_n}{\rho h} - \frac{\tau_{bottomn}}{\rho h} \tag{5.3}$$

where:

η : the water elevation
u: the velocity
g: the acceleration of gravity
f_{cor} : the Coriolis coefficient
τ_{wind} : the wind stress
F_{wave} : the wave stress
R: the Reynolds stress
τ_{bottom} : the bed shear stress
h: the water level
ρ : the water density

The circled terms are neglectable at the boundaries. The advection terms containing

across-shore gradients of the velocity $u_s \frac{\partial u_s}{\partial s}$ and $u_s \frac{\partial u_n}{\partial s}$ are not neglected, as they are important during the spin-up of the model or in in-stationary conditions, or in 3D simulations.

The *s* direction, along the boundary, is perpendicular to the shoreline, while the *n* direction is along the shoreline (Fig 5.2).

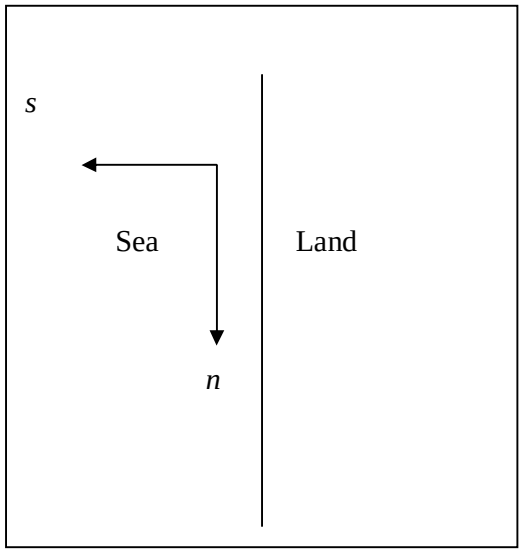

Fig 5.2 The *s*, *n* direction definition

In the case of tidal wave propagating along the coast, the tidal water level can be described as the following:

$$\eta(s,t) = \sum_{j=1}^{N} \eta_j \cos(w_j t - k_j n - \varphi_j) \tag{5.4}$$

where:

η_j : the amplitude of the j-th component,

ω_j : the angular frequency

k_j : the alongshore wave number of the tidal component

n : the alongshore distance

φ_j : phase lag

Then the alongshore gradient is:

$$\frac{\partial \eta}{\partial s}(s,t) = \sum_{j=1}^{N} k_j \eta_j \sin(w_j t - k_j n - \varphi_j) = \sum_{j=1}^{N} k_j \eta_j \cos(w_j t - k_j n - \varphi_j - \frac{\pi}{2}) \tag{5.5}$$

In this case, the area dimension is about 70km alongshore from Noordwijk to Schouwen and 30km in cross shore direction. The tidal amplitudes are extracted from the result of

the coarse grid ZUNO model based on scale linage theory described above (Part 1.4.1). The tidal alongshore wave length is 400km.

Then wave number $k = {2\pi}/{400km} = 1.57*10^{(-5)}$

And phase lag is: $\varphi = {70}/{400km} * 360^{o} = 63^{o}$

The phase lag for the gradient is : $63^{o}+90^{o} = 153^{o}$.

Thus the boundary conditions are set as Table 5.1.

Table 5.1 Boundary condition in the schematized model

Boundary	**Type**	**Frequency**	**Amplitude begins**	**Phase begins (deg)**	**Amplitude ends (m/s)**	**Phase ends (deg)**
North	Von Neumann	30	$1.33*10^{-5}$ (m/s)	153	$1.33*10^{-5}$ (m/s)	153
South	Von Neumann	30	$2*10^{-5}$ (m/s)	153	$2*10^{-5}$ (m/s)	153
SeaSide alongshore	Water level	30	1.28 (m)	0	0.85 (m)	63

The water levels at both boundaries are extracted from the result of the coarse grid ZUNO model based on scale linage theory described above (Part 1.4.1).

Measured discharge data from Niuewe Waterweg is used as operational boundary.

5.2.1.3.2 Boundary of Haringvliet Sluice

It is known that the Haringvliet Sluice opens now and then to the sea and this influences the Haringvliet Mouth area, especially during the ebb tide period.

The data of the operation of Haringvliet Sluice has been interpolated from 1 day interval value to every 6 minutes during the ebb tide period (Fig 5.3, Fig 5.4).

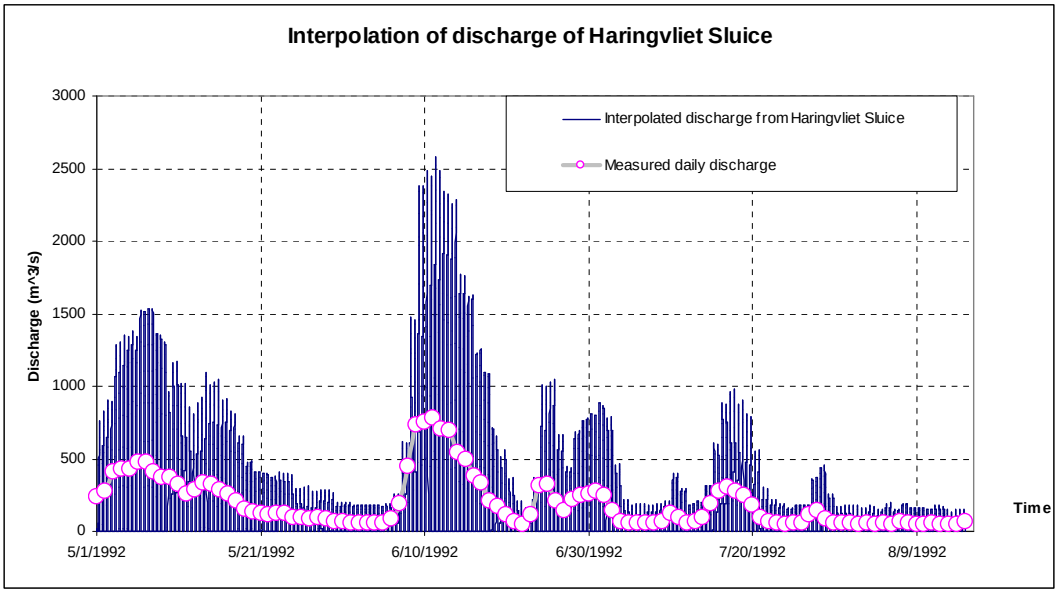

Fig 5.3 The interpolated discharge from Haringvliet Sluice

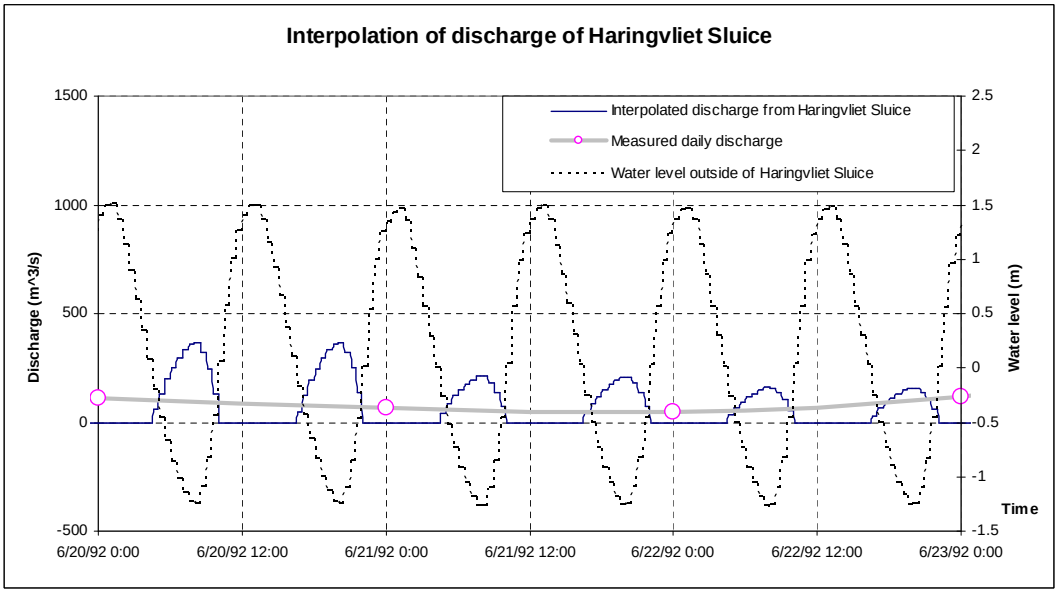

Fig 5.4 The interpolated discharge from Haringvliet Sluice during ebb tide period

5.2.1.3.3 Boundary of salinity process

The salinity process is essential to the dynamics of transportation, deposition and resuspension of cohesive sediments due to its characteristics. It is included in the model with a boundary value of 30ppt at the seaside, and 0ppt at the river side.

5.2.1.3.4 Boundary of suspended sediments

The SPM concentration boundary at the south boundary is set followed the measured

time series at the point called Schouwen 20 km uit de kust from Rijkswaterstaat (www.waterbase.nl) (Fig 5.5). The model simulation starts from May 1st to Aug 15th, during which not so many measurements happened. The interval values between the measurements are interpolated linearly.

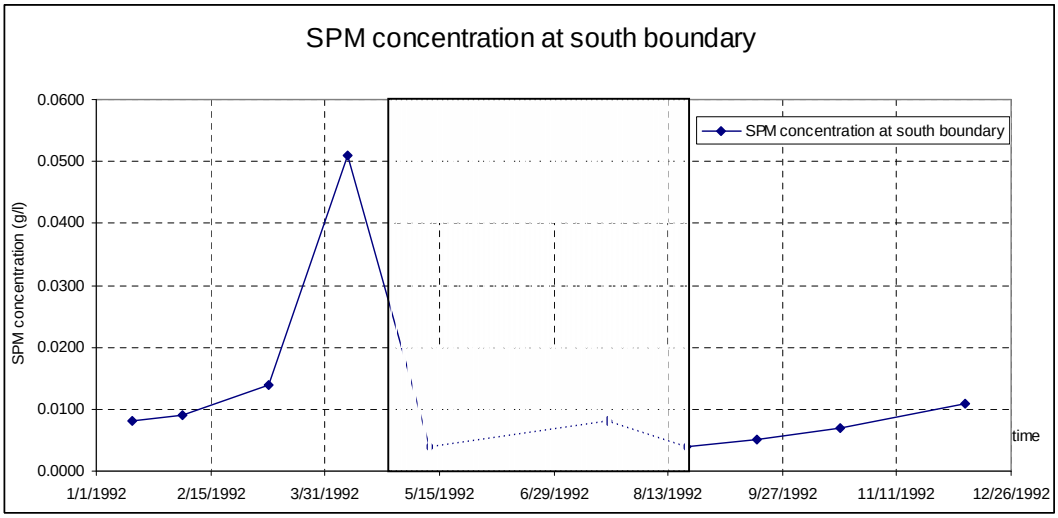

Fig 5.5 The SPM concentration at the south boundary (The shade shows the model simulation time window)

5.2.2 Wave model

5.2.2.1 Grid

The wave grid covers much bigger area and coarser than the flow grid.

5.2.2.2 Bathymetry

The bathymetry of wave is using the previous bathymetry given with ZUNO grid. In addition, the detailed bathymetry in the Haringvliet Mouth is provided by a more finer RIJMAMO grid of WL | Delft Hydraulics (Winterwerp, 2005).

5.2.2.3 Boundary for wave model

Measured wave (provided by www.waterbase.nl) and wind condition (provided by www.knmi.nl) during the whole year of 1992 in Europlatform are used as wave boundary (Fig 5.6).

Due to some reasons, there are some vacant values during Aug 26th to Sept. 21st, Sept 24th to Sept 27th, Dec 6th to Dec 16th,1992. With the data from real wave climate website (www.golfklimaat.nl/data), some storm events are found during those time interval, which are selected as the verification data for the schematized model in Part 5.4.

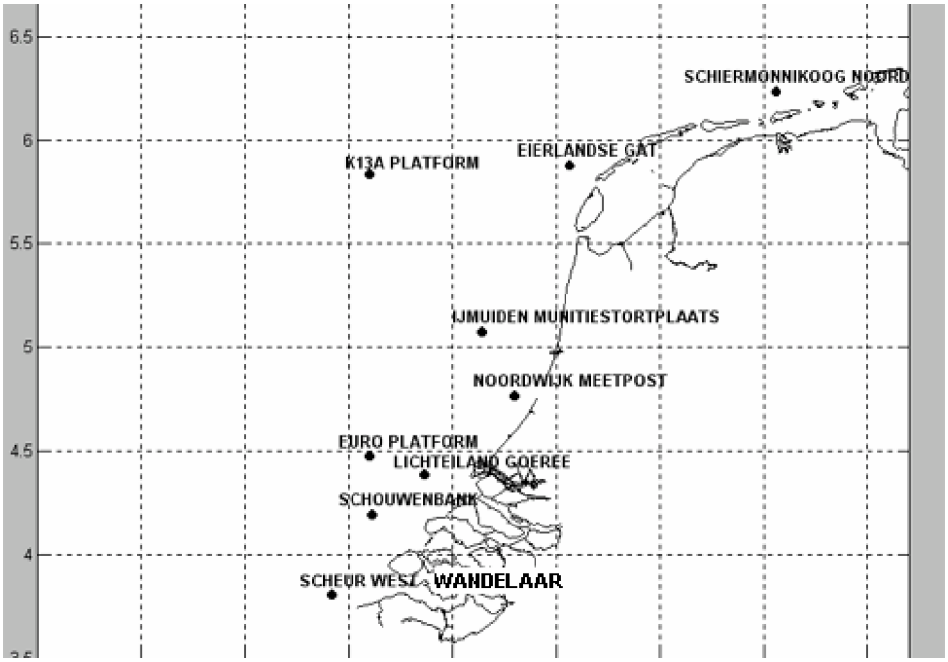

Fig 5.6 Location of Euro Platform

5.3 Model calibration

5.3.1 Calibration of hydrodynamic model

The parameters for flow model are listed as table 5.2:

Table 5.2 Parameters calibrated in the flow model

Parameter	Value	Lower limit	Upper limit	Unit
Gravity	9.81	9.5	12.0	m/s^2
Water density	1023	900	1500	kg/m^3
Air density	1.25	0.5	1.5	kg/m^3
Temperature	15	0	60	ºC
Salinity	30	0	100	ppt
Wind drag coefficient 1	0.00063	0	1	-
Wind drag coefficient 2	0.00723	0	1	-
Wind speed 1	0	0	100	-
Wind speed 2	100	0	100	-
Roughness Manning	0.026	0	0.04	-
Horizontal Eddy viscosity	1	0	100	m^2/s
Horizontal eddy diffusivity	10	0	1000	m^2/s
Vertical eddy viscosity	0.0001	0	100	m^2/s
Vertical eddy diffusivity	0.0001	0	1000	m^2/s

Parameters for wave model (WL|Delft Hydraulics, 2006) (Table 5.3):

Table 5.3 Parameters calibrated in the wave model

Parameter	Options	Value in this case	Units
Hydrodynamics involved in wave	Bathymetry	Yes	-
	Water level	Yes	-
	Current	No	-
Acceleration of gravity	9.8-10	9.81	m/s^2
Density of water	950-1050	1025	kg/m^3
North	-	90	deg
Minimum depth	-	0.05	m

Processes of wave model (Table 5.4):

Table 5.4 Process used in the wave model

Processes	Options	Value in this case	Units
Wave setup	-	Not included	-
Generation mode for physical formulations	$1^{st}/2^{nd}/3^{rd}$	2nd	-
Wind growth	-	Activated	-
White capping	-	Activated	-
Quadruplet	-	Activated	-
Refraction	-	Activated	-

Because the tidal boundary is provided with a harmonic sinusoidal for a schematized model, the wave characters are the key points to calibrate for the hydrodynamic model.

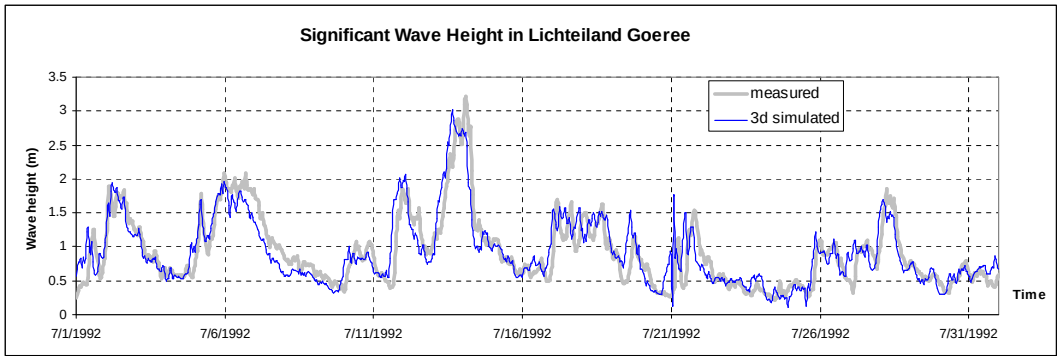

Fig 5.7 Simulated significant wave height and measured value at Lichteiland Goeree (offshore 20 km)

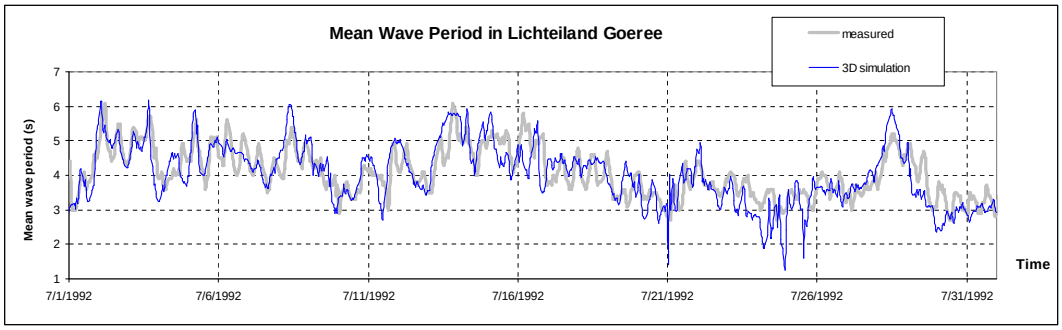

Fig 5.8 The simulated mean wave period and measured value at Lichteiland Goeree (offshore 20 km)

The model reproduces the significant wave height and mean wave period quite well in Lichteiland Goeree compared with the measured data, which indicates that the model reproduced the wave dynamic pattern.

Both the peaks and trends of significant wave height, which implies the wave energy, are quite accurately represented, even with a few hours of phase lag at some time points. The magnitude of significant wave height, which is more important to the resuspension of cohesive sediments, is well reproduced (Fig 5.7).

Sometimes the wave period is smoothed by the simulation compared with the measured wave period data. The simulated wave period is regarded as good representation in acceptable accuracy (Fig 5.8).

5.3.2 Calibration of cohesive sediment model

Parameters calibration at the sediment model (Table 5.5):

Table 5.5 Parameters calibrated in the Sediment model

Parameter	Value	Lower limit	Upper limit	Unit
Reference density	1600	100	-	kg/m^3
Specific density	2650	100	4000	kg/m^3
Dry bed density	500	mud: 100.0 sand: 500.0	3000	kg/m^3
Settling velocity	0.25	>0	30	mm/s
Median sediment diameter	-	64	2000	micron
Critical shear stress for sedimentation	0.1/1000	0	1000	N/m^2
Critical shear stress for erosion	1	0.001	100	N/m^2
Sediment erosion rate	0.0001	0	1	$Kg/m^2/s$
Initial sediment layer at bed	0	0	mud: 10.0 sand: 50.0	m

5.3.2.1 Suspended sediment concentration

The comparison of the SPM concentration is carried out at different points in the model domain (Fig 5.9).

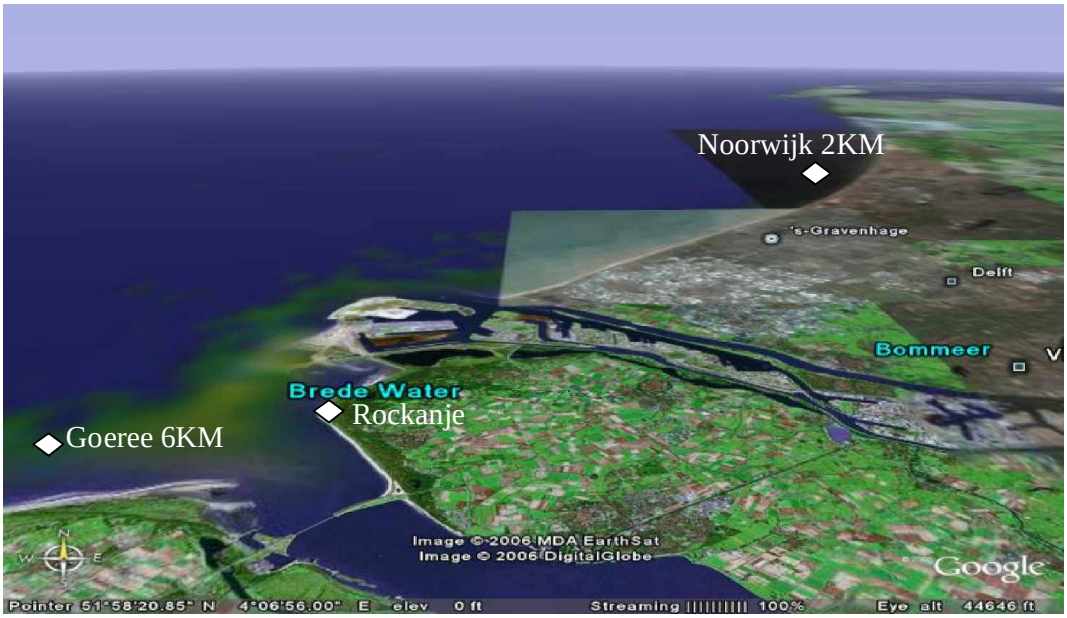

Fig 5.9 The location of comparison points

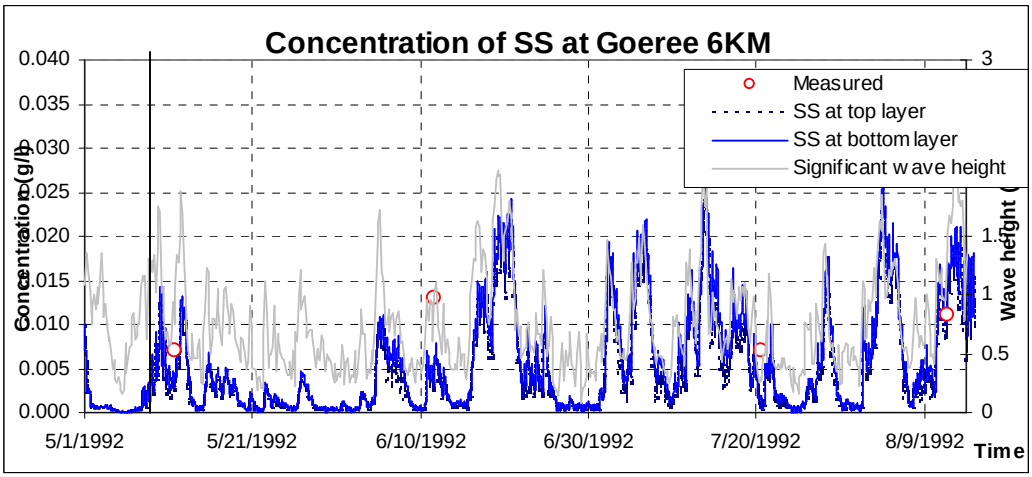

(a)

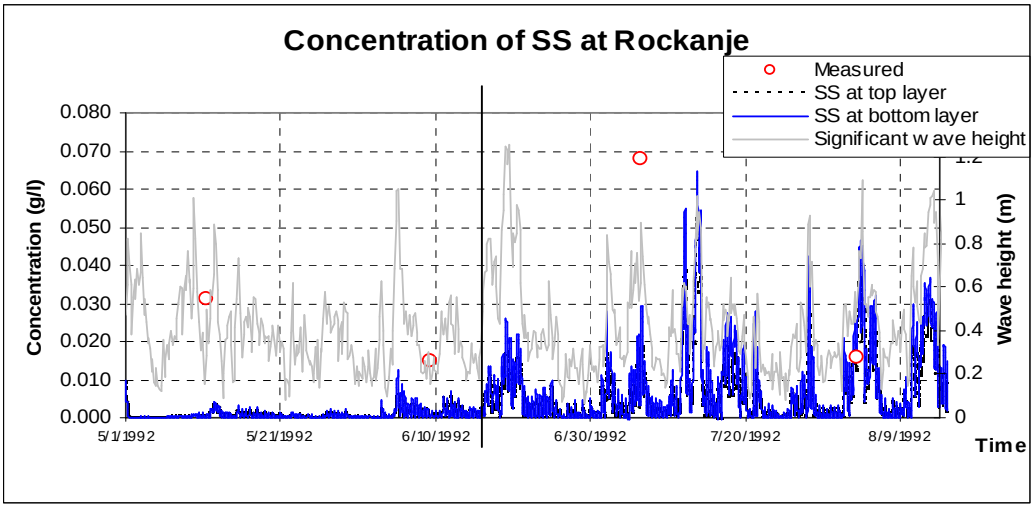

(b)

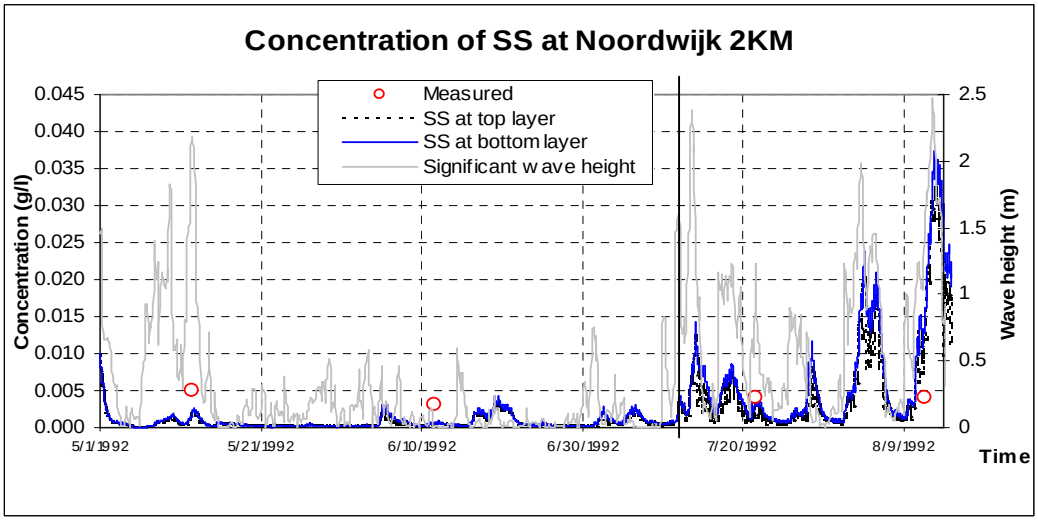

(c)

Fig 5.10 The simulated suspended sediments concentration and measured value at 3 points along the Dutch coast WITH wave effects (from south to north)

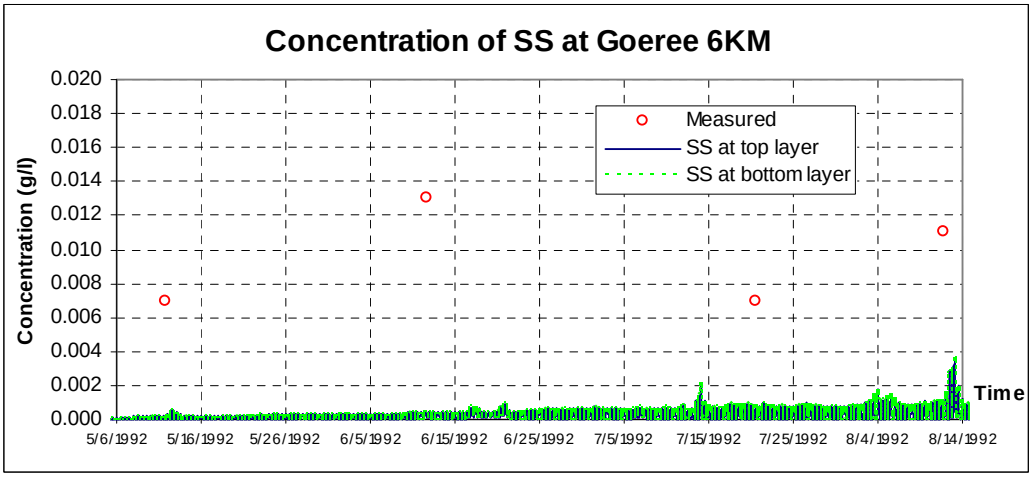

(a)

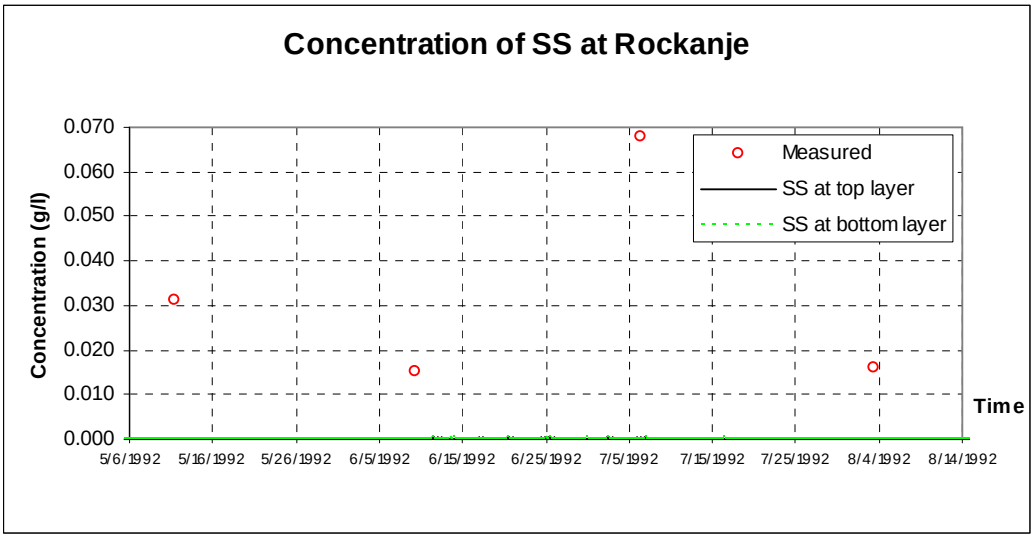

(b)

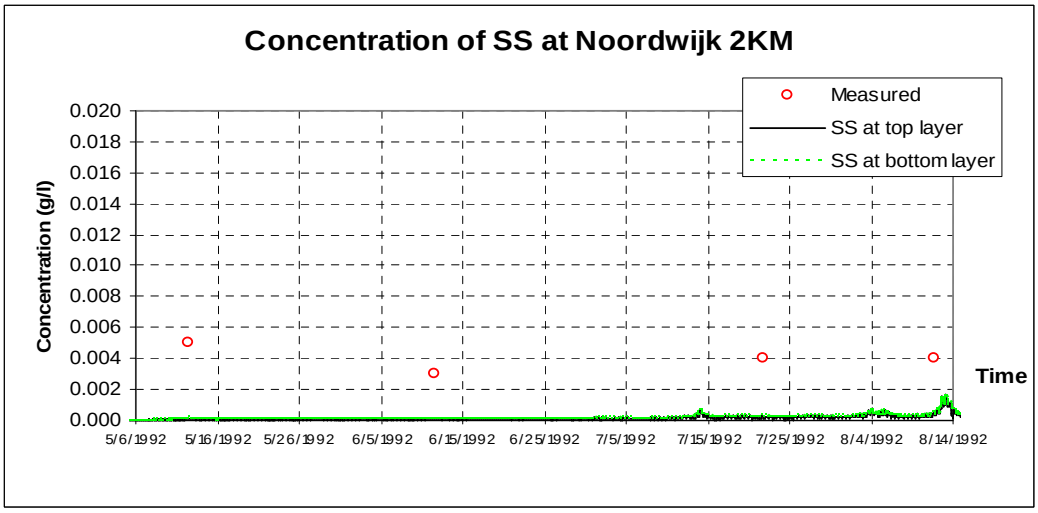

(c)

Fig 5.11 The simulated suspended sediments concentration and measured value at 3 points along the Dutch coast WITHOUT wave effects (from south to north)

In Fig 5.10 and Fig 5.11, the dynamics of the suspended cohesive sediment is described as the following:

- The cohesive sediments are moving northwards from the south boundary. It takes 10 days for the sediments travel from the south boundary to the Goeree point, where simulation concentration gets around 15mg/l. The concentration is also corresponding with to the significant wave height (Fig 5.10a).

- Then the sediments continue to travel northwards. About six weeks later, an amount of sediments arrive the Rockanje point, and settle down there and are resuspended by the wave. There are some big wave happened in the Rockanje point before June 10th, 1992, but because there is no sediments mass there (the initial thickness of sediment is 0 in our study), no sediments is resuspended into the water body (Fig 5.10b). From the Fig 5.9b, till July 11th, 1992, there are plenty of sediments settled in the bed at Rockanje eventually. After that, when

the wave is strong enough, proportional amount of sediments are stirred up and peak SPM concentration match the peak wave conditions.

- To the Noordwijk, it takes more than 10 weeks for the cohesive suspended sediment travelling from the south boundary. Even till Aug. 4th, 1992, the peak of wave condition starts to match the peak of SPM concentration (Fig 5.10c).

In summary, the time for the sediments travelling from the south boundary is about 10 to 12 weeks to the north boundary in the model.

The effects of wave dynamics are demonstrated distinguishably.

With waves, the peak value of SPM concentration at the Goeree point (water depth is about 6.5 m) is about 15mg/l in the surface and even higher concentration happens in the bottom layer, which is verified by the measured data. Without wave, the simulation concentration is generally lower than 2mg/l during the whole period (Fig 5.11a).

The effect of wave is more significant to the point Rockanje (water depth is about 3 m) which is located inside the Haringvliet mouth. Fig 5.11b shows the SPM concentration is quite low without wave effects, which fails to represent the reality as measured data.

To the point located in offshore 2 km of Noordwijk (water depth is about 10 m), the influence of waves is quite significant, less than 2mg/l as well, which fails to represent the reality as measured SPM concentration again (Fig 5.11c).

Fig 5.11 shows that the wave dynamics is essential to the high SPM concentration along the coastal line.

5.3.2.2 Available mass of sediments

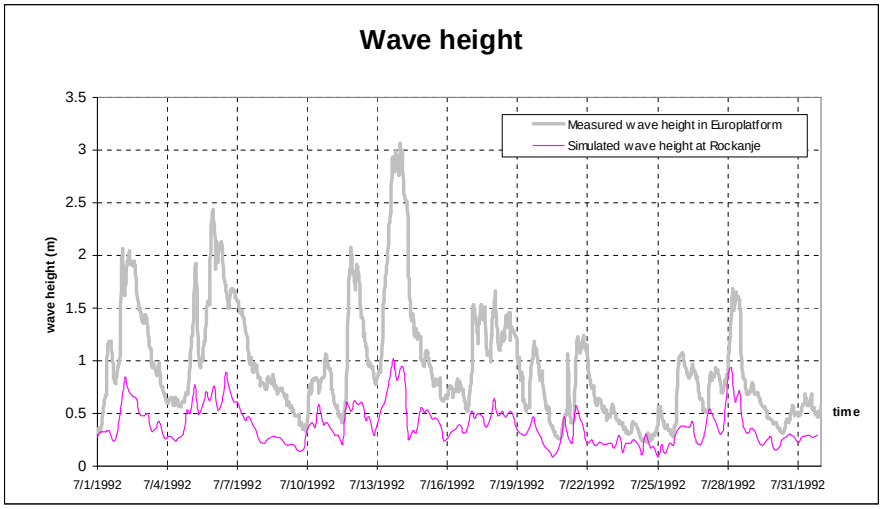

Fig 5.12 The significant wave height measured at Europlatform and simulated value at Rockanje (in shade area)

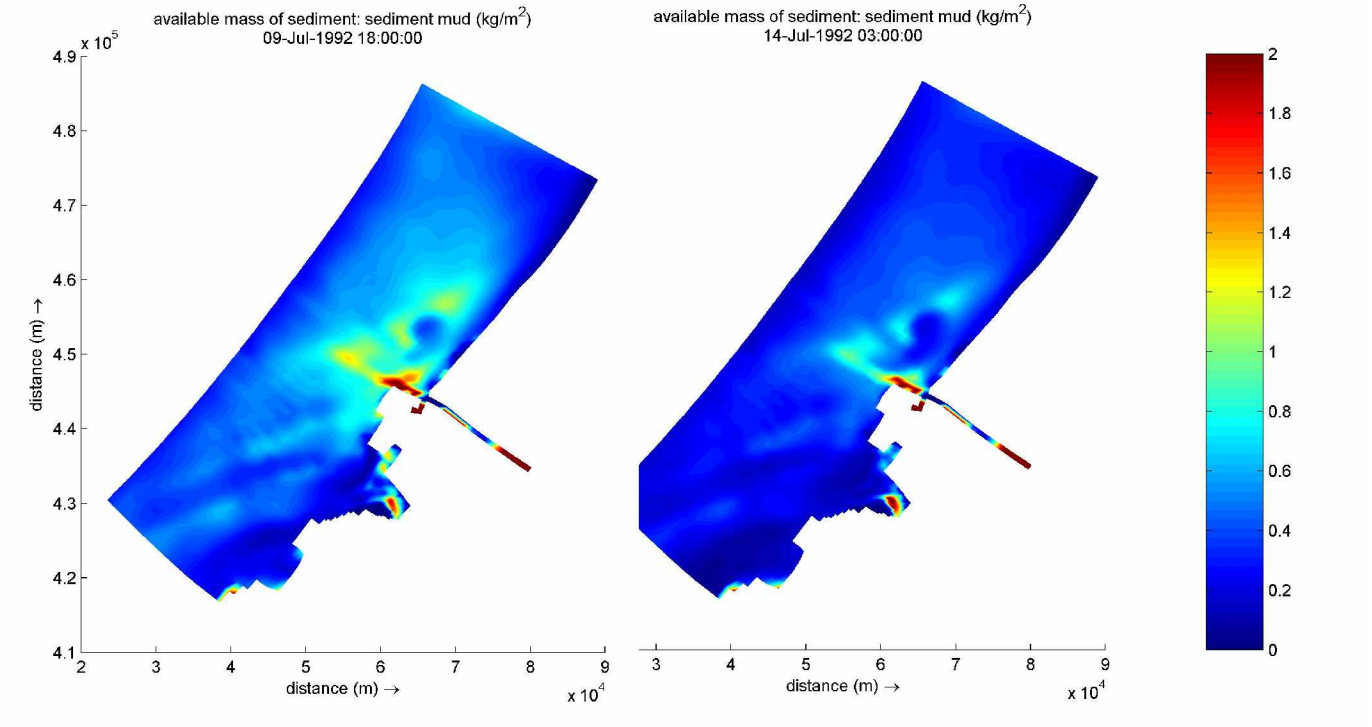

Fig 5.13 The available mass of sediments in the model domain under different wave conditions

Fig 5.12 depicts the significant wave height measured at the Europlatform and Rockanje. Two time points are chosen as examples to demonstrate to what extent the wave condition affects the available mass of sediments in the bed.

The left part of Fig 5.13 shows that the available mass of sediments is high when the significant wave height is 0.41 m at Europlatform (July 9th, 18:00:00, 1992). And the right part of Fig 5.13 shows the available mass of sediments is relatively lower than the left, which can be explained by the significant wave height at that time is as high as 2.63 m (July 14th, 3:00:00, 1992).

Some details are worth to notice as well. In the left part of Fig 5.13, the available mass of sediments at Rockanje is higher with relative mild wave condition showed in the right part of Fig 5.13. The value is as high as 1.2 kg/m^2, which is about 2.4mm thick of sediment available at Rockanje with low wave, while the value is about 0.7 kg/m^2, which means 1.4 mm thick of sediment available on the bed during the wild wave condition. About 1mm thick is eroded due to the wave.

However, the front area of Haringvliet Sluice behaves different. The available mass of sediments is relatively consistent, which implies that if such definite amount sediments arrived at the Haringvliet Sluice, it is not only influenced by the wave resuspension. Because the water level at July 9th, 18:00:00, 1992 is low, there are some fresh water is discharged out from the Haringvliet Mouth. The high available mass of sediments may subject to the special flow dynamics in the front of Haringvliet Sluice, which is the meeting point of salt water and fresh water and some vertical circulations may be driven

by density gradient. And during the July 14th, 3:00:00, 1992, the water level is quite high, and wave is wild at that time, no freshwater is discharged. It implies that the wave resuspension effects cause that amount of mass of sediments at the shoaling area next to the Slufter area by the orbital movements; however, it is quite shallow and most of the wave energy is dissipated there. Thus less wave can propagate inside to the front area of the Haringvliet Sluice, where quite an amount of sediments are available there.

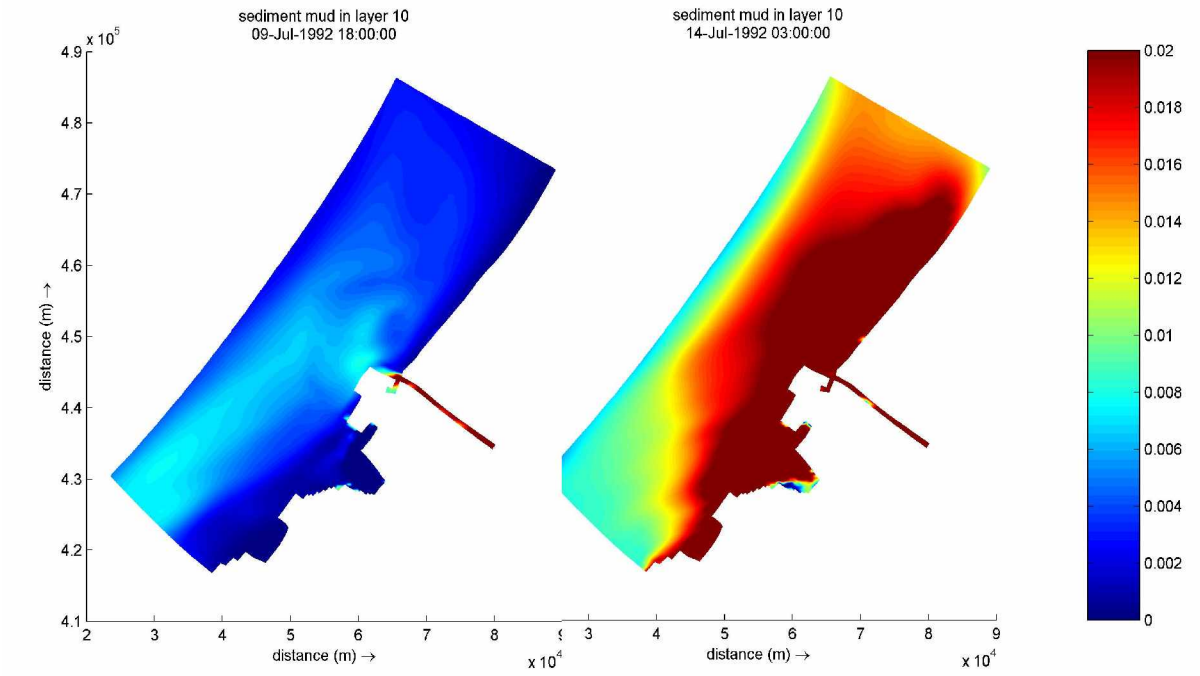

Fig 5.14 The near-bed SPM concentration in the model domain under different wave conditions (layer 10 is the bottom layer)

The left part of Fig 5.14 shows that the SPM concentration is low when the significant wave height is 0.41 m at Europlatform (July 9th, 18:00:00, 1992). And the right part of Fig 5.14 shows the SPM concentration is relatively lower than the left, which can be explained by the significant wave height at that time is as high as 2.63 m (July 14th, 3:00:00, 1992).

Fig 5.13 and Fig. 5.14 show that the total sediment mass at the studied domain is in equilibrium approximately after some time when the flow carries enough amount of sediment. The mass will change between suspended sediments and bed sediments due to the wave resuspension mechanisms. Wave dynamics is the dominant role in the resuspension and sedimentation in the Haringvliet Mouth and adjacent area.

5.3.2.3 Salinity

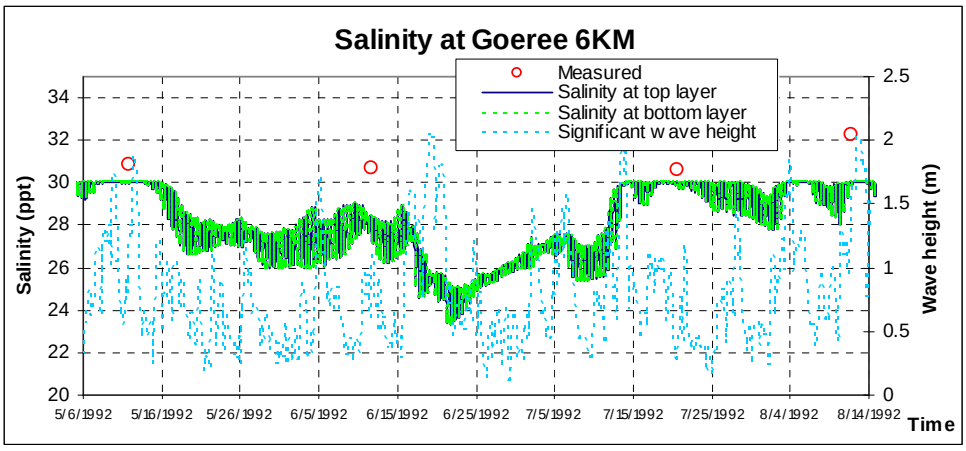

(a)

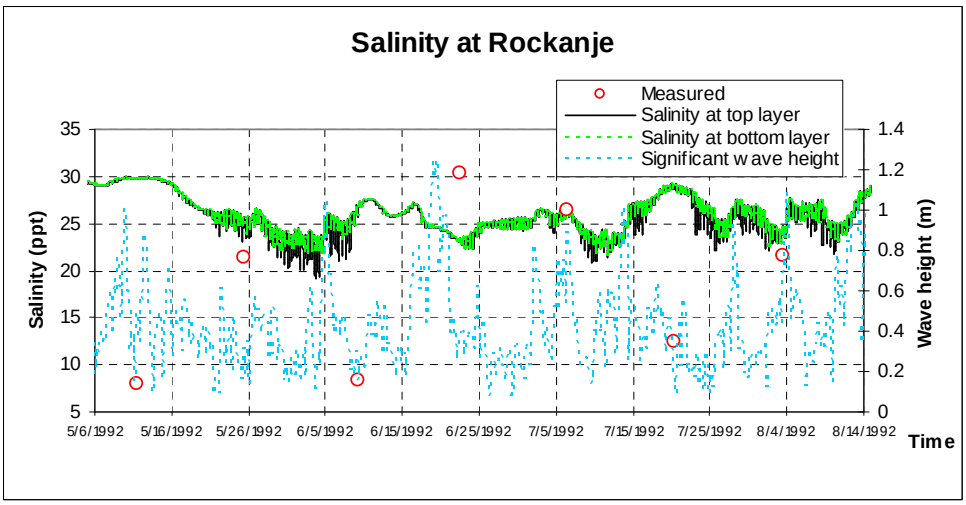

(b)

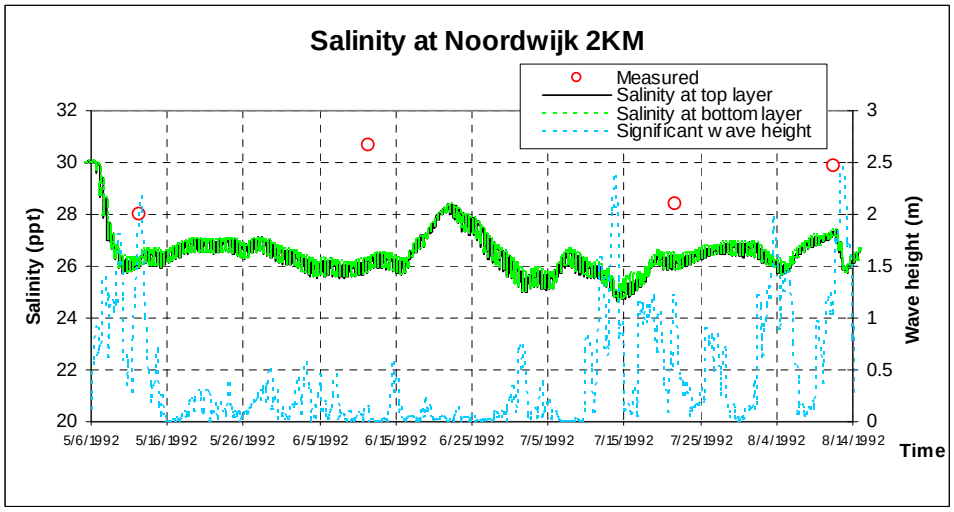

(c)

Fig 5.15 The simulated salinity and measured value at 3 points along the Dutch coast WITH wave effects (from south to north)

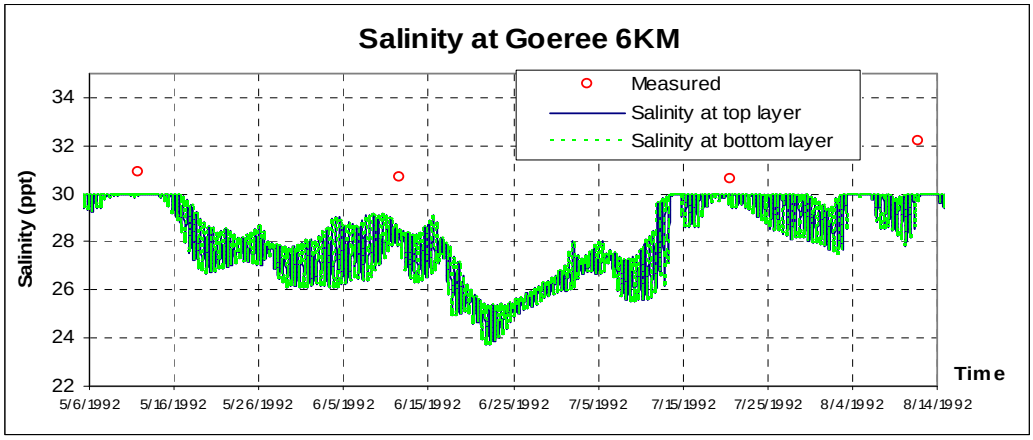

(a)

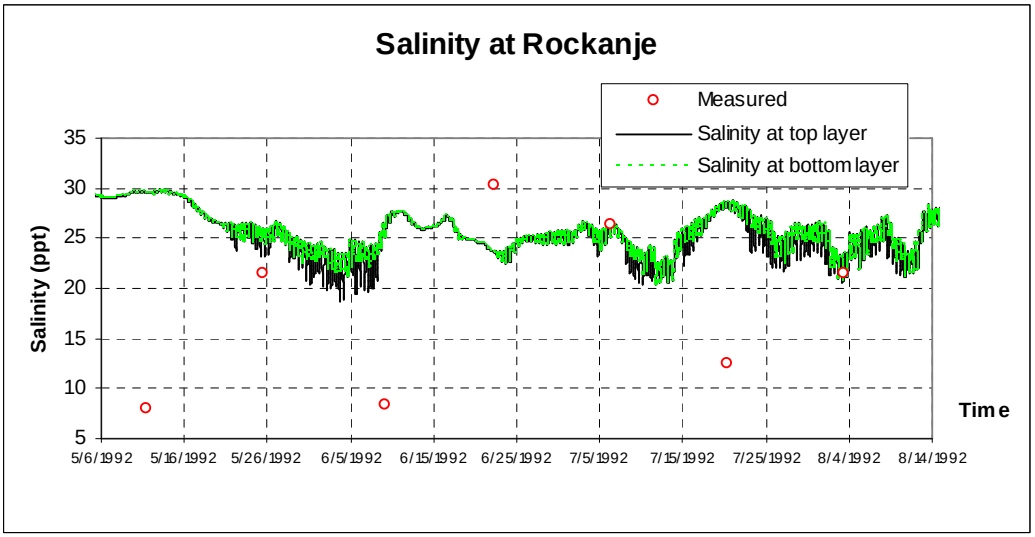

(b)

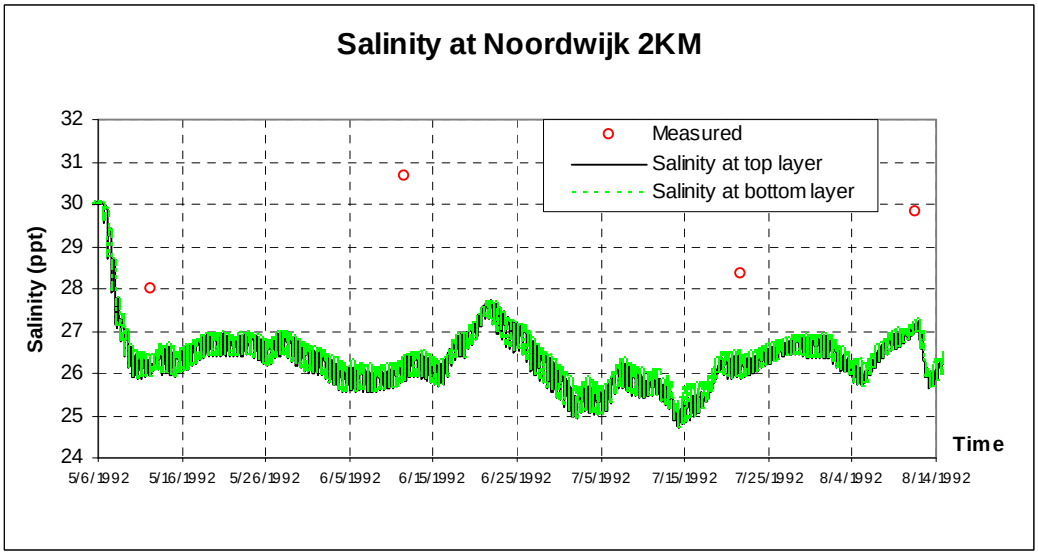

(c)

Fig 5.16 The simulated salinity and measured value at 3 points along the Dutch coast WITHOUT wave effects (from south to north)

The salinity computation is not so perfectly compared with the measured data. Generally the simulated salinity is lower than the measured data (Fig 5.15a, Fig 5.15c). The salinity in the Rockanje is at the right pattern, while it fails to reproduce some measured low salinity caused by the flush of fresh water from the Haringvliet Sluice (Fig 5.15b).

The main reason is that the salinity boundary is not set as a realistic value. As mentioned above (Part 5.2.1.3.3), the value is set as 30ppt at the seaside, and 0ppt at the river side.

There are also some other ways to improve the salinity model: one is to add a temperature process with heat flux boundary; another is to introduce high frequent measured data inside the model domain to get the correct pattern of salinity distribution.

Probably, the grid size in the Haringvliet Mouth is still too coarse for the salinity model to describe the details in this study, which need further study.

However, salinity may be not so sensitive to the wave in the simulation (Fig 5.16a, Fig 5.16b and Fig 5.16c). Anyway, it needs further study.

5.3.2.4 Sediment balance

The sediment balance in the model is also studied.

The values in literature of the residual SPM transport through the Dover Strait vary between [2.5–57.8] × 10^6 ton/year. These variations are due to differences in measurement techniques as well as to naturally occurring fluctuations. Eisma and Kalf (1987) calculated a SPM transport of [11.5–15.0] × 10^6 ton/year. McManus and Prandle (McManus, 1997) used numerical models and measurement data to obtain a yearly averaged value of 44.4 × 10^6 ton/year ([21.8–57.8] × 10^6 ton/year). The most recent value is of 22.2× 10^6 ton/year (seasonal variation: [11.9–28.9] × 10^6 ton/year) and is based on the data of McManus and Prandle (1997).

In the model, the cumulative flux of suspended sediments are calculated at the cross-sections located at two boundaries, south boundary as an input to the system, north boundary as an output to the system (Fig 5.17).

The dry density of cohesive sediments in our model is set to be 0.5 ton/m^3, thus the total input of the cohesive sediment in the simulated 3 months is 600,000×0.5 = 0.3 × 10^6 ton, i.e. the whole volume is 1.2 × 10^6 ton/year. From the value it is a little bit small. However, the domain covers only 1/5 or 1/6 width of the north exiting channel out of Dover Strait. And some other reasons like, that the vertical profile of SPM concentration is quite uniform with such a small settling velocity (0.25mm/s) while the bottom SPM concentration is normally much higher that at the water surface, and the measurement of the SPM are taken place during the mild weather condition in general, which ignores the high SPM concentration events during the wild storms, may cause the underestimation of the cumulative flux of suspended sediments in the model compared with the quantity that the literatures showed.

The output of the system with wave effects is about 400,000×0.5 = 0.2 × 10^6 ton in the 3 months, i.e. the whole volume is 0.8 × 10^6 ton/year. It is a reasonable ratio that 2/3 of the input sediments flux outputs to the model domain.

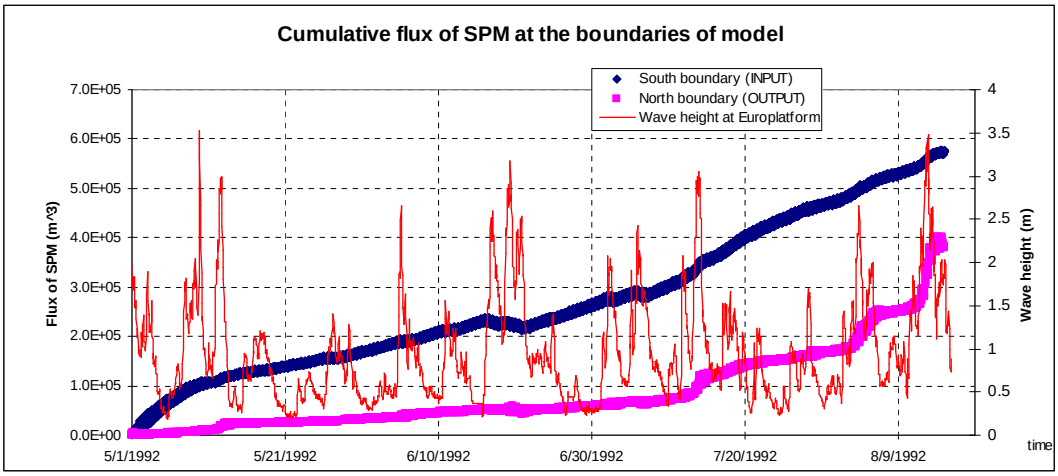

Fig 5.17 The cumulative flux of suspended sediments at the boundary of model WITH wave effects

Fig 5.17 also shows some correlation between the high wave height and increasing of the outflow in the north boundary. It is reasonable that during high wave climate condition, more sediment are resuspended and carried by the current out of the system, which is distinguishable after 10 weeks, even more remarkable after Aug 1, 12 weeks after the sediments travels from the south (refer to Part 5.3.2.1).

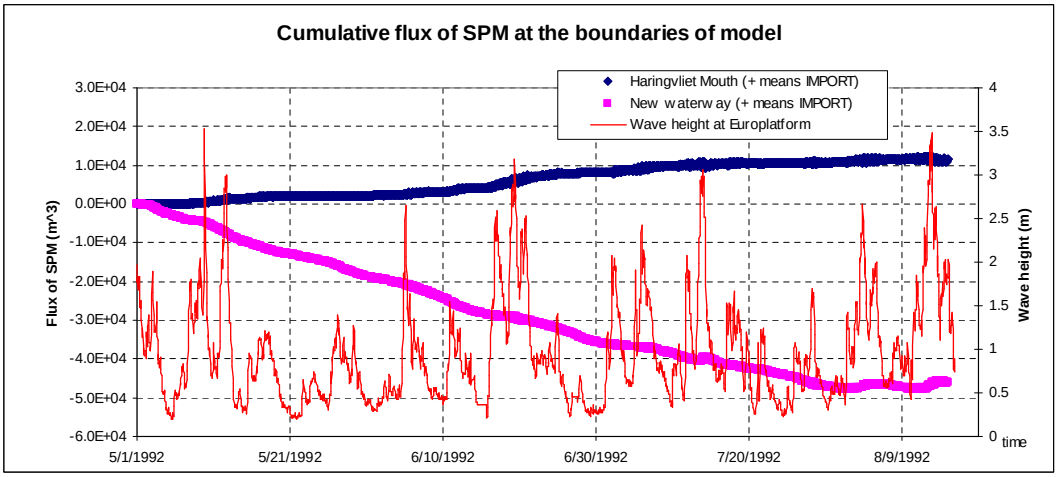

Fig 5.18 The cumulative flux of suspended sediments at the Haringvliet Mouth and Nieuwe Waterweg of model WITH wave effects

Fig 5.18 shows the cumulative flux of suspended sediments. In the Haringvliet Mouth, there is 10,000 m^3 sediments import from the seaside, which is averagely thickness of 0.1 mm to the whole Haringvliet Mouth area. In the Nieuwe Waterweg, about 50,000 m^3 the net export is flushed out from the river in the 3 months.

There are some correlations between the high wave height and cumulative sediments flux as well. To the Haringvliet, the import of SPM from the out sea tends to be a constant after 10 weeks, which proves the time value as the comparison of SPM concentration at Rockanje at Fig 5.10b. After 10 weeks, the import and export of the Haringvliet Mouth are almost equal, which means the equilibrium status has been achieved after 10 weeks. As to the Nieuwe Waterweg, no significant influence from the marine side, i.e. it acts as consistent sediments source for the system.

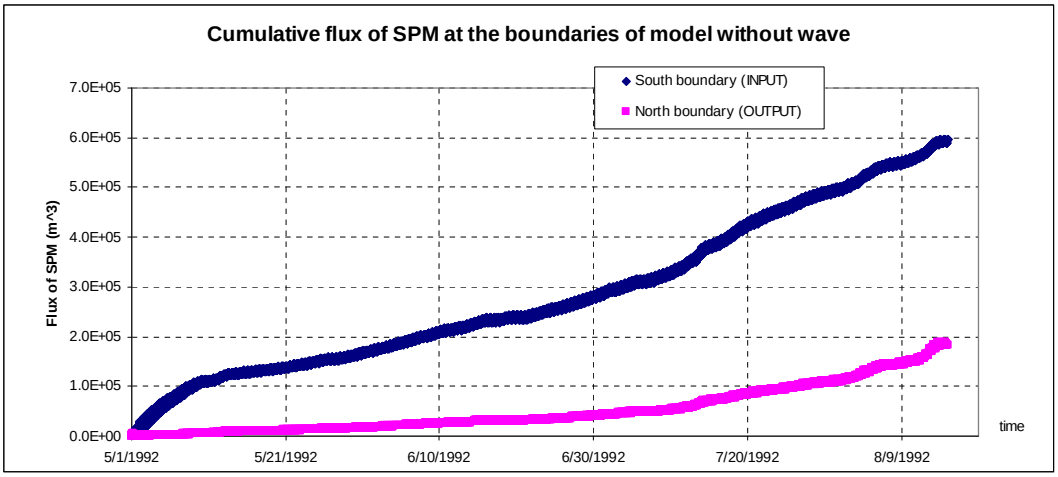

Fig 5.19 The cumulative flux of suspended sediments at the boundaries of model WITHOUT wave effects

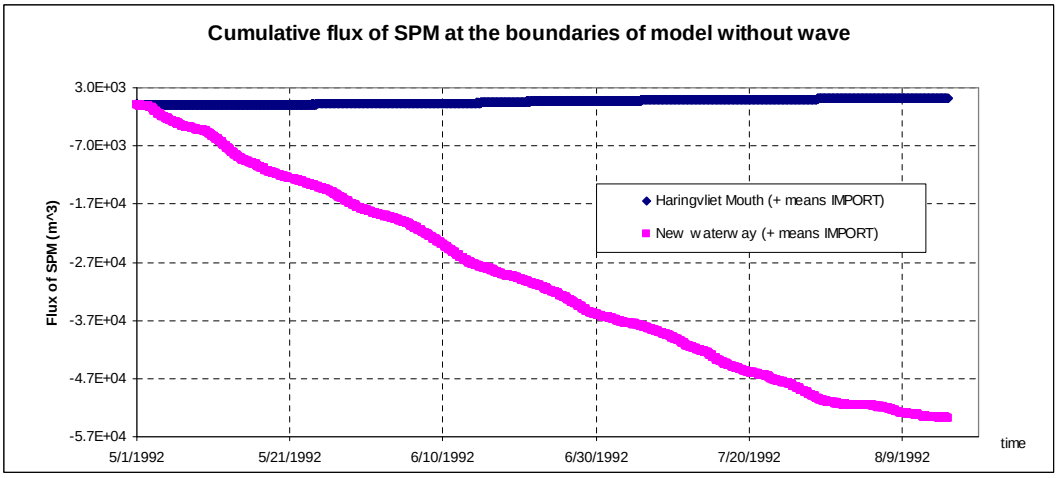

Fig 5.20 The cumulative flux of suspended sediments at the Haringvliet Mouth and Nieuwe Waterweg of model WITHOUT wave effects

Comparing Fig 5.19 and Fig 5.17, there is no significant change of flux of SPM from the south boundary, but without wave effects, only 200,000 m^3, half of the volume 400,000 m^3 with wave effects, is flushed out to the north boundary.

To the Haringvliet Mouth, the net import of the SPM is less than 2,000 m^3 without wave effects, which is not realistic at all (Fig 5.20).

No obvious influence with or without wave to the output of Nieuwe Waterweg, which acts as a sediment source to the system.

5.3.2.5 Summary of settings during calibration process

During the calibration process, several scenarios have been examined, which is summarized as the following table (Table 5.6).

Table 5.6 Summary of runs with different settings

Nr. of runs	Modification of outflow of Haringvliet sluice	With North Boundary input	BarocP	Sediment input of Nieuwe Waterway	τ_d in Nieuwe Waterway channel (Pa)	Thecher-Harlemann time lag (mins)
0	no	no	yes	no	1000	0
1	yes	no	yes	no	1000	0
2	yes	yes	yes	no	1000	0
3	yes	yes	no	no	1000	0
4	yes	yes	no	0.03g/l	1000	0
5	yes	yes	no	0.03g/l	0.1	0
6	yes	yes	no	0.03g/l	0.1	3800

General observations

From visual inspection of figures and corresponding animations (which is provided with slides), the following initial conclusion can be made:

- Two sources of sediments flowing into the system are observed, one is marine source from the south boundary, the other is riverside source from the Neiewe Waterweg.

- A clearly visible sediment flume is observed from the south to north along the modelling part of Dutch coast, which is identified as marine source of mud. And the river source of mud from Nieuwe Waterway channel influence the SPM concentration along the middle part of Dutch coast. The river segment in the upstream of Haringvliet sluice acts like a sink for the fluvial sediments. Therefore, the main source of sediments in Haringvliet Mouth is marine source.

- Persistent and high concentration of suspended sediments in the shoaling area in the Haringvliet Mouth indicates that the sediment is of high mobility and can be easily resuspended and entrained.

- The model results show that the simulations of SPM concentration are in reasonable agreement with the measurement and the knowledge on the large scale sediment transport in the North Sea.

Effects of Modification of outflow of Haringvliet sluice

Because the interval of outflow discharge record of Haringvliet sluice is once one day, it is not realistic. After manipulation the discharge with the water level outside sluice, it shows the sedimentation outside the Haringvliet sluice is varied with the tidal flow regularly.

Effects of North Boundary input

The suspended sediment concentration at the north boundary is set to be zero because the algorithm of the computation considers the concentration as an input sediment flux, which is not true. Without the north boundary input of the sediment flux, the narrow strip of sediments alongshore to the north can be distinguished clearly.

Effects of BarocP setting

The parameter BarocP setting, which is defined as the flag for activating barocline pressure term at open boundaries, is set as YES by default. The barocP setting is turned off to remove the influence of density or temperature gradient at the boundary, as a result, to decrease the disturbance from the boundary

Effects of sediment input and τ_d setting in Nieuwe Waterweg channel

The input of sediments of Nieuwe Waterweg channel causes a high SPM concentration strip along the coastline. The input sediment concentration is set as 0.03g/l, with a very low τ_d, less sediment will settle down in the channel, alternatively, that amount of sediments flows into the system and distributed and contributes to the strip of high concentration of SPM along the coast line.

Effects of Thacher-Harleman time lag

The *Thacher-Harleman time lag* setting describes the return time for concentrations from their value at outflow to time lag their value specified by the boundary condition at inflow.

At the sea-side boundary a common problem for numerical models of estuarine areas is encountered when the boundary conditions for a constituent are to be prescribed. In a physical (unbounded) world, the inflowing water mass immediately after low water slack originates from the outflowing water mass a moment earlier. Consequently, the concentration of the inflowing water is commonly not equal to the concentration $C_{\max}$ which has been prescribed along this open boundary. It will take some time before the concentration along this open boundary reaches the $C_{\max}$ value. In numerical models, this time lag (return time) is often modelled by means of a "Thatcher-Harleman" boundary condition (Thatcher, 1972). The return time depends on the flow conditions outside the estuary. If there is a strong circulation the return time is short.

Longer Thecher Harlemann time lag decrease the influence of ebb flow in this case.

5.4 Discussions and conclusions for the schematized model

The wave characters and SPM concentration of schematized model are calibrated and verificated with measured data from 1st, May till 15th, Aug of 1992, during which several storms events happened. some conclusions and discussions are carried out after analysis.

5.4.1 Conclusions

1. With subtle setting of the boundary conditions, the schematized model reproduces the hydrodynamics pattern and the transportation, deposition and resuspension pattern of suspended cohesive sediments in the Haringvliet Mouth and adjacent area.

2. It shows that the wave effect is the essential process for the cohesive sediment transportation, deposition and resuspension inside the Haringvliet Mouth area.

3. The cohesive sediments are moving northwards from the south boundary, and it takes about 1 week to move to the Goeree point, about 6-10 weeks to Rockanje, and around 10-13 weeks to Noordwijk. This time phase is concluded from the simulation from May 1st to August 15th, with a mild wave condition during summer. The time phase during the winter storm needs further study.

4. After that amount of time, there is enough sediment to be stirred up by the wave, eventually, the peaks of significant wave height match the peaks of the SPM concentrations compared with the limited number of measured points.

5. The model also exposes that the available sediment mass is also effected significantly with wave. Higher waves indicate that less sediments could stay on the bed, as a result, the suspended cohesive sediments concentrations increase and available sediment mass decreases.

6. Salinity is not simulated accurately in the model because of the schematized boundary conditions. The wave conditions affect little on salinity.

7. Sediment balance shows that the magnitude of flux of SPM input / output of the model is lower than the literatures showed due to some operational reasons in the model simulation period. However, the order is at the right range. Waves affect the output of sediments of the system, and the flux import and export from the Haringvliet remarkably.

5.4.2 Discussions

The wave field pattern has been well reproduced. The significant wave height and mean wave period are selected to compare with the measured data in Lichteiland Goeree, which indicates that he model reproduced the wave dynamic pattern.

The cohesive sediment transportation and deposition, then resuspension pattern has been well reproduced in addition. Even though, there are some discussions on the results.

The comparison of SPM concentration of the simulation and measured data is carried out in 3 points, each of which has 4 measured data during the model simulation period. The figures show that the simulated SPM concentrations in all the points are in good agreement with measured data in quantities with the wave process effects, while the model fails to reproduce the measured SPM concentration without wave effects. However, the measured data for SPM concentration is quite limited.

There are some spatial differences on the importance of wave dynamics apparently. In the Goeree 6KM, which located closer to the south boundary, the high SPM concentration occurs soon after the simulation starts, while in Noordwijk, far from the south boundary, the high SPM concentration occurs at the end of the simulation. It may imply that the system may need longer time than the simulation time in this case study to get deposition and erosion equilibrium in the whole model domain.

With wave, the peak value of SPM concentration at Goeree 6km point (water depth is about 6.5m) is about 15mg/l in the surface and even higher concentration happens in the bottom layer, which is verified by the measured data. Without wave, the simulation concentration is generally lower than 10mg/l during the whole period. Whether the high SPM concentration strip is related to the tide current need further study.

The effect of wave is more significant to the point Rockanje (water depth is about 3m) which located inside the Haringvliet mouth. With wave effects, the model represents measured SPM concentration, and similarly, the net cumulative flux of sediment in the Haringvliet Mouth is very reasonable. However, how the high SPM concentration affect by the salinity distribution and to what extent, still need further study.

Longer simulation is needed to validate the travelling time for the mud in the system. Some sensitivity tests on the sediment erosion rate, critical shear stress for erosion and settling velocity may benefit the correct magnitude for the cumulative flux of the SPM input / output of the system.

Part 6 Conclusions

The main objective of this study is to increase the understanding of the complex patterns of cohesive sediments transportation, deposition and resuspension due to wave effects with tide, wind, density-driven flow in the Dutch coastal area.

The study focuses on the case studies of areas adjacent to the approach channel of the port of Rotterdam and Haringvliet Mouth, which are characterized by complex interactions between hydrodynamics and sedimentation.

The following results have been achieved:

- **The study carries out analyses on the measurement data and reproduces the hydrodynamics pattern by ZUNO model in macro scale. Some sensitivity tests are carried out.**

  The study starts from the extension of the existing calibrated ZUNO model with wave module, and get the right pattern of sediment movement under wave dynamics with various verifications and sensitivity tests.

  Based on the analyses on the measured data and simulation result, the verification shows that the model reproduced the flow dynamic pattern, even though there is a one hour time lag between the simulation and measured velocity magnitude, which may be caused by the given boundary condition time lag, and some discrepancies of the higher water level and lower water level appears. The further study showed that may happen because of numerical processes.

  Analyses on the measured ADCP data, near the bottom, the long-term residual current has a significant onshore directed component, with values of 0.025 - 0.035 m/s, while near the surface, the long-term residual current is offshore directed. This pattern is ascribed to an estuarine-like cross-shore circulation due to horizontal and vertical variation in the density field related to the outflow of the system. The effect of onshore wind on the cross-shore residual currents shows a characteristic down welling pattern. Near-bottom currents are offshore directed, whereas near-surface currents are onshore directed, both opposite to the persistent density-driven cross-shore pattern.

  Near the surface, long-term residual currents are larger, 0.07 - 0.11 m/s, and are mainly in the alongshore direction with an onshore component increasing with distance from shore. Variability in the alongshore residual current is correlated to variations in the alongshore wind stress, particularly for the near-bottom currents.

  The simulation accurately reproduced the alongshore residual flow, while the cross residual flow pattern is a little bit under predicted.

  Sensitivity test of different turbulence closure models shows that the most complicated k-epsilon model did not lead to the best result compared with measured water level data.

Sensitivity test of the numerical coefficient of DPSOPT/ DPUOPT exposed some flaws of the default sets in the Delft-3D model. The value of DPSOPT=MAX and DPUOPT=MIN or MOR leads to a general deepening at the velocity points. The effects, in a relatively coarse model such as ZUNO, are very severe in this case. It still need further proof.

Wave modelling coupled with the coarse ZUNO grid flow model shows the wave periods and significant wave heights at the verified point are acceptable. Apparently, there are some discrepancies which show that, to such a big area, the wave field is affected by so many factors which cause difficulties to accurate simulation.

- **A refined grid model with domain decomposition technology has been set up and has been run successfully. However, because of the time restriction of this study, this part is not finalized.**

  With domain decomposition technology, a refined grid model is setup to simulate the detailed dynamic pattern and sediment transportation in a relatively small area – Haringvliet Mouth, which is covered by one element of coarse ZUNO model, with online simulation of flow/wave/sediments/morphology change models. The calibration and verification are not ready yet because of time limitations. This also raises a difficult question to modellers: to make a more detailed model which need long-time simulation, or to setup a coarse model which cannot depict the detailed physical phenomena?

- **A schematized model has been setup and calibrated. It reproduces hydrodynamics pattern and cohesive sediments transport pattern in the Haringvliet Mouth successfully and delineates the cohesive sediments transportation, deposition and resuspension pattern mainly due to wave effects in meso-temporal and spatial scale.**

  Based on the scale linkage theory of de Vriend (1991) and rules to keep model simple of Roelvink (2005b), a model with schematized dynamics and processes is setup using local grids coupling with online flow/wave dynamics and sediment transportation model. The subtle boundary condition of model is built deliberately with harmonic tidal forcing and real time discharge from the Haringvliet Sluice. After the calibration of the wave model and cohesive sediment transportation model, the coupled online models show the correct pattern of the cohesive sediment distribution in the area. It reproduces successfully the cohesive sediment transportation, deposition and resuspension pattern mainly due to wave effects in the areas adjacent to the approach channel of the port of Rotterdam and Haringvliet Mouth, which has been verified by measured sediments data of three month (1992) at three points located near the Haringvliet Mouth.

  The model results show that the wave dynamics is the most significant process in the Haringvliet Mouth.

  With a simple model determine the correct solution at the boundary by imposing the alongshore water level gradient (a so-called Neumann boundary condition) and some other settings of boundary conditions, a schematized model is just the

compromise for the modellers who are in the difficult dilemma of more processes and shorter time, that is, more complex physics are handled in shorter time.

As a result of the study, the model has been calibrated for the summer time, and after validation for the winter time with some sensitivity tests, it can be used as a predictive model in the future studies.

- **The distributed simulation solution tool is developed to utilize the distributed computation abilities in the local area network based on the named pipe technology. It has been proved to be efficient during the model simulations.**

Part 7 Recommendations

The following points are recommended in the future study:

1. Due to time limitation of this study, the model using domain decomposition technology has not been full calibrated. It would be challenge to calibrate the model using domain decomposition technology and use it to predict the physical processes with on-spot measured boundary conditions in the local area. Therefore it is recommended to do this, taking into account the two conflicting resources: the inadequate time and insufficient measured data. If the measured data is plenty, the area model covered, which is only restricted by the boundary influence, can be very small. If the computation time is not a limitation, a model with the wider area can be introduced and it is not difficult to find reasonable boundary condition for the existing global models.

2. The schematized model is using harmonic water level in the boundary introduced with a so-called Von Neumann boundary condition. The case study shows it works well if the boundary condition is set properly. However, it also is useful to include a series of tide components, with spring-neap cycle successively, by analysing the measured tide data from the measurement stations along the Dutch coast.

3. The measured concentrations data of suspended particulate matter (SPM) used in this case are quite limited. The number of points of measured data for verification and calibration in the case study for the schematized model is 3 points, one of which are located at the entrance of the Haringvliet Mouth, another is inside the Haringvliet mouth, while the other is located along the middle straight part of Dutch coast line. The interval of the measurement of SPM is about 20 to 30 days. During the simulation time, only 3 or 4 measured data for each point are available. More measured dataset, for instance, SILTMAN, can be significantly helpful for the model calibration and verification.

4. The seasonal dynamics in the SPM concentration is not considered in this study, which can be a very interesting topic for future studies.

5. Due to the characteristics of cohesive sediments, salinity process can be another significant effect to the distribution of SPM concentration. A more detailed salinity model can be introduced.

6. The uncertainty analysis of the parameter sets, the ranges of which are imposed in the part 5.3.1 and 5.3.2, and from other sources can be analysed in the future, which can help the decision makers to estimate the reliable extent of the model results.

7. The schematized model demonstrated the pattern in the area, and the result of the model can be used as a reasonable input for building data driven models.

8. The meso-scaled schematized model can be extended with longer time scale and the morphodynamics can be modelled based on the calibrated hydrodynamics and sediment transportation model.

References

Andrews, D.G., McIntyre, M.E., 1978. An exact theory of nonlinear waves on a Lagrangian-mean flow. Journal of Fluid Mechanics 89 (4): 609- 646.

Ariathurai, C.R., 1974. A finite element model for sediment transport in estruaries, University of California, Berkley, USA.

Battjes, J.A., Jansen, J.P.F.M., 1978. Energy loss and set-up due to breaking of random waves, Proc. 16th Int. Conf. on Coastal Engineering. ASCE, New York, pp. 570- 587.

Bhattacharya, B., 2005. Learning from data for aquatic and geotechnical environments. Taylor & Francis Group, 251 pp.

Booij, N., Ris, R.C., Holthuijsen, L.H., 1999. A third generation wave model for coastal regions: 1. Model description and validation. J. Geophys. Res. 104: 7649- 7666.

Dean, R.G., 1973. Heuristic models of sand transport in the surf zone, Proceedings of Conference on Engineering Dynamics in the Surf Zone, Sydney, Australia, pp. 208-214.

Dingemans, M.W., 1997. Water wave propagation over uneven bottoms. Part 1 -linear wave propagation. Advanced Series on Ocean Engineering, 13. World Scientific, 471 pp.

Dingemans, M.W., Radder, A.C., De Vriend, H.J., 1987. Computation of the driving forces of wave-induced currents. Coastal Engineering, 11: 539- 563.

Dronkers, J., 2005. Dynamics of coastal systems. Advanced series on ocean engineering, Volume 25. World scientific.

Eisma, D., Kalf, J., , 1987. Dispersal, concentration and deposition of suspended matter in the North Sea. Journal of the Geological Society of London 144, 161-178.

Fettweis, M.a.E., Dries Van den, 2003. The mud deposits and the high turbidityin the Belgian–Dutch coastal zone, southern bight of the North Sea. Continental Shelf Research 23: 669-691.

Fredsøe, J.F., 1984. Turbulent boundary layer in wave-current interaction. J. Hydraul. Eng 110: 1103 - 1120.

Godin, G., 1972. The Analysis of Tides. Liverpool University Press, Liverpool, 264 pp. pp.

Groeneweg, J., 1999. Wave-current interactions in a generalised Lagrangian Mean formulation, Delft University of Technology, Delft, The Netherlands.

Groeneweg, J., Klopman, G., 1998. Changes of the mean velocity profiles in the combined wave-current motion in a GLM formulation. Journal of Fluid Mechanics 370: 271- 296.

Hasselmann, K., T.P. Barnett, E. Bouws, H. Carlson, D.E. Cartwright, K. Enke, J.A. Ewing, H. Gienapp, D.E., Hasselmann, P. Kruseman, A. Meerburg, P. Müller, D.J. Olbers, K. Richter, W. Sell and H. Walden, 1973. Measurements of wind-wave growth and swell decay during the Joint North Sea Wave Project (JONSWAP). Dtsch. Hydrogr. Z. Suppl., 12, A8.

Holthuijsen, L.H., 2005. Waves in Oceanic and Coastal Waters. Cambridge University Press, Delft.

Janssen, G., Mulder, S. , 2005. Zonation of macrofauna across sandy beaches and surf zones along the Dutch coast. OCEANOLOGIA, 47 (2): pp. 265-282.

Johan Boon, H.W., Hans Los, 2001. Description and model representation T0 situation Part 1: The transport of fine-grained sediments in the southern North Sea.

Krone, R.B., 1984. The significance of aggregate prperties to transport processes.

estuarine cohesive sediment dynamics; workshop on cohesive sediment dynamics with special reference to physical processes in estuaries, Lecture notes on coastal and estuarine studies 14, Tampa.
Krumbein, 1941. Measurement and geological significance of the shape and roundness of sedimentary particle. Journal of Sedimentary Petrology, 11(Geotechnical spacial publications, No.21, ASCE, New York): 330-345.
Leendertse, J.J., 1987. A three-dimensional alternating direction implicit model with iterative fourth order dissipative nonlinear advection terms, WD-333-NETH, The Netherlands Rijkswaterstaat.
Lesser, G.R., Roelvink, J.A.,van Kestera, J.A.T.M., Stelling,G.S. , 2004. Development and validation of a three-dimensional morphological model. Coastal Engineering, 51: 883- 915.
Liu, K.a.C.C.M., 1989. Effects of wave-induced friction on a muddy seabed as a Bingham plasic fluid. Journal of Coastal Research, 5: 777-789.
Manning, A.J.a.D., K.R., 2002. A Comparison of Floc Properties Observed During Neap and Spring Tidal Conditions. In: J.C.a.K.C. Winterwerp (Editor), Fine Sediment Dynamics in the Marine Environment. Eksevier Science.
McLachlan, A., Jaramillo, E., Donn, T.E.,Wessels, F., 1993. Sandy beach macrofauna communities and their control by the physical environment: a geographical comparison. J. Coastal Res., 15: 27-38.
McManus, J.P., Prandle, D., 1997. Development of a model to reproduce observed suspended sediment distributions in the southern North Sea using Principal Component Analysis and Multiple Linear Regression. Continental Shelf Research, 17: 761-778.
Mehta, A.J., 2002. Mudshore dynamics and controls, in: Muddy Coasts of the World. In: Y.W. T. Healy, J-A. Healy (Editor), Proceedings in Marine Science. Elsevier, pp. 19-60.
Mei, C.C., 1983. The applied dynamics of ocean surface waves. Wiley, New York, 740. pp.
Molen, J.v.d., Dijck, B. van 2000. The evolution of the Dutch and Belgian coasts and the role of sand supply from the North Sea. Global and Planetary Change, 27: 223–244.
Odum, H.T., 1996. Scales of ecological engineering. Ecological Engineering, 6: 7-19.
OSPAR Commission, 2004. Geography, hydrography and climate, http://www.ospar.org. OSPAR Commission
Partheniades, E., 1965. Erosion and Deposition of Cohesive Soils. Journal of the Hydraulic Division, ASCE, No. HY1, Vol 91.
Port Of Rotterdam, 2005. Doing business on Maasvlakte 2. Port of Rotterdam.
Ris, R.C., Holthuijsen, L.H., Booij, N., 1999. A third generation wave model for coastal regions: 2. Verification. J. Geophys. Res. 104: 7667- 7681.
Roelvink, J.A., 2005a. Coastal Hydrodynamics Lecture Notes. UNESCO-IHE Institute for Water Education, Netherlands Centre for Coastal Research | NCK, Delft.
Roelvink, J.A., Broker, I., 1993. Cross-shore profile models. Coastal Engineering, 21: 163-191.
Roelvink, J.A., D.J.R. Walstra, 2005b. Keeping it simple by using complex models Advances in Hydro-Science and Engineering, Vol. VI.
Roelvink, J.A., T.Van der Kaaij, Ruessink, B.G., 2001a. Calibration and verification of large scale 2D/3D flow models--Phase 1, WL|Delft Hydraulics.
Roelvink, J.A., T.Van der Kaaij, Ruessink, B.G., 2001b. Reference scenarios and design alternatives Phase 1, WL|Delft Hydraulics.
Ross, M.A., and Mehta,A.J, 1989. On the mechanics of lutoclines and fluid mud.

Journal of Coastal Research(Special Issue 5: High concentration cohensive sediments transport): 51-61.
Short, A.D., 1996. The role of wave height, period, slope, tide range and embaymentisation in beach classifications: a review. Rev. Chil. Hist. Nat.,, 69: 589-604.
Short, A.D., 2006. Australian Beach Systems-Nature and Distribution. Journal of Coastal Research 22: 11-27.
Soulsby, R.L., Hamm, L., Klopman, G., Myrhaug, D., Simons, R.R.,Thomas, G.P., 1993. Wave-current interaction within and outside the bottom boundary layer. Coastal Engineering, 21: 41-69.
Stelling, G.S., 1984. On the construction of computational methods for shallow water flow problem. Rijkswaterstaat Communications, vol. 35.
Stelling, G.S., Leendertse, J.J., 1991. Approximation of convective processes by cyclic AOI methods, Proceeding of the 2nd ASCE Conference on Estuarine and Coastal Modelling, Tampa. ASCE,New York pp. pp. 771- 782.
Stelling, G.S., van Kester, J.A.T.M., 1994. On the approximation of horizontal gradients in sigma coordinates for bathymetry with steep bottom slopes. International Journal for Numerical Methods in Fluids, 18: 915-955.
Stive, M.J.F., Wind, H.G., 1986. Cross-shore mean flow in the surf zone. Coastal Engineering, 10: 235- 340.
Svendsen, I.A., 1985. On the formulation of the cross-shore wavecurrent problem, National Technical University of Athens, Athens.
Tchouani, n.J.M., 2004. Graded Sediment Transport Modeling, UNESCO-IHE, 132 pp.
Terwindt, J.H.J., 1967. Mud transport in the Dutch DELTA area and along the adjacent coastline. Netherlands Journal of Sea Research, 3,4: 505-531.
Thatcher, M.L., and R.F. Harleman,, 1972. A mathematical model for the prediction of unsteady salinity intrusion in estuaries. Report no 144., Massachusetts Institute of Technology.
Tonis, I.E., Stam, J.M.T., J. van de Graaf, 2002. Morphological changes of the Haringvliet estuary after closure in 1970. Coastal Engineering 192 44 191-203.
Uittenbogaard, R.E., J.A.Th.M. van Kester and G.S. Stelling, 1992. Implementation of three turbulence models in 3D-TRISULA for rectangular grids, Delft Hydraulics.
Van Kessel, T., 1997. Generation and transport of subaqueous fluid mud layers, Delft University of Technology, Delft.
Van Rijn, L.C., 1993. Principle of Sediment Transport in Rivers, Estuaries, Coastal Seas and Oceans. Aqua Publications, 1993, Amsterdam.
Vriend, H.J.d., 1991. Mathematical modelling and large-scale coastal behaviour. Journal of Hydraulic Research, 29: 727-740.
Vriend, H.J.d., Zyserman, J., Nicholson, J., Roelvink, J.A., Pechon, P. and Southgate, H.N., 1993. Medium-term 2DH coastal area modelling. Coastal Engineering, 21: 193-224.
Walstra, D.J.R. and Roelvink, J.A., Groeneweg, J., 2000. Calculation of wave-driven currents in a 3D mean flow model. In: B.L. Edge (Editor), Coastal Engineering pp. 1050- 1063.
Whitham, G.B., 1974. Linear and nonlinear waves. Wiley, New York, 636 p. pp.
Winterwerp, J.C., 1998. Rapid siltation from saturated mud suspensions. In: A.J.M. William H.McAnally (Editor), InterCOH'98. Elsevier, pp. 125-145.
Winterwerp, J.C., and Kessel Thijis van 2005. Personal communication.
Winterwerp, J.C., Kesteren, W.G.M.V, 2004. Introduction to the physics of cohesive sediment in the marine environment. Developments in Sedimentology, 56. Elsevier, 466 pp.

WL|Delft Hydraulics, 2005. User Manual Delft3D-Flow, B-76 pp.
WL|Delft Hydraulics, 2006. Delft3D-WAVE, Simulation of short-crested waves with SWAN.

Appendix I

User defined distributed simulation solution

I.1 Introduction

The computational architecture allowing for the distributed simulation solution is developed during this study.

As mentioned above, the modellers always have the difficult dilemma when they need to get compromise between the simulation time and the detailed physical processes.

On one hand, modellers intend to involve processes as much as possible to expose the intrinsic rules underneath the phenomena, which means more complicated model will be introduced and more computational time and more working labours are needed.

On the other hand, the result should be presented in acceptable short time.

There are some ways to solve the problem.

One way is to modify the models itself.

Nevertheless, it is a good try to use the domain decomposition to get a compromise. It make the modellers can just refine the interest area only, which can save quite a mount of time and can get relatively accurate result. Yet, it cannot help much in our study case.

It is also a good way to use the schematized model, just as what has been done in the study. The disadvantage is that this way demands a subtle setting of boundary conditions.

The other way is to utilize the available computation ability entirely, which is the motivation for the computational architecture allowing for the distributed simulation solution.

The solution is to use the Microsoft defined Name pipe basic class.

I.2 Basic concepts

Pipe is one of the technologies for inter-process communications, not only for Windows system, but also for Unix (personal communication with D.P. Solomatine).

A pipe is a section of shared memory that processes use for communication. The process that creates a pipe is the pipe server. A process that connects to a pipe is a pipe client. One process writes information to the pipe, then the other process reads the

information from the pipe.

There are two types of pipes: anonymous pipes and named pipes. Anonymous pipes require less overhead than named pipes, but offer limited services.

The term pipe, as used here, implies that a pipe is used as an information conduit. Conceptually, a pipe has two ends. A one-way pipe allows the process at one end to write to the pipe, and allows the process at the other end to read from the pipe. A two-way (or duplex) pipe allows a process to read and write from its end of the pipe.

In this study, we use named pipe.

A named pipe is a named, one-way or duplex pipe for communication between the pipe server and one or more pipe clients. All instances of a named pipe share the same pipe name, but each instance has its own buffers and handles, and provides a separate conduit for client-server communication. The use of instances enables multiple pipe clients to use the same named pipe simultaneously.

Any process can access named pipes, subject to security checks, making named pipes an easy form of communication between related or unrelated processes.

Any process can act as both a server and a client, making peer-to-peer communication possible. As used here, the term pipe server refers to a process that creates a named pipe, and the term pipe client refers to a process that connects to an instance of a named pipe.

Named pipes can be used to provide communication between processes on the same computer or between processes on different computers across a network. If the server service is running, all named pipes are accessible remotely. If a named pipe is intended to use locally only, access to NT AUTHORITY\NETWORK could be denied or local RPC can be switched off.

Thus the study starts based on a basic hypothesis: all the computational capacity can be accessed, which limits the usage of this solution in a local network system, where the accesses between computers are trusted.

I.3 Applications

The utilization of named pipe starts from the definition of the pipe.

- First, create the pipe with a prescribed name with status. In this case, fife pipe are defined as following:

```
// 1 for administration pipe
// 2 used to get the process in the remote computer
// 3 used to send and retrieve the application or process name the user will start.
// 4 used to kill the process in the remote computer
// 5 used to shutdown the pipe
```

// function name ConnectToRemoteService!

```
TCHAR szRemoteAdminPipeName[_MAX_PATH]              = _T("");
TCHAR szRemoteAdminProcessInfoPipeName[_MAX_PATH]   = _T("");
TCHAR szRemoteAdminProcessExecutePipeName[_MAX_PATH] = _T("");
TCHAR szRemoteAdminProcessKillPipeName[_MAX_PATH]   = _T("");
TCHAR szRemoteAdminSysShutdownPipe[_MAX_PATH]       = _T("");

HANDLE hCommandPipe = INVALID_HANDLE_VALUE;

// Remote service communication pipe name
::sprintf(
   szRemoteAdminPipeName,
   _T("\\\\%s\\pipe\\%s"),
   strRemoteMachineIP.GetBuffer(0),
   REMOTE_ADMIN_PIPE
   );

// Remote service communication pipe name
::sprintf(
   szRemoteAdminProcessInfoPipeName,
   _T("\\\\%s\\pipe\\%s"),
   strRemoteMachineIP.GetBuffer(0),
   REMOTE_ADMIN_PROCESS_INFO_PIPE
   );

// Remote service communication pipe name
::sprintf(
   szRemoteAdminProcessExecutePipeName,
   _T("\\\\%s\\pipe\\%s"),
   strRemoteMachineIP.GetBuffer(0),
   REMOTE_ADMIN_PROCESS_EXECUTE_PIPE
   );

// Remote service communication pipe name
::sprintf(
   szRemoteAdminProcessKillPipeName,
   _T("\\\\%s\\pipe\\%s"),
   strRemoteMachineIP.GetBuffer(0),
   REMOTE_ADMIN_PROCESS_KILL_PIPE
   );

// Remote shutdown pipe
::sprintf(
   szRemoteAdminSysShutdownPipe,
   _T("\\\\%s\\pipe\\%s"),
   strRemoteMachineIP.GetBuffer(0),
   REMOTE_ADMIN_SYS_SHUTDOWN_PIPE
   );
```

```
SECURITY_ATTRIBUTES SecAttrib = {0};
SECURITY_DESCRIPTOR SecDesc;
::InitializeSecurityDescriptor(&SecDesc, SECURITY_DESCRIPTOR_REVISION);
::SetSecurityDescriptorDacl(&SecDesc, TRUE, NULL, TRUE);

SecAttrib.nLength = sizeof(SECURITY_ATTRIBUTES);
SecAttrib.lpSecurityDescriptor = &SecDesc;;
SecAttrib.bInheritHandle = TRUE;

// Connects to the remote service's communication pipe
while(dwRetry--)
{
   if (::WaitNamedPipe(szRemoteAdminPipeName, 5000))
   {
      hCommandPipe = ::CreateFile(
                  szRemoteAdminPipeName,
                  GENERIC_WRITE | GENERIC_READ,
                  0,
                  &SecAttrib,
                  OPEN_EXISTING,
                  FILE_ATTRIBUTE_NORMAL,
                  NULL
                  );

      ::CloseHandle(hCommandPipe);

      CMachineInfo* pMachineInfo = GetMachineInfo(strRemoteMachineIP);
      //pMachineInfo->SetRemoteAdminPipe(hCommandPipe);

      ::Sleep(10000);
      if (::WaitNamedPipe(szRemoteAdminProcessInfoPipeName, 5000))
      {
         hCommandPipe = ::CreateFile(
                  szRemoteAdminProcessInfoPipeName,
                  GENERIC_WRITE | GENERIC_READ,
                  0,
                  &SecAttrib,
                  OPEN_EXISTING,
                  FILE_ATTRIBUTE_NORMAL | FILE_FLAG_OVERLAPPED,
                  NULL
                  );

         pMachineInfo->SetRemoteAdminProcessInfoPipe(hCommandPipe);
      }

      if (::WaitNamedPipe(szRemoteAdminProcessExecutePipeName, 5000))
      {
         hCommandPipe = ::CreateFile(
                  szRemoteAdminProcessExecutePipeName,
                  GENERIC_WRITE | GENERIC_READ,
```

```
                0,
                &SecAttrib,
                OPEN_EXISTING,
                FILE_ATTRIBUTE_NORMAL,
                NULL
                );

        pMachineInfo->SetRemoteAdminProcessExecutePipe(hCommandPipe);
      }

      if (::WaitNamedPipe(szRemoteAdminProcessKillPipeName, 5000))
      {
        hCommandPipe = ::CreateFile(
                szRemoteAdminProcessKillPipeName,
                GENERIC_WRITE | GENERIC_READ,
                0,
                &SecAttrib,
                OPEN_EXISTING,
                FILE_ATTRIBUTE_NORMAL,
                NULL
                );

        pMachineInfo->SetRemoteAdminProcessKillPipe(hCommandPipe);
      }

      if (::WaitNamedPipe(szRemoteAdminSysShutdownPipe, 5000))
      {
        hCommandPipe = ::CreateFile(
                szRemoteAdminSysShutdownPipe,
                GENERIC_WRITE | GENERIC_READ,
                0,
                &SecAttrib,
                OPEN_EXISTING,
                FILE_ATTRIBUTE_NORMAL,
                NULL
                );

        pMachineInfo->SetRemoteAdminSysShutDownPipe(hCommandPipe);
      }


      break;
    }
    else
    {
      // Let's try it again
      ::Sleep(dwRetryTimeOut);
    }
  }
```

§ Secondly, after pipes are constructed, build the connection.

//EstablishAllConnections

```
  // Remote resource, \\remote\ipc$, remote\admin$, ...
   ::sprintf(szRemoteResource,  _T("\\\\%s\\%s"),  strRemoteMachineIP.GetBuffer(0),
strResource.GetBuffer(0));

   //
   // Disconnect or connect to the resource, based on bEstablish
   //
   if (bEstablish)
   {
      NETRESOURCE nr;
      nr.dwType = RESOURCETYPE_ANY;
      nr.lpLocalName = NULL;
      nr.lpRemoteName = (LPTSTR)&szRemoteResource;
      nr.lpProvider = NULL;

      //Establish connection (using username/pwd)

// makes a connection to a network resourc and redirects a local device to the network
resource.
      dwRetVal = ::WNetAddConnection2(
                  &nr,
                  strPwd.GetBuffer(0),
                  strLogon.GetBuffer(0),
                  FALSE
                  );

      // Let the caller generate the error message
      /*if (dwRetVal != NO_ERROR)
      {
         //::PopError(dwRetVal);
         /*CString strFromatAPIMsg = ::FormatError(dwRetVal);
         CString strDisplayMsg;
         strDisplayMsg.Format("Machine IP %s: %s",
strRemoteMachineIP.GetBuffer(0), strFromatAPIMsg.GetBuffer(0));

         ::AfxMessageBox(strDisplayMsg);*/
      //}*/
   }
   else
   {
      // Disconnect
      dwRetVal = ::WNetCancelConnection2(szRemoteResource, 0, NULL);

      // Let the caller generate the error message
      /*if (dwRetVal != NO_ERROR)
      {
```

```
        //::PopError(dwRetVal);
        /*CString strFromatAPIMsg = ::FormatError(dwRetVal);
        CString strDisplayMsg;
        strDisplayMsg.Format("Machine IP %s: %s",
strRemoteMachineIP.GetBuffer(0), strFromatAPIMsg.GetBuffer(0));

        ::AfxMessageBox(strDisplayMsg);*/
      //}*/
    }

   // Prepare the return value
   if (dwRetVal == NO_ERROR)
   {
                ::LeaveCriticalSection(&g_CriticalSection);
     return TRUE; // indicate success
   }
```

- Thirdly, copy a client service for the pipe to the remote computer, which will act as a client, the other end of the pipe, without interruption to the remote users.

```
//CopyServiceExeToRemoteMachine

  HMODULE hInstance = ::GetModuleHandle(NULL);

  // Find the binary file in resources
  HRSRC hServiceExecutableRes = ::FindResource(
                        hInstance,
                        MAKEINTRESOURCE(IDR_REMOTEADMIN),
                        _T("EXECUTABLES")
                        );

  HGLOBAL hServiceExecutable = ::LoadResource(
                        hInstance,
                        hServiceExecutableRes
                        );

  LPVOID pServiceExecutable = ::LockResource(hServiceExecutable);

  if (pServiceExecutable == NULL)
    return FALSE;

  DWORD dwServiceExecutableSize = ::SizeofResource(
                       hInstance,
                       hServiceExecutableRes
                       );

  TCHAR szServiceExePath[_MAX_PATH];

  ::sprintf(
     szServiceExePath,
```

```
    _T("\\\\%s\\ADMIN$\\System32\\%s"),
    strRemoteMachineIP.GetBuffer(0),
    REMOTE_ADMIN_SERVICE_EXE
    );

  // Copy binary file from resources to \\remote\ADMIN$\System32
  HANDLE hFileServiceExecutable = ::CreateFile(
                                szServiceExePath,
                                GENERIC_WRITE,
                                0,
                                NULL,
                                CREATE_ALWAYS,
                                FILE_ATTRIBUTE_NORMAL,
                                NULL
                                );

  if (hFileServiceExecutable == INVALID_HANDLE_VALUE)
  {
     return FALSE;
  }

  ::WriteFile(hFileServiceExecutable, pServiceExecutable, dwServiceExecutableSize,
&dwWritten, NULL);

  ::CloseHandle(hFileServiceExecutable);
```

- Fourthly, install and run the client service for the pipe on the remote computer, which will act as a client, the other end of the pipe, without interruption to the remote users.

```
// InstallAndStartRemoteService


  // Open remote Service Manager
   SC_HANDLE hSCM = ::OpenSCManager(
                  strRemoteMachineIP.GetBuffer(0),
                  NULL,
                  SC_MANAGER_ALL_ACCESS
                  );

   if (hSCM == NULL)
   {
      return FALSE;
   }


   // Maybe it's already there and installed, let's try to run
   SC_HANDLE hService =::OpenService(hSCM, SERVICENAME,
SERVICE_ALL_ACCESS);
```

```
// Creates service on remote machine, if it's not installed yet
if (hService == NULL)
{
   hService = ::CreateService(
                hSCM,
                SERVICENAME,
                LONGSERVICENAME,
                SERVICE_ALL_ACCESS,
                SERVICE_WIN32_OWN_PROCESS,
                SERVICE_DEMAND_START,
                SERVICE_ERROR_NORMAL,
                _T("%SystemRoot%\\system32\\")REMOTE_ADMIN_SERVICE_EXE,
                NULL,
                NULL,
                NULL,
                NULL,
                NULL
                );
}


if (hService == NULL)
{
   ::CloseServiceHandle(hSCM);
   return FALSE;
}

// Start service
if (!::StartService(hService, 0, NULL))
{
   return FALSE;
}

::CloseServiceHandle(hService);
::CloseServiceHandle(hSCM);
```

After the pipe is setup, local computer can send a command to execute the local executable command to start a model simulation. In our case, a batch generate by Delft3Dis a good example.

The sample application screen dump looks like the following:

Fig A.1 the RCMI sample application screen dump